NUMERICAL MODELING OF GROUND MOVEMENTS ASSOCIATED WITH TRENCHLESS BOX JACKING TECHNIQUE

by

BABAK HAJI MOHAMMAD HASAN MAMAQANI

Presented to the Faculty of the Graduate School of

The University of Texas at Arlington in Partial Fulfillment

of the Requirements

for the Degree of

DOCTOR OF PHILOSOPHY

THE UNIVERSITY OF TEXAS AT ARLINGTON

August 2014

Acknowledgements

Foremost, I would like to express my sincere gratitude to my advisor, Dr. Mohammad Najafi, for his continuous support of my Ph.D. degree study and research, for his patience, motivation, enthusiasm, and immense knowledge. His guidance helped me immeasurably while researching and writing this dissertation. I could not imagine having a better advisor and mentor. In addition to my advisor, I would like to thank the rest of my dissertation committee, Drs. Chao, Ghandehari, Han, Hoyos, and Sattler for their encouragement, insightful comments, and hard questions.

I am deeply grateful to the Texas Department of Transportation (TxDOT) for providing the funding and support of the Vernon Box Jacking Project. I would like to thank Mr. Richard Williammee, Jr., M.S., P.E., (District Materials Engineer, Fort Worth District, TxDOT) and Dr. Ghassan Khankarli, P.E., (Director of Transportation Planning and Development, Amarillo District, TxDOT) who served as the Project Managers representing TxDOT. Their strong support of the project, close monitoring of project activities, and valuable suggestions and information greatly facilitated the study.

I would like to express my sincere gratitude to Mr. Art Daniel, President, AR Daniel Construction Services Inc., and Mr. Wayne Wright, Superintendent, AR Daniel Construction Services Inc., for allowing us to monitor and observe the box jacking project in Vernon, TX and Navarro, TX and providing us with information and valuable insight on the box jacking operation.

I am thankful to the following engineers in the Wichita Falls District: Mr. Chris C. Henry, P.E., Mr. Douglas Beer, P.E., Mr. Michael Beaver, P.E., Mr. Brad Catlett, and Mr. Monty Brown.

I would like to thank my friends, especially Abhay Jain, Hossein Tavakoli, Sajjad Moradi, Soheil Shafiee, Siavash Motlagh, Bhaumi Chaurasia, Alimohammad

Entezarmahdi and Manouchehr Teimouri for helping me get through the difficult times, and for all their support, entertainment, and caring. Without them, this research would have been impossible.

Lastly, and most importantly, I wish to thank my wife, Maryam Zavieh, and my parents, Ahmad Mamaqani and Shahnaz Esteva. They supported me, encouraged me, taught me, and loved me unconditionally. To them I dedicate this dissertation.

July 16, 2014

Abstract

NUMERICAL MODELING OF GROUND MOVEMENTS ASSOCIATED WITH TRENCHLESS BOX JACKING TECHNIQUE

Babak Haji Mohammad Hasan Mamaqani, Ph.D., E.I.T.

The University of Texas at Arlington, 2014

Supervising Professor: Mohammad Najafi

The Trenchless Technology (TT) is defined as a family of methods used to install, renew, replace or renovate new pipe/box or existing pipe/box underground with little or no surface disruption. TT is divided into two main categories including Trenchless Construction Methods (TCMs) and Trenchless Renewal Methods (TRMs). TCMs are used to install new utilities and pipes underground while TRMs are used to renew, renovate and replace an existing utility or pipe.

Box jacking (BJ) is a TCM used to install rectangular box culverts under existing facilities such as highways and railroads. In this method, box culverts are pushed through the ground using the thrust power of a hydraulic jack. Due to excavation methods and space requirements, the box culverts need to be large enough to provide adequate space for excavation. The sizes of box culverts usually range from 1.2 m x 1.2 m (4 ft x 4 ft) to 24.4 m x 12.2 m (80 ft to 40 ft).

Installing box culverts underground, like other trenchless methods, may cause surface settlement and consequently damage existing road pavement or railroad bed. As a result, the need to better understand ground movements induced by the BJ process is important to minimize damage to adjacent infrastructures and facilities. Settlement in BJ projects are divided into two main categories including advance settlement, and trailing settlement. This research is focused on trailing settlement.

The main objective of this research is to develop a surface vertical displacement prediction model using Artificial Neural Network (ANN). In this research, the ANN model was developed and trained using eight parameters including 1) modulus of elasticity (E), 2) friction angle (ϕ), 3) unit weight (γ), 4) cohesion (c), 5) box culvert height (h), 6) box culvert width (w), 7) overcut size (s), and 8) depth of box culvert from surface (H_1). Exactly 300 finite element models were generated using PLAXIS 2D and used to train the ANN model. Twenty-two new finite element models were generated to verify the final ANN model. Moreover, the final ANN model was verified by collected data from two case studies and by new finite element models. The secondary objectives of this research are to evaluate the effects of different parameters on surface vertical displacement, to study arching effects and to evaluate applicability of available methods to estimate vertical stress at the top of box culverts.

Results obtained from the final ANN model was in a good agreement with collected data from case studies and new finite element models. It was observed that the empirical method, suggested by Milligan and Marshal (1995) and originally developed for tunneling and pipe jacking (PJ), overestimated the maximum surface vertical displacement and underestimated the width of settlement trough (channel). Results showed that soil cohesion and box depth from ground surface had the highest impact on determining maximum surface vertical displacement, and soil friction and dilation effect have negligible impact on surface vertical displacements.

Analysis of stress redistribution due to soil collapsing into the overcut area showed that stress was reduced due to arching effect above the box culvert. However, both Terzaghi and Marston's theories underestimated vertical stress.

Table of Contents

List of Illustrations

List of Tables

Chapter 1

Introduction

Background

The demand for installing new underground utility and drainage systems under existing facilities has posed numerous challenges that necessitate the use of innovative construction methods. Pipelines play important roles in all communities because they can transport large quantities of different types of fluids; such as, water, sewer, and oil efficiently and at a low cost (Association of Pipelines, 2013).

The following methods are used to install new pipes or utilities underground:

1. Open-cut (OC)
2. Trenchless technology (TT)

Open-cut (OC): Open-cut (OC) method has been the conventional technology for construction, replacement and repair of underground utilities. Pipeline installation using OC methods may seem like a straightforward procedure which includes digging a trench, laying the pipe and backfilling. However, pipe installation using OC method involves several important engineering and construction decisions and activities. OC method includes the following main activities (Najafi, 2010):

1. Trench excavation,
2. Foundation placement if required
3. Trench wall (e.g., vertical trench or sloped trench)
4. Bedding preparation
5. Laying pipe
6. Embedment and backfill

Figure 1-1 illustrates a new pipe installation using open-cut method. A Trench box is installed to provide a safe working area for laborers inside the trench as per OSHA 29 CFR guidelines (OSHA, 2002).

(a) (b)

(c)

Figure 1-1 Pipeline Installation Using Open-cut Method: a) Trench Excavation, b) Trench Box Installation, and c) Backfilling and Embedment

Trenchless technology (TT): Advancements in technology and the development of new equipment have led to the development of new methods to facilitate utility-pipe work and decrease social costs and surface disruption. These new methods are called trenchless technology (TT) (Najafi and Gokhale, 2004). Environmental concerns, social (indirect) costs, new safety regulations, difficult underground conditions (existence of

natural or artificial obstructions, high water table, etc.) and new developments in equipment have increased the demand for trenchless technology design and specifications. TT includes the methods, materials and equipment that are used to install, repair or replace underground facilities with little or no excavation of the surface (Piehl, 2005). Different types of TT methods are available such as pipe jacking, utility tunneling, and horizontal earth boring that will be discussed in Chapter 2.

Social costs of construction include inconvenience to general public, and damage to environment and existing structures. Social costs are major elements in calculating the total life cycle costs, and they extensively impact method adoption procedures for installing pipelines and utilities underground. Due to the nature of the OC method, it involves high social costs versus trenchless technology which has lower social costs as presented in Figure 1-2 (Najafi and Gokhale, 2004).

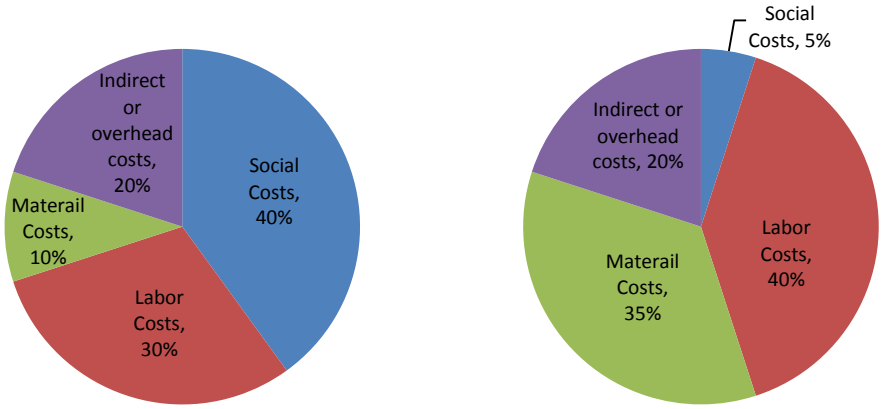

(a) (b)

Figure 1-2 Sample Costs Breakdowns: a) Open-Cut Method, and b) Trenchless Methods (Najafi and Gokhale, 2004)

General Description of Pipe Jacking

Pipe jacking (PJ) is a TT method for installation of a new prefabricated pipe underground from a drive shaft to a reception shaft. The term pipe jacking can be used to describe TT or a specific method or requirement essential to the process. When PJ refers to a specific TT method, it can apply to several methods such as the auger boring method. In the auger boring method a casing pipe is jacked through the ground as the spoil is transported through the casing by a continuous flight auger. Therefore, the process is a form of PJ. When PJ is a generic method, it refers to a cyclic method that uses the thrust power of hydraulic jacks to propel each segment of the pipe through the ground (Iseley & Gokhale, 1997). PJ is considered to be a conventional installation method or technique and was used at the end of 19th century for the first time. New PJ capabilities were added in the 1950s and 1960s by the Europeans and Japanese. These capabilities include extended drive length, upgraded line and grade accuracy, enhanced joint mechanism, new pipe materials and improve excavation (Najafi & Gokhale, 2005).

In the PJ method, the jacked pipe is sufficiently large to allow workers to enter the pipe. To apply this method, a jacking pit or shaft is dug on one side of the road to be crossed and contains the jacking machine and sections of the pipe to be jacked. Directly across the road, a receiving pit or shaft is dug to receive the pipe that will lie underneath the road. Excavation at the face of the PJ shaft can be done using a variety of excavation machines including the hand shield, backacter,[1] cutter boom, tunnel boring machine (TBM) and earth pressure balance machine (EPBM). Excavated soil is removed using carts or other means. A space between the outer diameter of the installed pipe section and excavated bore, referred as overcut, is maintained to reduce friction forces and to facilitate steering of the tunneling machine. Overcut sizes of 25.4 to 50.8 mm (1 to 2 in.)

[1] Backacter is an open-face shield with mechanical means of excavation.

over diameter are typical. To reduce the contact friction between the advancing pipe and the surrounding earth, and to balance the pressure around the pipe, bentonite slurry is pumped into the overcut space immediately outside the pipe to serve as a lubricant. The process of pipe jacking is summarized follows (Najafi, 2013):

1. Excavate and prepare the drive shaft.
2. Set up the jacking frame and the hydraulic jack.
3. Install the laser guidance system.
4. Lower the tunnel boring machine (TBM) if excavation method is not hand mining.
5. Mate the jacking push plate.
6. Begin excavation using TBM or any other excavation methods.
7. Remove spoils from the shaft.
8. Provide space for the pipe segment by retracting the jacks and push plates.
9. Place a segment of the pipe.
10. Mate the push plate to pipe and pipe to the shield or TBM.
11. Start pushing the pipe.
12. Repeat pipe jacking cycles until the complete pipe assembly is installed.
13. Grout the space between pipes and excavated area.
14. Remove the shield or TBM.
15. Remove jacking equipment and auxiliary equipment.
16. Restore the site as required.

The pipe must have a relatively thick wall to withstand the horizontal pressure required for jacking and vertical soil pressure; otherwise, the pipe may be damaged by the large thrust developed from the jacking operation or excessive fill height. Therefore, the jacking pipe material must be relatively stiff and strong, which means it usually made

of steel reinforced concrete (Najafi, 2013). This consideration causes the cost of pipe material to be higher than the in OC method. Figure 1-3 shows typical components of a pipe jacking operation.

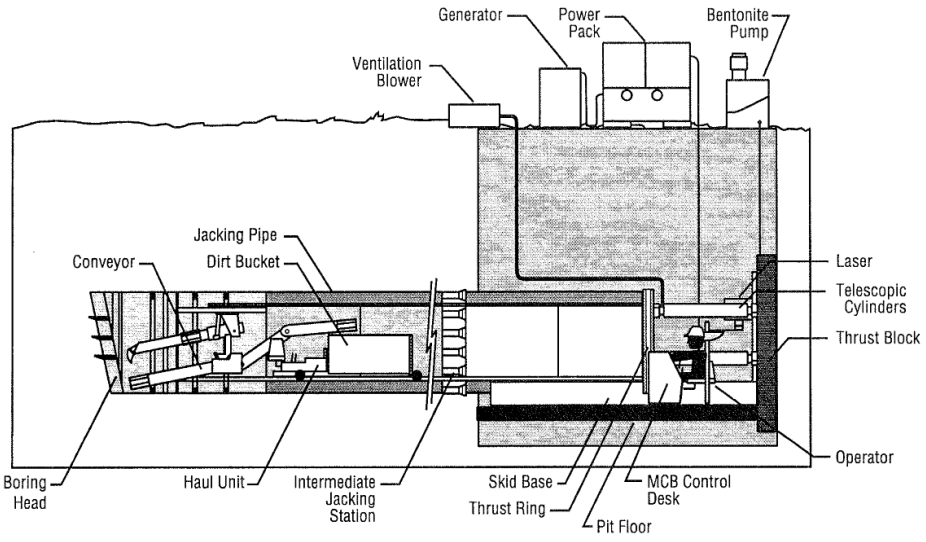

Figure 1-3 Typical Components of a Pipe Jacking Operation (Iseley & Gokhale, 1997)

Similar to other TT methods, PJ has specific characteristics and limitations. Table 1-1 shows main characteristics of the PJ method.

Table 1-1 Main Characteristics of Pipe Jacking Method (Najafi, 2013)

Method	Diameter Range m (in.)	Maximum Length m (ft)	Pipe Material[1]	Typical Application	Accuracy
Pipe Jacking	1 (42) and up	457 (1,500)	RCP, GRP, Steel	Pressure and Gravity	± 1

[1]RCP- Reinforced Concrete Pipe, GFRP- Glass-Fiber Reinforced Polyester

Pipe jacking (PJ) method is not applicable in all types of soils. Cohesive soils are the most suitable soils for the PJ method. Dewatering and closed-face or earth pressure balance machines (EBM) may be required when PJ method is used underwater and/or in

unstable soil conditions. Table 1-2 presents applicability of PJ method in different soil conditions (Najafi, 2013).

Table 1-2 Applicability of Pipe Jacking Method in Different Soil Conditions (Najafi, 2013)

Type of Soil	**Applicability**
Soft to very soft clays, silt, and organic deposits	Marginal
Medium to very stiff clays and silts	Yes
Hard clays and highly weathered shales	Yes
Very loose to loose sands above the water table	Marginal
Medium to dense sands below the water table	No
Medium to dense sands above the water table	Yes
Gravels and cobbles with less than 50- to 100-mm diameter	Yes
Soils with significant cobbles, boulders, and obstructions larger than 100- to 500-mm diameter	Marginal
Weathered rocks, marls, chalks, and firmly cemented soils	Marginal
Significantly weathered to unweathered rocks	No

General Description of Box Jacking (BJ)

Box jacking (BJ) method is a unique TT method for installing a box culvert underground from a drive shaft to its receiving shaft beneath critical facilities such as railways, major highways and airport runways without surface disruption (Hung et al., 2009). The basic process of installing a box culvert includes setting a box culvert in a launch shaft and then jacking into the ground with excavation taking place within an open face shield (Najafi, 2013). Figure 1-4 shows a BJ project.

Figure 1-4 BJ Project

Box jacking (BJ) method was originally developed from the PJ method and includes many of the same features as the PJ method. The first development from PJ method to BJ was made in the 1960's because it was found that the circular pipe sections were not suitable for shallow installations. In the past 40 years, the BJ method has developed to include a wide variety box dimensions ranging from 4 ft x 4 ft to 80 ft x 40 ft (Hung et al, 2009). Figure 1-5 illustrates a typical cross section of a box culvert.

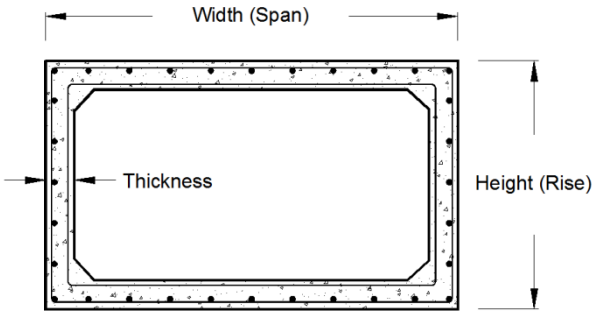

Figure 1-5 Cross Section of a Box Culvert

Box jacking (BJ) method can be used in variety of ground conditions, including soft clays, granular material, filled ground and mixed ground (Taylor and Winsor 1998). However, similar to best soils for the PJ method, cohesive soils are the most suitable soils for BJ method.

Similar to the PJ method, overcut excavation is required to reduce friction forces and facilitate steering during construction. Bentonite slurry is pumped into the overcut space to reduce the friction forces between box culverts and surrounding soils. Overcut space needs to be grouted after completion of the project to prevent soils from collapsing into the overcut space.

Since box culverts have rectangular shapes, TBM and EPBM machine cannot be used for excavation purposes. Dependent on box culvert size, excavation in BJ method can be implemented by hand mining, small size backhoe or roadheader (Hung et al,

2009). In relatively small size box culverts, hand mining is the only applicable excavation option while in large box culverts backhoe and roadheader can be used. Figure 1-6 and Figure 1-7 illustrate box jacking operations with hand mining and roadheader excavation respectively.

Figure 1-6 Box Jacking (BJ) Operation with Hand Mining Excavation

Figure 1-7 Box Jacking (BJ) Operation with Roadheader Excavation

(Hung et al, 2009)

Box Jacking (BJ) Operation

Similar to PJ method, BJ operation process involves several activities as follows:

1. Lift, Placement and Line Adjustment of Each Reinforced Concrete Box: An excavator lifts a new box from the stockpile and places it into the lunch shaft as presented in Figure 1-8.

Figure 1-8 Excavator Hoists a Box Section from the Stockpile (Tavakoli, 2012)

2. Lift, Placement and Line Adjustment of the Jacking Frame: The excavator lifts the jacking frame and places it into the launch shaft as shown in Figure 1-9. Laborers help to place the frame in the correct alignment.

Figure 1-9 Excavator Placing Jacking Frame into Launch Shaft (Tavakoli, 2012)

3. Lift, Placement and Line Adjustment of the Rail: Excavator lifts the two pieces of the rail and placed it into the launch shaft. Laborers place the rails on a wood frame and adjust them. These rails are used to transport the soil spoil from the tunnel. A rail is shown in Figure 1-10 .

Figure 1-10 Spoil Cart Rail (Tavakoli, 2012)

4. Installing Pipes and Hoses for Bentonite Slurry Movement: Laborers install the pipes that will be used to pump the bentonite slurry. In Figure 1-11, a laborer is shown preparing the bentonite slurry.

Figure 1-11 Bentonite Lubricant Preparation (Tavakoli, 2012)

5. Installing the Air Supply Line: Laborers installs air supply lines in the tunnel. These lines are used to flow fresh air to the face of the tunnel while the workers are inside excavating the soil in front of the first box. Air supply lines are shown in Figure 1-12.

Figure 1-12 Air Supply Lines (Tavakoli, 2012)

6. Alignment Check: The hydraulic jack operator checks the alignment and extends the jacks to push the box culvert forward. A laser, as illustrated in Figure 1-13 a, is used to check the grade and alignment. Figure 1-13 b shows the jacking control handle.

(a) (b)

Figure 1-13 a) Laser for Alignment and b) Jacking Control Handle (Tavakoli, 2012)

7. Excavation Cycle: Spoil buckets are used to transfer excavated soil out of the bore. Figure 1-14 a, illustrates how the excavator unloaded the bucket with the help of a laborer. Figure 1-14 b, shows the spoil cart going into the tunnel to be loaded again.

Figure 1-14 a) Excavator Unloads Spoil Cart, b) Empty Spoil Cart (Tavakoli, 2012)

8. Jacking the box: Figure 1-15 illustrates a hydraulic jack pushing the box culvert into the bore.

Figure 1-15 Pushing Box by Hydraulic Jacks (Tavakoli, 2012)

9. Removing Mud Rail, Air Supply Line and Hose for Bentonite Supply: Once one box is fully jacked into the tunnel and the jacking process is completely

finished, the mud rail, air supply lines and hose for the bentonite supply are removed.

10. Removing Jacking Frame: Once all items are removed, laborers detach the jacking frame from the previous jacked box and attach it to the excavator. Then, the excavator lifts the jacking frame out of the launch shaft.
11. Applying Box Culvert Joint Adhesive to the Front End of The Previously Jacked Unit: The process of preparation for the next box section starts with applying joint adhesive to the end of the previously jacked box section. Figure 1-16 shows the joint sealant.

Figure 1-16 Polymer Modified Concrete Joint Sealant (Tavakoli, 2012)

12. Cleaning the Spoil over the Guide Rail: The next activity is to clean the dirt from the launch shaft and to prepare it for receiving the next box section (Tavakoli, 2012).

Pipe Jacking (PJ) versus Box Jacking (BJ)

Pipes are commonly used to transfer water, sewer, etc. A circular section is the best geometrical section in terms of hydraulic performance because the area of flow is minimized for a given discharge (Humes, 2013).

Box culverts are commonly used under highways and railroads as drainage structures, pedestrian crossings, and are mainly used to transport storm water.. Rectangular box sections are used when a large flow is required especially when the hydraulic head is limited. This is because the height of the box culvert can be reduced to have less impact on upstream water level and downstream flow velocities while the equivalent area of circular pipes are fixed and cannot be reduced. Figure 1-17 shows a comparison of a pipe and a box with equivalent area in terms of hydraulic head effects. Moreover, a box culvert's width can be reduced for difficult site conditions such as very loose or very stiff soils to reduce excavation and backfilling (Humes, 2013).

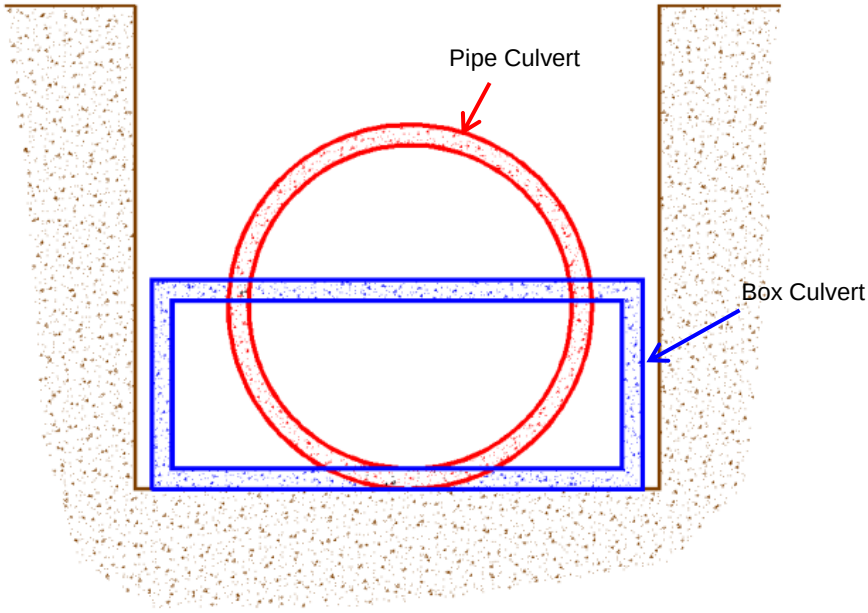

Figure 1-17 Hydraulic Head Effects in Box and Pipe Culverts

Another difference between PJ and BJ method is required jacking load in each method. Since a box culvert has more contact area with surrounding soils than an equivalent pipe culvert, the frictional force is higher in the BJ method; therefore, a higher jacking load is required to push box culverts.

Installing a box culvert underground impacts a wider area of surrounding soils and consequently has higher ground movement potential than pipe installation. Table 1-3 present a summary of differences between PJ and BJ methods.

Table 1-3 Comparison of Pipe Jacking and Box Jacking

Criteria	**Pipe Jacking (PJ)**	**Box Jacking (BJ)**
Culvert Shape	Circular	Rectangular
Jacking Frame Shape	Circular	Rectangular
Culvert Weight	Relatively Low	Relatively High
Culvert Dimensions	48 in. to 72 in.	4 ft x4 ft to 80 ft x 40 ft
Jacking Load	Relatively Low	Relatively High
Favorable Soil	Cohesive	Cohesive
Associated Ground Movement	Relatively Low	Relatively High
Excavation Method	TBM, EBPM, Hand Mining	Hand Mining, Roadheader
Hydraulic Performance	Relatively High	Relatively Low
Hydraulic Head Effect	Relatively High	Relatively Low

Ground Movements Associated with PJ, BJ, and Tunneling

Although the PJ method provides the greatest safety with regards to soil displacement and the protection of the surface compared to other trenchless technology methods, soil deformation may occur during project execution. Cautions need to be taken during construction to avoid damage to nearby structures and ground surface (Stein, 2005).

Soil deformations are divided into horizontal and vertical displacement of the soil surface or within the body of the soil. Vertical displacement in the direction of ground surface is called heaving and displacement in the opposite direction is referred as subsidence, settling or settlement (Stein, 2005). Since both PJ and BJ include bore excavation underground, settlement may occur during project execution.

Types of Settlement in BJ and PJ Methods

Settlement associated with BJ and PJ methods are dependent on site conditions and can be divided into two main categories:

1) Advanced settlement

2) Trailing settlement

Advanced settlement: Depending on jacking methods, penetration resistance may include cutting edge resistance (P_S), contact pressure force (P_A), and support pressure (P_{st}). Cutting edge resistance (P_S) is defined as a force generated during pushing the cutting edge of jacking machine into the soil. Type and position of excavating equipment greatly influence cutting edge resistance. The contact pressure force (P_A) is referred to the force generated due to pushing the excavation tool in the boring direction. The support pressure (P_{st}) is the pressure applied manually, mechanically or by compressed air at the working face to support the earth pressure and keep the soil from collapsing inside the bore. Figure 1-18 presents penetration pressure in PJ method which includes support pressure at the working face (P_{st}) and contact pressure (P_A).

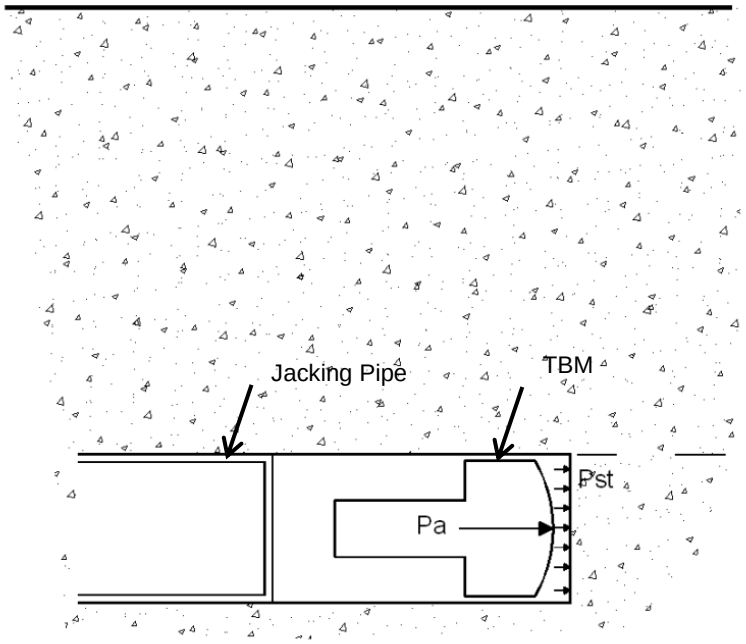

Figure 1-18 Penetration Resistance Combinations for PJ Using TBM (Stein, 2005)

Advanced settlement, as illustrated in Figure 1-19; occurs because of soil movements towards the face of the boring (working face) due to too little head pressure (P_a), too little support pressure at the working face (P_{st}), or loosening of soil as a result of excavation (Stein, 2005). As presented in Figure 1-19, advance settlement may reach the ground surface and causes surface settlement.

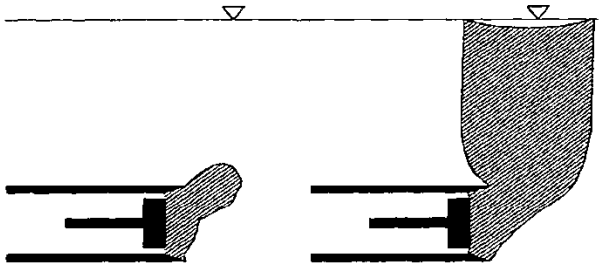

Figure 1-19 Advance Settlement in Front of Working Face (Duan, 2001)

Advance settlement can be prevented by grouting, freezing, or chemical stabilization of the soil, or use of earth-pressure balance or slurry support tunneling machines (Najafi, 2013). However, earth-pressure balance or slurry support tunneling machines cannot be used in BJ method due to the rectangular shape of the box culverts. Figure 1-20 illustrates an example of the mechanical support of work face by pressing trapezoidal flaps of steel plate against the soil with a hydraulic jack.

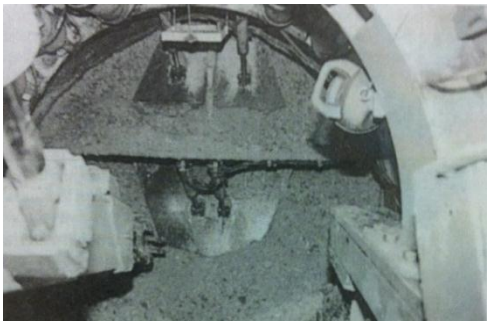

Figure 1-20 Work Face Protection by Means of Plate Flap Pressed by Hydraulic Jack (Najafi, 2014)

Trailing settlement: An overcut is required to reduce the frictional loads, and to facilitate steering of the pipe or box. The annular space due to overcut provides enough space to pump lubricators such as bentonite slurry during project execution. Soils around the pipe or box may collapse and cause subsurface and subsurface settlements. Trailing settlement occurs exactly above the jacking pipe or box segment due to collapsing of surrounding soils into the annular space, and missing or poor annular gap filling (Stein, 2005). Figure 1-21 (a and b) illustrates trailing settlement due to pipe and box installation underground respectively. As shown in Figure 1-21, installing a box culvert influences a wider area than the pipe culvert. The amount of trailing settlement depends on overcut size, shape of the culvert, soil properties and lubrication as well as grouting pressure during and after project execution. The possibility of trailing settlement can be reduced by injecting bentonite slurry into the annular space (overcut) during project execution or by grouting after project completion.

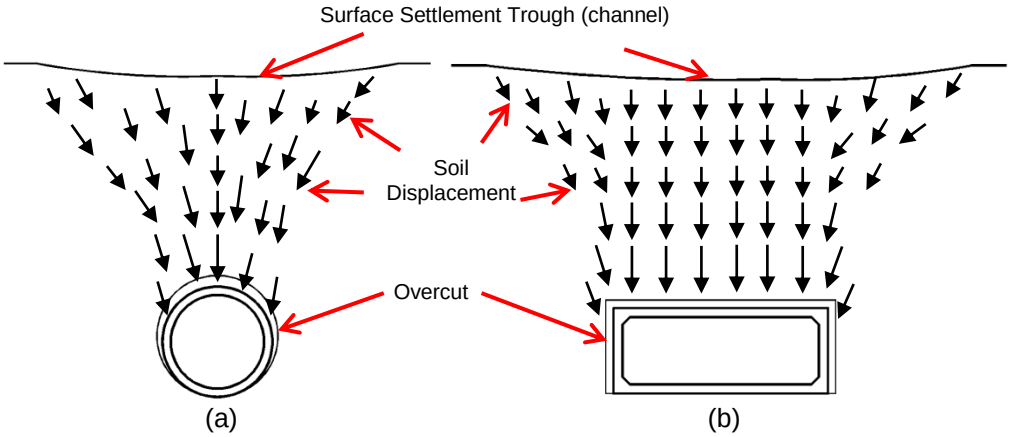

Figure 1-21 Trailing Settlement: a) Pipe Culvert, and b) Box Culvert

Settlement Trough (Channel) Associated with BJ and PJ Methods

If the soil movement reaches the ground surface, a three dimensional deformation occurs at the surface which is referred as settlement trough (channel).

Figure 1-22 shows settlement trough (channel) formation due to installation of a pipe at the depth of Z from the ground surface. Figure 1-22 implies that the settlement is formed as the pipe is advancing inside the bore and surrounding soils collapse into the overcut area. The maximum surface settlement (S_{max}) occurs exactly at the top of the advance pipe and the settlement magnitude decrease away from the centerline until it reaches zero (Stein, 2005).

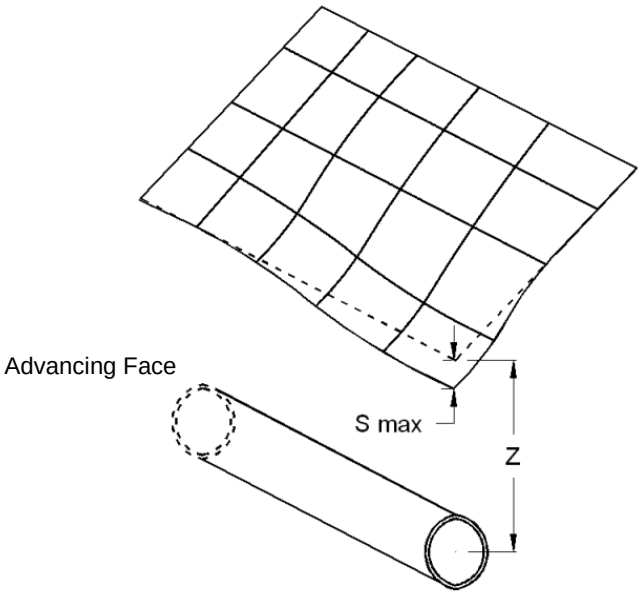

Figure 1-22 3D Surface Settlement Trough (Channel) due to Pipe Installation

(Stein, 2005)

Similar to pipe installation, underground box installation requires overcut around the box culvert. However, a wider overcut is needed in BJ method compared to PJ method due to rectangular shape of box culverts. Therefore, a wider area of surrounding soils may collapse into the annular space. Settlement trough (channel) volume in the BJ method is greater than the volume induced by the PJ method. The maximum surface settlement (S_{max}) happens at the top of the box culvert and the magnitude of settlement decreases slightly away from the center of the box culvert as illustrated in Figure 1-23.

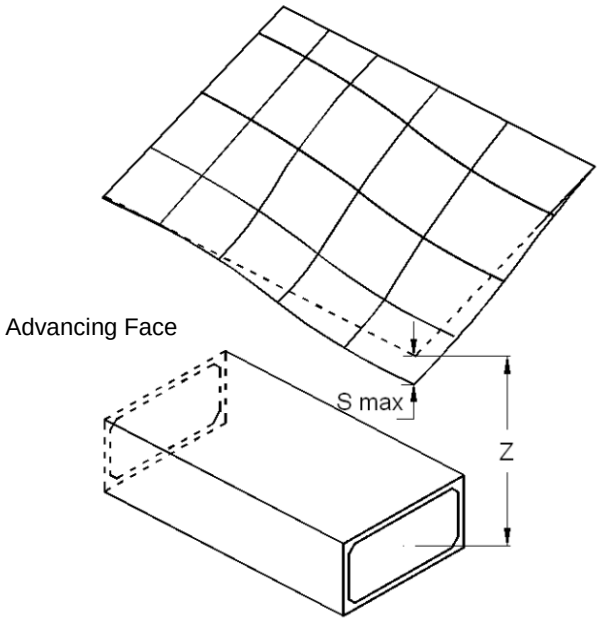

Figure 1-23 3D Settlement Trough (Channel) due to box Installation

The size and shape of the settlement trough (channel) are influenced by:

1) Operational limiting conditions: Includes lubrication process, grouting of the annular space, and the type of working face.
2) Geometric limiting conditions: Includes pipe/ box dimensions, and depth of pipe/ box from ground surface.
3) Geotechnical limiting conditions: Includes type of soil, soil properties such as unit weight, cohesion, modulus of elasticity, etc. (Stein, 2005)

It is important to identify any existing surface and subsurface facilities or infrastructures such as buildings, highways, railroads, underground utilities, piles, and piers to be able to evaluate the risk of settlements due to new trenchless pipe/box installation. Once the existing facilities and infrastructures are identified, the maximum allowable settlement for each feature should be determined. Table 1-4 presents maximum allowable settlements suggested by Wallin et al in 2008.

Table 1-4 Suggested Maximum Allowable Settlements of Site Features

(Wallin et al., 2008)

Site Feature	**Allowable Settlement mm (in.)**
Underground Utilities	25.4 (1)
Surface Streets	12.7-25.4 (0.5 to 1)
State Highway and Interstate Highways	6.35-12.7 (0.25 to 0.5)
Lined Canal Bottoms	6.35-12.7 (0.25 to 0.5)
Levee Crests	12.7-25.4 (0.5 to 1)
Railroads	6.35-12.7 (0.25 to 0.5)

According to pavement design guide published by TxDOT (2011), one inch settlement is the maximum allowable settlement in highways. However, this criterion is stricter when a pipe or box is installed under railroads. This is because railroads are more sensitive to surface settlement than highways. Moreover, the maximum allowable may change depending on type of pavement (e.g., flexible and rigid).

Arching Effect

Arching is described as force transfers between a yielding mass of soil and adjacent fixed structure, which results in stress redistribution in the body of the soil. The shearing stress prevents the yielding mass of soil from deformation resulting in a pressure change on both of the yielding mass's support and the adjacent part of soil (Terzaghi, 1943). Arching is divided into two main categories depending on relative stiffness of soil mass and buried structure

1. Active
2. Passive

If the soil mass is less compressible than the buried structure, active arching will occur as presented in Figure 1-24. Active arching decreases stress on top of a buried structure compared to adjacent soil (Tien, 1990).

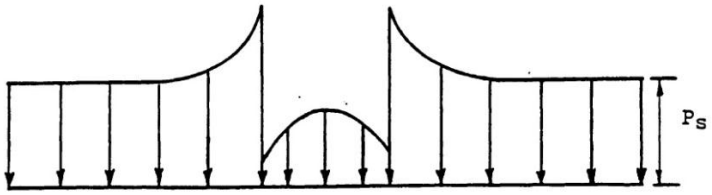

Figure 1-24 Stress Distribution on Top of a Buried Structure

in Active Arching (Evans, 1984)

The shear resistance appears upward in active arching to reduce stress at the base of the yielding part as presented in Figure 1-25. Figure 1-25 shows stress redistribution due to yielding a support with length of 2L on top of buried structure and applied pressure of P (Tien, 1990).

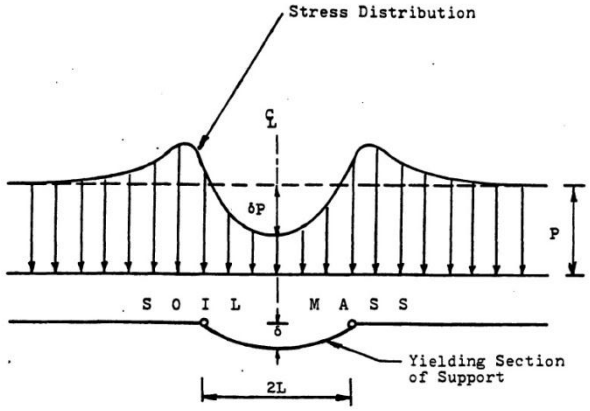

Figure 1-25 Stress Distribution in the Soil above a Yielding Base (Tien, 1990)

Passive arching occurs when the buried structure is stiffer than the surrounding soil. This causes stresses to increase on the buried structure and decrease in adjacent soil. The shear resistance appears downward in passive arching to block its movement and results in stress increase at the base of the yielding part. Determining arching effects play an important role in the development of soil load on buried structures (Tien, 1990). Figure 1-26 illustrates stress distribution in passive arching.

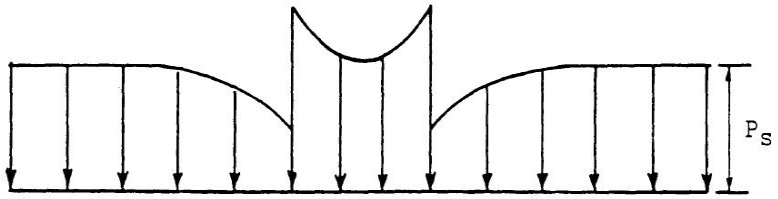

Figure 1-26 Stress Distribution on Top of a Buried Structure

in Passive Arching (Evans, 1984)

Terzaghi's Theory (Terzaghi, 1943)

Terzaghi conducted an experiment in 1936 to study arching effects. The experiment included a trap door with width of 2B mounted in a box with height h filled with dry sand. Figure 1-27 shows Terzaghi's trap door experiment and results with door movements for 0%, 1%, 2%, 3%, and 4% of the door width and associated measured stresses. The total load on the door and its displacement were monitored while the door was opened (Tien, 1990).

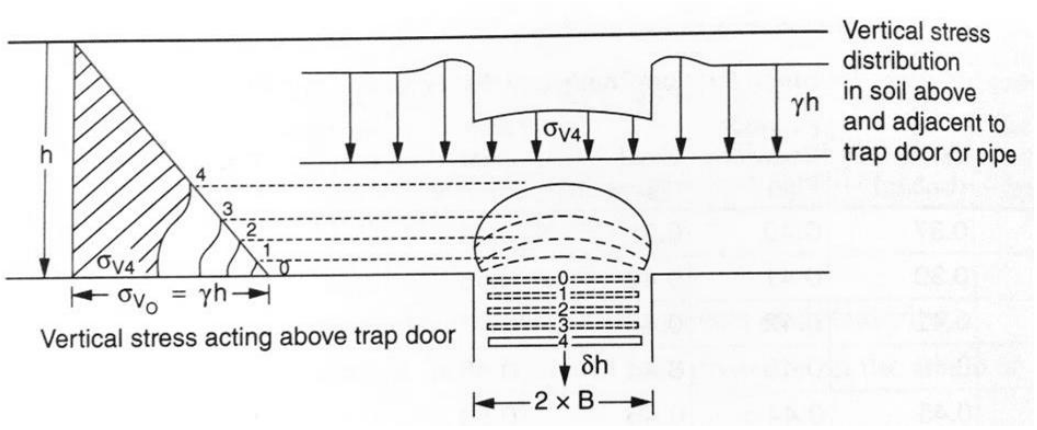

Figure 1-27 Terzaghi's Trap Door Experiment (Najafi, 2013)

Terzaghi found that the large decreases happened in vertical stress for very small trap door displacement. Terzaghi explained this fact as the arching effect creation on top of the trap door. He assumed that the sliding face was vertical, and therefore, the pressure of a yielding strip was the difference between the weight of the sand located at

the top of the strip and the shear resistance along the vertical sections. Figure 1-28 presents a free body diagram of yielding strip at the depth of H from ground surface (Evans, 1984).

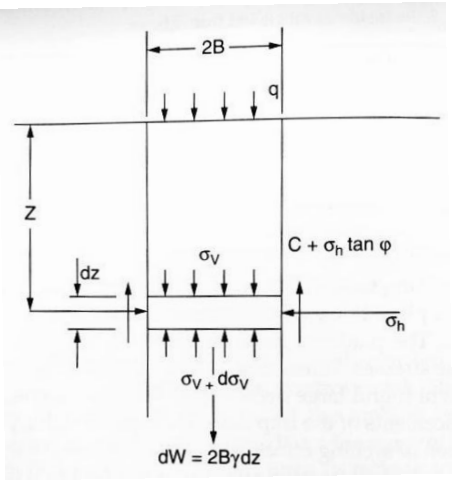

Figure 1-28 Free Body Diagram of a Yielding Strip (Najafi, 2013)

Terzaghi suggested Equation 1-1 to determine vertical stress in the soil above the yielding strip.

$$\sigma_v = \frac{B(\gamma - {}^{C}/_{B})}{K.\tan\phi}.(1 - e^{-\frac{k.\mathrm{H}.\tan\phi}{B}}) \qquad \text{Equation 1-1}$$

where:

B = Half width of opening (m)

H = Opening depth from ground surface (m)

γ = Soil Unit weight (kN/m^3)

c = Soil cohesion (kN/m^2)

ϕ = Soil friction angle (degree)

K = Lateral pressure coefficient (generally is 1-sin ϕ)

His investigations showed that the arching effect extended to a height of 5B. Therefore, the stress state did not change beyond 5B above the yielding strip.

Terzaghi extended his findings to tunnel design and realized that the stress state above a tunnel is similar to stress state above a yielding strip. He assumed that the adjacent soils to the tunnel yields toward the tunnel during construction and create an active pressure condition with inclined yielding boundary at about (45° + ϕ/2) (Tien, 1990). Figure 1-29 illustrates soil movements due to tunneling.

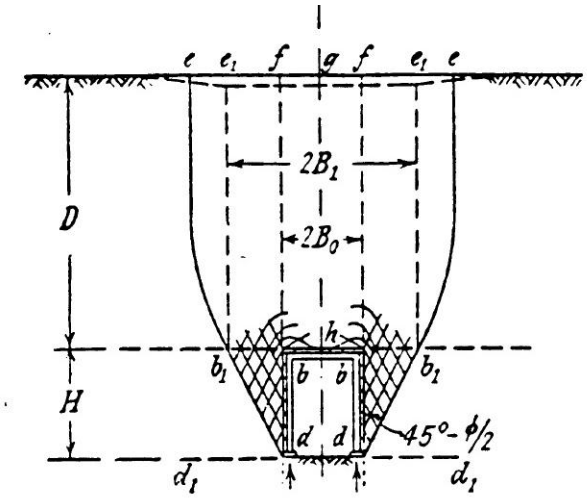

Figure 1-29 Soil Movements during Tunnel Construction (Tien, 1990)

The width of yielding strip ($2B_1$) at top of a rectangular tunnel is:

$$2B_1 = 2[B_0 + H.\tan\left(45 - \frac{\phi}{2}\right)] \qquad \text{Equation 1-2}$$

where:

$2B_0$ = Width of the tunnel

Therefore, if the tunnel is located at the depth of H from the ground surface, Equation 1-1 can be rewritten as follows:

$$\sigma_v = \frac{B_1\left(\gamma - {}^{c}/_{B_1}\right)}{K.\tan\phi}.\left(1 - e^{-\frac{k.\mathrm{H}.\tan\phi}{B_1}}\right) \qquad \text{Equation 1-3}$$

Marston's Theory (Marston, 1930)

In 1930, Marston developed a theory to explain soil characteristics above a buried structure such as a conduit. He found that the soil load does not fully act on a buried conduit because the load is transferred to adjacent soil due to arching effect. Buried conduits were categorized based on their installation procedure in Marston's theory as follows:

1. Conduits installed in an excavated trench below the ground surface (trench conduit) as presented in Figure 1-30 a.
2. Conduits installed above the ground surface where an embankment is subsequently placed on top of it as presented in Figure 1-30 b.

If the top of the conduit is above the ground surface it is referred as positive project conduit as illustrated in Figure 1-30 b. If the conduit is placed in a shallow trench and its top is below ground surface, it is referred as negative project conduit as presented in Figure 1-30 c.

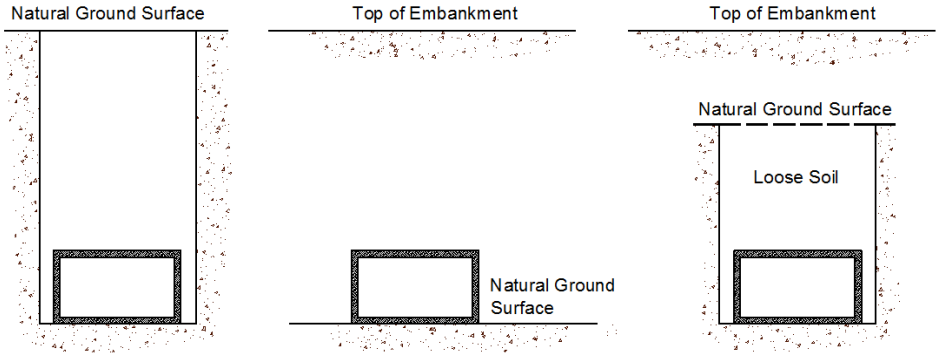

Figure 1-30 Types of Conduit Installations: a) Trench Conduit, b) Positive Project Conduit, and c) Negative Project Conduit (Adapted from Marston, 1930)

In the case of a negative project conduit, the load of soil prism above the buried conduit is reduced due to arching affect which is favorable (Figure 1-31 a). On the

contrary, in a positive project conduit, the arching effect is inverted and causes the load to significantly become greater than the weight of overlying soil prism as presented in Figure 1-31 b.

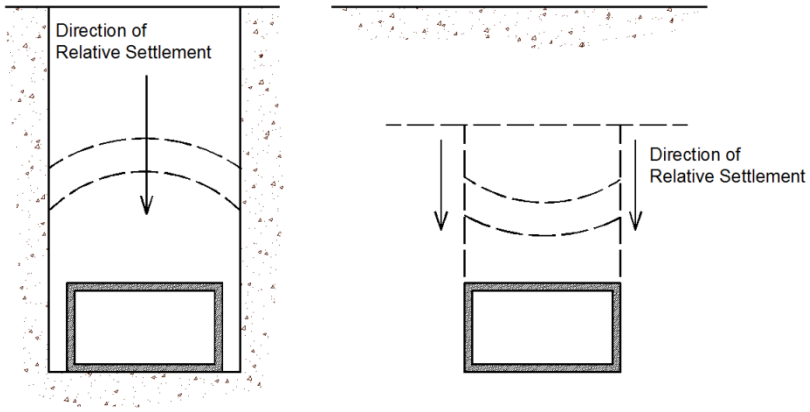

(a) (b)

Figure 1-31 Arching Effects in Buried Conduits: a) Favorable Arch Action, and b) Inverted Arch Action (Adapted from Spangler and Handy, 1984)

For type 1 conduits, trench conduits, Marston suggested Equation 1-4 to calculate the load on the conduit (W_c) where the conduit is stiffer than the surrounding soils.

$W_c = C_d \cdot \gamma \cdot B_d^2$ Equation 1-4

where:

$C_d = \frac{1-e^{-2K\mu'(H/B_d)}}{2K\mu'}$

K = Lateral stress coefficient (generally, Rankine's active ratio is applied: $K = \tan^2(45-\phi/2)$

μ' = Coefficient of friction between fill material and sides of trench ($\mu' = \tan \phi'$)

H = Depth of the conduit from ground surface to the top of it

B_d = Trench width at top of the conduit

γ = Soil unit weight (kN/m^3)

If the surrounding soil is stiffer than the buried conduit (e.g., flexible pipe), Equation 1-4 should be multiplied by the ratio B_c/B_d, where B_c is the outside width of the conduit. Therefore, the load on the flexible conduit is as follows:

$$W_c = C_d \cdot \gamma \cdot B_c \cdot B_d \qquad \text{Equation 1-5}$$

In positive project conduits, where the conduit is placed on top of ground surface, the magnitude and directions of relative displacements between the interior soil prism and the adjacent exterior prisms are affected by the settlement of the conduits and the surrounding soils. Marston suggested Equation 1-6 by combining different settlements into an abstract ratio, called the settlement ratio.

$$r_{sd} = \frac{(s_m + s_g) - (s_f + d_c)}{s_m} \qquad \text{Equation 1-6}$$

where:

r_{sd} = Settlement ratio

s_m = Compression strain of the side columns of soil with height of pB_c

p = Projection ratio

pB_c = Depth of conduit from embankment surface to top of the conduit

B_c = Width of the conduit

s_g = Natural ground surface settlement

s_f = Conduit settlement into its foundation

d_c = Vertical height of the conduit shortening

Marston suggested Equation 1-7 to calculate load on the conduits in positive projects.

$$W_c = C_c \cdot \gamma \cdot B_c^2 \qquad \text{Equation 1-7}$$

where:

$$C_c = \frac{e^{-2K\mu(H/B_c)}-1}{2K\mu}$$

μ = Coefficient of friction of embankment material (μ = tan ϕ)

Marston suggested imperfect ditch (trench) conduits to reduce the load on the conduit under the positive project. Imperfect ditch conduit, as presented in Figure 1-32, is first installed as a positive project conduit. Then, the embankment soil is placed and compacted up to a specific elevation above the conduit. Next, a trench is excavated above the conduit with the same width of the conduit and filled with very loose, compressible material such as sand. This procedure causes more settlements to occur in the interior soil prism than in the exterior prism and consequently generate upward friction force on the sides of the interior prisms and reduces load on the buried conduit.

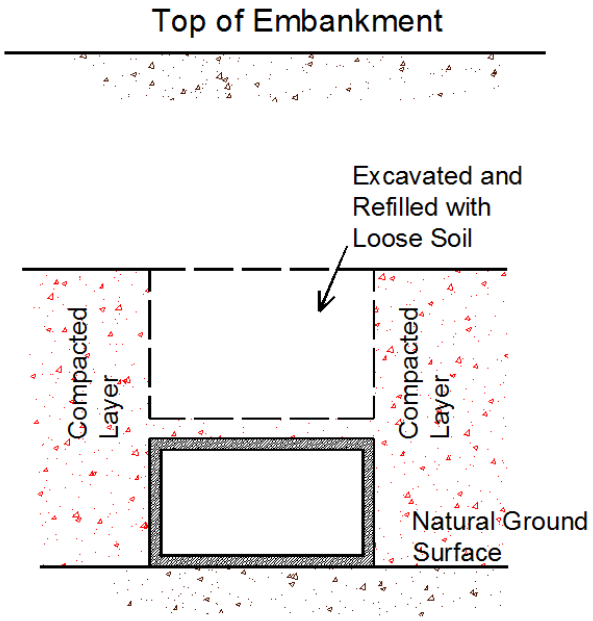

Figure 1-32 Imperfect Ditch Conduit (Adapted from Spangler and Handy, 1984)

The load on the imperfect ditch conduit is as follows:

$W_c = C_n \cdot \gamma \cdot B_c^2$ Equation 1-8

where:

C_n = Load coefficient which depends on height of the fill to the width of ditch ratio (H/B_c), the projection ratio p', and the settlement ratio r_{sd}.

Research Needs

The TT industry has radically changed and improved in the past 30 years providing better methods to install pipes, boxes, and utilities underground with less total cost and less disruption to the existing infrastructures. The BJ method is one of the trenchless technology methods to install box culverts under highways and railroads. Installing box culverts underground, like other trenchless methods, may cause surface settlement and consequently damage existing road pavement or railroad beds. As a result, the need to better understand ground movements induced by the BJ process is important to project completion without causing damage to adjacent infrastructures and facilities.

Several research studies and investigations such as Milligan and Marshall (1995), Bennett (1998), Rogers and O'Reilly (1991), and Liu and Lu (2012) have been conducted to study surface and subsurface ground movements due to pipe jacking or tunneling. Although some aspects of the BJ method are similar to the PJ method, there are significant differences between these two methods. It is noted that no research is performed to analyze ground movements associated with the BJ method. Therefore, there is a need to study ground movements associated with BJ.

Scope and Limitations

This research is focused on trailing settlement in BJ projects due to lack of collected data for advanced settlement from case studies. Moreover, 2D modeling which was adapted in this research could not simulate advanced settlementIt in BJ project since

it required 3D modeling. It was assumed that advance settlement can be controlled using available techniques such as freezing, grouting, and chemical stabilization. Since cohesive soils are the most favorable soils in the BJ method, sandy soils with small amount of cohesions was considered for use in this research. Table 1-5 shows the minimum and maximum range of soil properties considered herein. Soil properties listed in Table 1-5 are derived using Standard Penetration Test (SPT) relationships with modulus of elasticity (E), friction angle (ϕ), and unit weight (γ). Since there is no relation between SPT value and cohesion, a range of cohesion from 0 to 24 kPa (0 to 3.5 psi) is considered for soils in this study.

Table 1-5 Minimum and Maximum Soil Properties Considered in the Research

Property	Modulus of Elasticity, MPa (psi)	Friction Angle (Degree)	Cohesion, kPa (psi)	Unit Weight, kN/m^3 (lb/ft^3)
Min	9 (1,305)	30	0 (0)	14 (89.1)
Max	32 (4,640)	40	24 (3.5)	20 (127.3)

In this research, six groups of box culverts, as presented in Table 1-6, are considered. Box sizes are selected based on standard dimensions provided by manufactures catalogs. More detail about available box sizes is presented in Appendix A.

Table 1-6 Considered Box Dimensions

No.	Width (Span), m (ft)	Height (Rise), m (ft)
1	1.8 (6)	1.2 (4)
2	1.8 (6)	1.8 (6)
3	2.4 (8)	1.2 (4)
4	2.4 (8)	2.4 (8)
5	3 (10)	1.5 (5)
6	3 (10)	3 (10)

To analyze the effect of box depth from ground surface to top of the box culvert on a surface settlement, different box depths ranging from 2h, 3h, 4h, 5h and 6h, where h is the height of the box, were considered. Installing box culverts at a depth of less than h

is either not economical compared with open-cut method or requires special caution since it may causes large surface settlement. Since the depths of box culverts from surface are less than five times that of the yielding strip width (B_1), arching effect extends to the ground surface and is, therefore, considered in this study.

Since an overcut size of 1 to 2 in. (25 to 50 mm) is required to install box culverts, the overcut sizes of 30 mm (1.18 in.), 40 mm (1.57 in.), and 50 mm (1.97 in.) were used in this research.

This research incorporates two BJ projects to validate results obtained through BJ simulation. First BJ project was located in Vernon, near Wichita Falls, Texas. The project scope was about jacking of a new 1.8 m x 1.2 m (6 ft x 4 ft) box culvert through the ground. Subsurface and surface displacements were recorded during and after project execution.

The second BJ project was located in Navarro County, TX. The scope of the project was to install 2.7 m x 1.2 m (9 ft x 4 ft) under a railroad at the depth of 1.8 m (6 ft) from the surface to the top of the box culvert. Surface displacement was collected at 15 points to assure the railroad was not settled.

These two projects provided a good opportunity for a thorough study on ground movement of BJ operation with boxes.

Objectives

The main objective of this research was to develop a surface displacement prediction model using Artificial Neural Network (ANN). The final model may assist municipal agencies, consultants, and contractors to reduce the risk involved in box installation under existing facilities such as highways and railroads by predicting final surface displacement under different circumstances (e.g., site condition, box size, and depth of box from surface).

Secondary objectives of this research included:

1. Studying the effect of soil properties, depth of box from ground surface and box dimension variations on surface vertical displacement.
2. Studying arching effect in BJ projects.
3. Studying the applicability of available empirical methods, originally developed for pipe jacking and tunneling, for BJ projects.

The final model in this research will provide information to answer to the following questions:

1. What is the associated risk in a BJ project?
2. Will the surface displacement (settlement) damage the existing pavement?
3. Which parameters can be changed to prevent excessive surface displacement (settlement) and meet project requirements at the same time?
4. Are available experimental methods, originally developed for pipe jacking and tunneling, able to predict surface vertical displacement associated with BJ projects?
5. Does arching occur at top of rectangular box culverts? If so, are available theories (e.g., Terzaghi and Marston), originally developed for circular sections, able to predict effective stress at top of box culvert accurately?

Hypothesis

In this research, it is assumed that the conventional empirical methods, originally developed for PJ and tunneling, are not applicable for BJ and that the current suggested error function based on Gaussian normal distribution is not able to represent surface vertical displacement associated with BJ projects.

Different methods are available to estimate surface vertical displacement due to PJ and tunneling projects and numerical method is one of the methods used to analyze

ground movements in this type of projects. Finite Element Modeling (FEM) is widely used to simulate field projects and obtain results in terms of surface displacement. However, in most research papers, a specific project condition is modeled and results cannot be extended to any other project conditions.

Different methods are available to analyze the relationships between inputs and outputs and develop predictive models such as regression analysis, and Artificial Neural Network (ANN).

In this research, it is assumed that a predictive ANN model can be developed and trained using results obtained from numerical analysis (e.g., FEM) and be used to estimate surface settlement in BJ projects. Combining FEM with ANN enhances its capabilities to be applicable for different types of project conditions within considered assumptions.

Methodology

This dissertation starts with a review of different trenchless technology methods focusing on the BJ method and continuing with a comprehensive literature search on ground movements due to PJ and tunneling using various research databases such as Engineering Village, and the American Society of Civil Engineers (ASCE) publications. A research on FEM by PLAXIS 2D and ANN was conducted. Scenarios were simulated in PLAXIS 2D and the results were recorded. ANN code was written in MATLAB program and the network was trained by inputs and results obtained from PLAXIS 2D.

New finite element models were generated by PLAXIS 2D, and results were compared with results calculated with the trained ANN model. Next, collected data from field projects were used as validation tools to assure that the trained ANN model was in good agreement with real projects. Meanwhile, a null scenario was generated in PLAXIS 2D to conduct a sensitivity analysis and evaluate the effect of previously mentioned

parameters on the surface vertical displacement. Stress redistribution due to arching effect at the top of box culverts was studied. Conclusions and recommendations are presented at the end. Figure 1-33 presents s methodology flow chart.

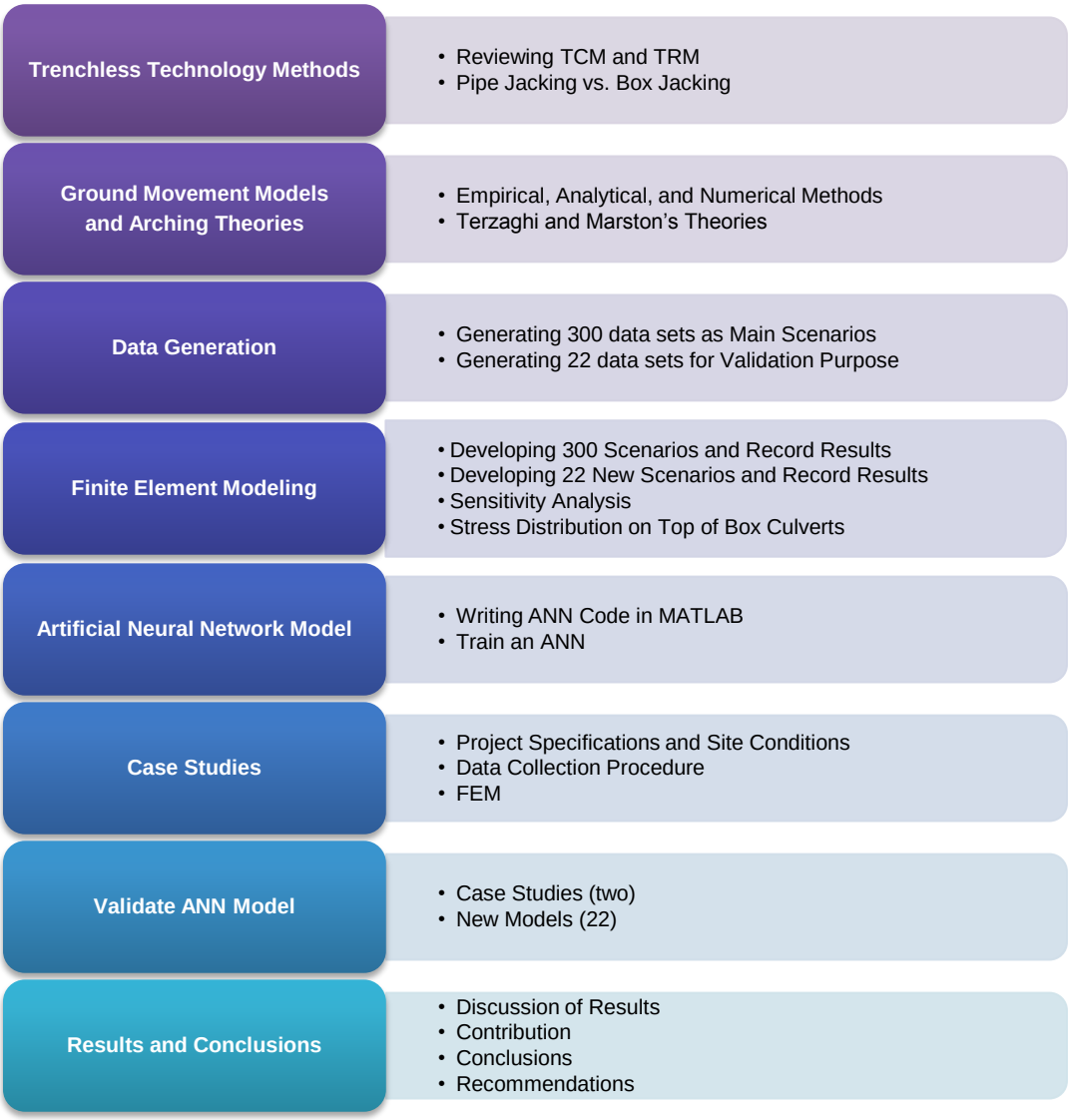

Figure 1-33 Methodology Flowchart

Dissertation Organization

This dissertation includes five chapters following Chapter 1 (Introduction) as listed below:

Chapter 2 consists of a comprehensive literature review on available methods to estimate surface/subsurface ground movements due to pipe jacking and tunneling.

Chapter 3 presents adopted methodology and includes case studies considered in this research. Also, a review of finite element modeling software, PLAXIS 2D, and Artificial Neural Network (ANN) are presented.

Chapter 4 describes case studies specifications, data collection procedure and collected field data. Results from this chapter are used for verification purposes.

Chapter 5 presents the results obtained from literature search, case studies, PLAXIS 2D and ANN. Comparison of results in terms of surface vertical displacement is included in this chapter. Moreover, case study simulation results obtained by the PLAXIS 2D and ANN model are compared with collected data from the field project.

Chapter 6 provides conclusions and recommendations for future work.

Chapter Summary

This chapter presented an introduction to open-cut and trenchless technology methods and discussed pipe jacking and box jacking (BJ) methods and delineated their differences. Ground movements associated with PJ, BJ and tunneling were discussed, and available theories for arching effects were presented. This research's main goal, objectives, scope of the research, and a brief methodology description were also presented in this chapter.

Chapter 2

Fundamental Concepts and Literature Review

Introduction

Trenchless Technologies (TTs) are methods used to install or renew pipelines, such as oil and gas pipelines, water distribution and sewer collection systems and are used when other conventional methods, such as open-cut methods are not applicable. Also, TT methods have other advantages compared to conventional open-cut method, such as lower cost per foot of installed pipe, lower environmental impacts and lower social costs (Najafi, 2013). These advantages make TTs a popular choice for installation and renewal of pipes and utilities especially in urban areas where blocking traffic flow result in high social costs. However, TT methods have some disadvantages such a decreased flow capacity in renewal TT methods, a higher level of engineering skills are required and grade or alignment corrections can be difficult (Piehl, 2005).

In TT method when a bore or tunnel is excavated, the ground around the bore or tunnel moves towards the excavated area and may cause damage to nearby structures and public lifeline facilities. Therefore, ground movements should be studied along with the magnitude of soil movement and their effect should be evaluated in pipe/box jacking projects (Lee et al. 2004).

Trenchless Technology Methods

Trenchless Methods are divided into two main areas:

1) Trenchless construction methods (TCM).
2) Trenchless renewal methods (TRM).

TCM include methods used to install new pipes or utilities such as pipe jacking (PJ) and horizontal directional drilling (HDD). TRM refers to methods that are used to

repair, renew or renovate an existing pipeline such as close-fit pipe (Najafi and Gokhale, 2005). Figure 2-1 shows different types of trenchless technology methods.

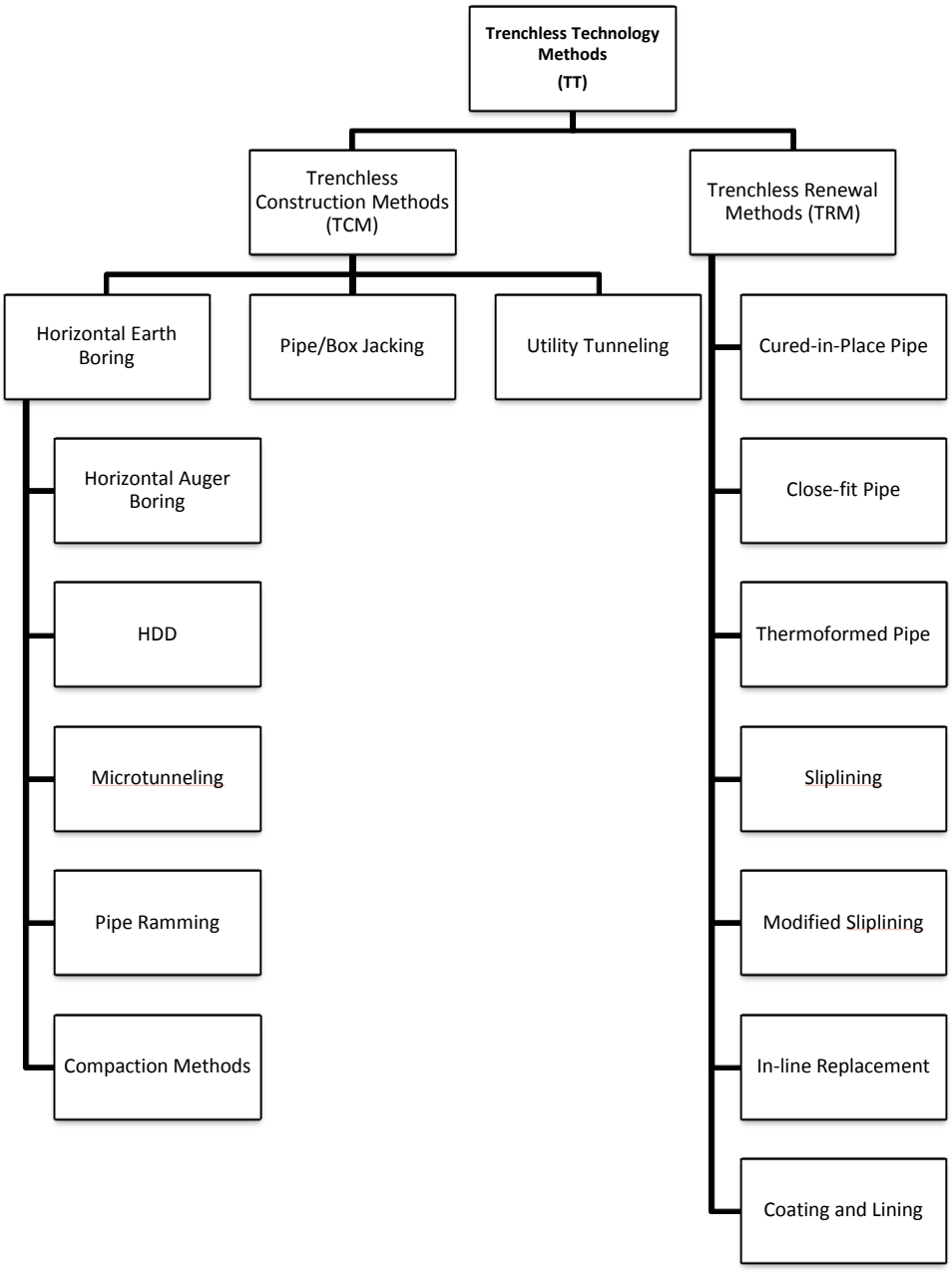

Figure 2-1 Trenchless Technology Methods (Najafi & Gokhale, 2005)

As presented in Figure 2-1, TCM methods are divided into three main categories:

1. Horizontal earth boring (HEA)
2. Pipe/box jacking (PJ/BJ)
3. Utility tunneling (UT)

Horizontal Earth Boring

Workers do not need to enter inside the bore in horizontal earth boring method and small size pipes can be installed using this method. Horizontal earth boring consists of five main methods: 1) Horizontal auger boring (HAB), 2) Horizontal Directional Drilling (HDD), 3) Microtunneling (MT), 4) pipe ramming, and 5) compaction methods.

Horizontal Auger Boring (HAB)

Horizontal auger boring (HAB) is a technique that is widely used to install steel pipes and casing under railway beds, road embankments, airport taxiways, etc. A rotating auger which is connected to a cutting head inside the steel casing is used to excavate bore hole and haul spoils out of the casing (Najafi, 2013).

Horizontal Directional Drilling (HDD)

Horizontal directional drilling (HDD) is a steerable system for the installation of pipes, conduits, and cables in an arc shape using a surface launched drilling rig. This method requires the execution of a pilot bore which is then enlarged with the use of a reamer prior to installation of the product pipe. Depending on the diameter of the product pipe, multiple enlargements may be required. The excavation is performed by fluid assisted mechanical action of a cutterhead (Najafi, 2013).

Microtunneling (MT)

Microtunneling (MT) is used to install pipe with an accuracy of $\pm$1 inch (25.4 mm) in both the horizontal and vertical alignments. The most common types of underground infrastructure systems installed by microtunneling are gravity sanitary sewers and storm

sewer. The spoil removal system for microtunneling can be a slurry transportation system or a small encased helical auger conveyor system. Different spoil removal systems categorized microtunneling into slurry microtunneling and auger microtunneling. Microtunneling methods are applicable to all types of soils and can achieve a large variety of depths (up to about 160 ft (48.8 m) below ground) either above or below the groundwater table (Najafi, 2013).

Pipe Ramming

Pipe ramming is a technique for installing steel casing from a drive shaft to a reception shaft utilizing the dynamic energy from a percussion hammer attached to the end of a pipe. In this method, the tool does not create a borehole; rather, it acts as a hammer to drive the pipe through the soil. The pipe can be used for water, sewer, electric, gas, or any other utility (Table 1), and, it can be installed under roads, highways, railroads, rivers, etc. A continuous casing support is provided by the pipe and over-excavation is not required. The pipe can be driven either by having the leading end of the pipe in a wedge or cone shape or by having the leading end of the pipe open. The wedge or cone shaped end can be used for pipes up to 203 mm (8 in.) in diameter. For pipes larger than 203 mm (8 in.), the leading end is usually left open. In this case a band is installed around the outside edge of the leading section when the pipe face is left open. This serves a dual purpose: (1) it reinforces the leading edge; (2) it decreases the friction around the casing. Open-faced pipe ramming is a 2-stage process, where the pipe is hammered open face inside the soil and then the spoil is pushed out. Figure 5 illustrates a schematic of the open-faced PR operation (Najafi, 2013).

Utility Tunneling (UT)

Utility tunneling (UT) is another TT method used to install new pipe or utilities underground. The UT procedure is the same as PJ method except temporary supports

are needed in this method. Pipe jacking is a one-step operation where pipe is installed while soil is excavated. Utility tunneling, on the other hand, is a two-step operation, where soil is excavated, a liner is installed, and then the pipe is transported inside the tunnel. The liner can be special steel or concrete liner plates, wood box tunnels, or steel rib and wood lagging systems.

Pipe Jacking (PJ) and Box Jacking (BJ)

Both PJ and BJ methods are previously discussed in Chapter 1.

Ground Movement Analysis

Methods of Calculations

So many research papers and investigations have been conducted and this section presents a summary of literature and research regarding ground movement of the free-field soils mass due to trenchless construction. Three main methods are recognized for modeling and estimating the free-field ground movements listed below:

1. Empirical methods
2. Analytical methods
3. Numerical methods

Empirical Methods

Empirical methods are based on mathematical relationships between measured values from previous projects. Regression analysis is widely used in empirical methods to find the relationships between project specifications such as pipe diameter, depth of pipe and soil properties and estimate soil deformation.

Scherle (1977) conducted a research to estimate surface settlement due to pipe jacking. He suggested that loss of soil due to jacking and the overcut were two main causes for settlement. Scherle idealized surface settlement by a trapezoidal with respect to the existing conditions and developed his results. He considered a pipe with diameter

d_a located at the depth of h from the ground surface and assumed that the width of the settlement trough (channel) is d_a + 2 (h/2).

Figure 2-2 illustrated surface settlement idealization suggested by Scherle (1977).

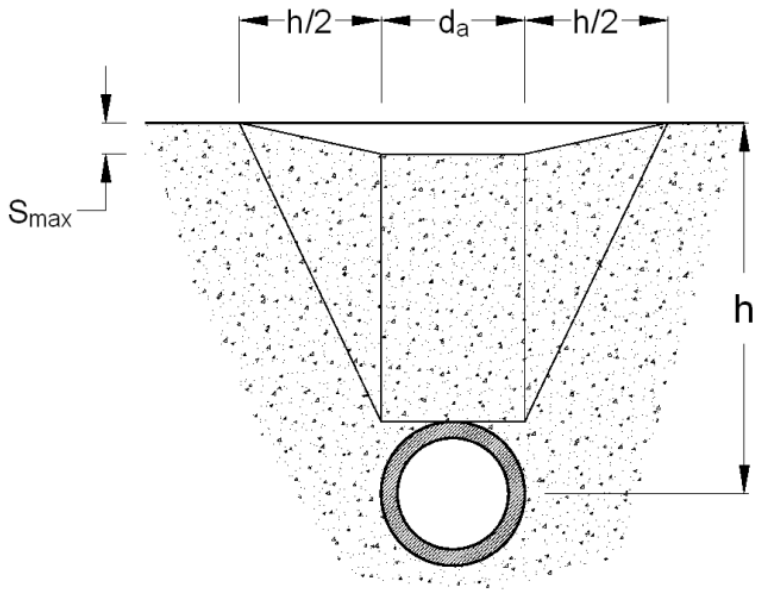

Figure 2-2 Surface Settlement Approximation by Trapezoidal Shape (Sherle, 1977)

Sherle (1977) suggested that the maximum surface settlement can be calculated by Equation 2-1.

$$S_{max} = \frac{d_a}{1+\frac{h}{2d_a}} . B_k \qquad \text{Equation 2-1}$$

where

S_{max} = Maximum surface settlement at pipe centerline (mm)

d_a = Outer diameter of the pipe (m)

h = Depth of the pipe from ground surface to top of the pipe (m)

B_k = Soil index

B_k is a dimensionless index which was depended on the type of soils and soil density as presented in Table 2-1.

Table 2-1 Soil Index, B_k (Scherle, 1977)

Soil Type	**Non-cohesive soils**				**Cohesive soils**			
Density	Very Dense	Dense	Loos	Very Loos	Stiff	Firm	Soft	Very Soft
B_k	1.5	2	3	4	2	3	4	6

O'Reilly and New (1982) determined that trapezoidal idealization cannot accurately estimate surface settlement. Sherle's method was not developed to estimate ground movement associated with BJ. Moreover, the effect of soil properties such as modulus of elasticity (E), and friction angel were ignored in determining soil index and surface settlement.

Martos (1958) suggested an error function curve, Equation 2.2, based on a statistical evaluation of field observation of settlement above tabular mine openings. The equation was suggested to estimate the shape of the settlement trough (channel) above a tunnel. It was assumed that the settlement trough (channel) shape can be represented by a dimensionless Gaussian normal distribution function.

$$S_z(y) = S_{max}.e^{\left(-\frac{y^2}{2.i_z^2}\right)}$$ Equation 2-2

where:

S_z (y) = Vertical displacement as a function of z

S_{max} = Maximum settlement at the tunnel centerline (y=0)

y = Horizontal distance from tunnel centerline

z = Depth of the interest point from the surface

i_z = Horizontal distance of the inflection point of the settlement trough (channel) from the pipe/tunnel centerline as a function of z

Figure 2-3 shows the Gaussian normal distribution function and its dependency on depth of tunnel from the surface. As illustrated in Figure 2-3, maximum settlement (S_{max}) occurs exactly at the top of the opening and settlement magnitude decreases away from opening centerline. Moreover, inflection point distance forms opening (e.g., pipe/tunnel) centerline (i) increases as moving toward the ground surface.

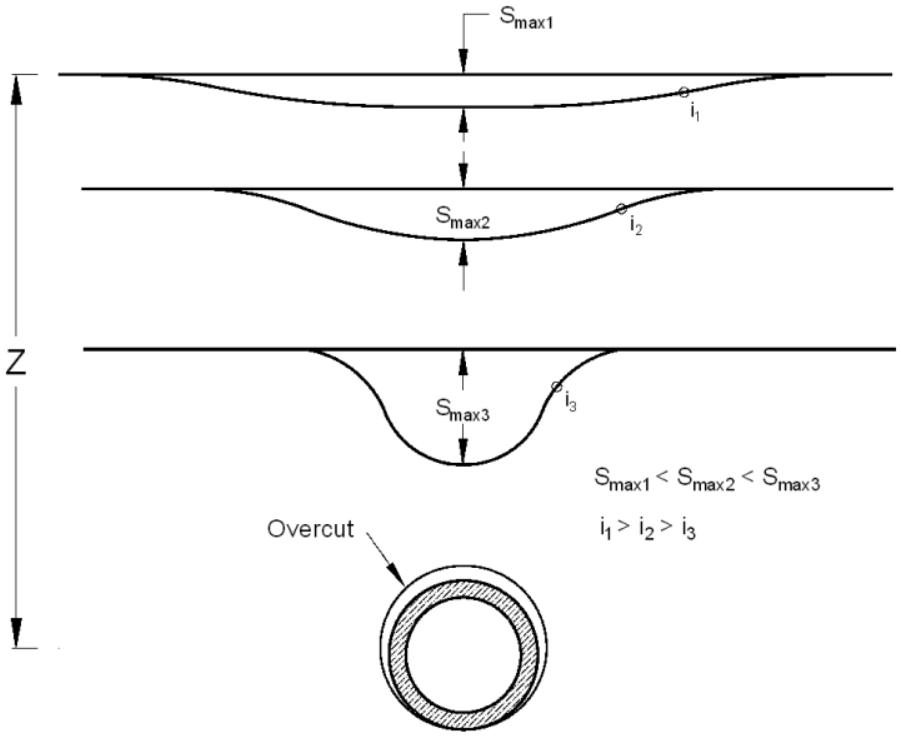

Figure 2-3 Error Function Curve in Different Depth (Schmidt, 1969)

Schmidt (1969) and Peck (1969) showed that the error function curve can model the shape of the settlement trough (channel) caused by tunneling in soft soil. If only surface ground deformation is considered, Equation 2-2 can be simplified as Equation 2.3.

$$S(y) = S_{max}.e^{\left(-\frac{y^2}{2i^2}\right)} \qquad \text{Equation 2-3}$$

Therefore, the ground slope and curvature can be derived by integration of Equation 2-3 which is shown in Equation 2-4 below.

$$V_s = \int_{-\infty}^{\infty} S.dy = \int_{-\infty}^{\infty} S_{max}.\exp\left(-\frac{y^2}{2i^2}\right).dy = \sqrt{2\pi} i S_{max} \approx 2.5i.S_{max}$$ Equation 2-4

where V_s is the volume of surface settlement. Equation 2-3 can be rewritten by substituting S_{max}.

$$S(y) = \frac{V_s}{2.5i}.e^{\left(-\frac{y^2}{2i^2}\right)}$$ Equation 2-5

Then the slope of the settlement at surface can be derived by differentiating of Equation 2-5 which is presented in Equation 2-6.

$$\frac{ds}{dy} = \frac{-V_s y}{2.5i} e^{\left(-\frac{y^2}{2i^2}\right)} = 0.606\ \frac{S_{max}}{i}$$ Equation 2-6

and the second differentiation leads to the approximate curvature.

$$\frac{d^2S}{dy^2} = \frac{V_s}{2.5i^3}.\left[\frac{y^2}{i^2} - 1\right].e^{\left(-\frac{y^2}{2i^2}\right)}$$ Equation 2-7

Figure 2-4 shows form and principal features of settlement trough (channel) using presented equations.

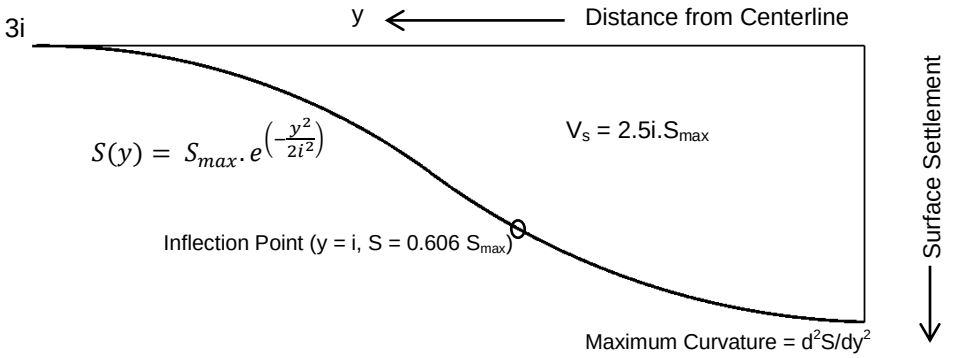

Figure 2-4 Surface Settlement Trough (Channel) Presentation by Gaussian Normal Function (Schmidt, 1969)

Some relationships have been suggested to determine the parameter of settlement trough (channel), i. O'Reilly and New (1982) performed an analysis to

estimate i parameter in error function curve at the surface for tunneling in granular and cohesive soils. It was assumed that that all movements in the clayey soil occurred along radial paths toward the tunnel axis and it was suggested that the flow was directed towards a sink, located close to the pipe invert as shown in Figure 2-5.

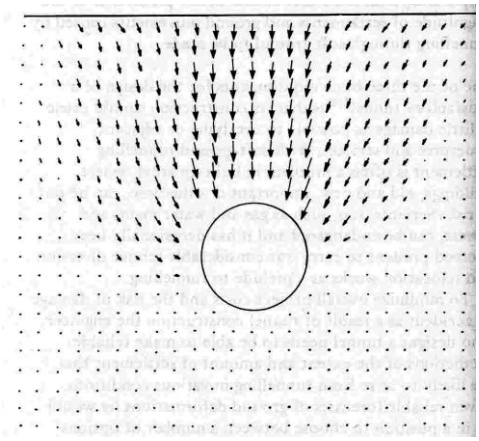

Figure 2-5 Soil Displacement around Model Tunnel in Clay (O'Reilly and New, 1982)

Studies by Potts (1976) and Cording et al. (1976) indicated that a rapid narrowing with large inward displacements of the settlement trough (channel) near the ground surface occur in sandy soils as presented in Figure 2-6.

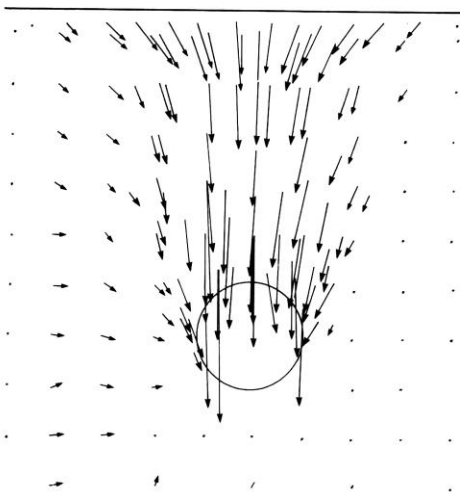

Figure 2-6 Soil Displacement around Tunnel in Sandy Soils (O'Reilly and New, 1982)

O'Reilly and New (1982) conducted statistical analysis (regression analysis) on collected data to evaluate the relationships between trough (channel) width parameter, i, and depth of the tunnel. Figure 2-7 illustrates collected data and the relationship between settlement troughs (channel) parameter, i, and the depth of tunnel axis below the ground surface for both cohesive and granular soils.

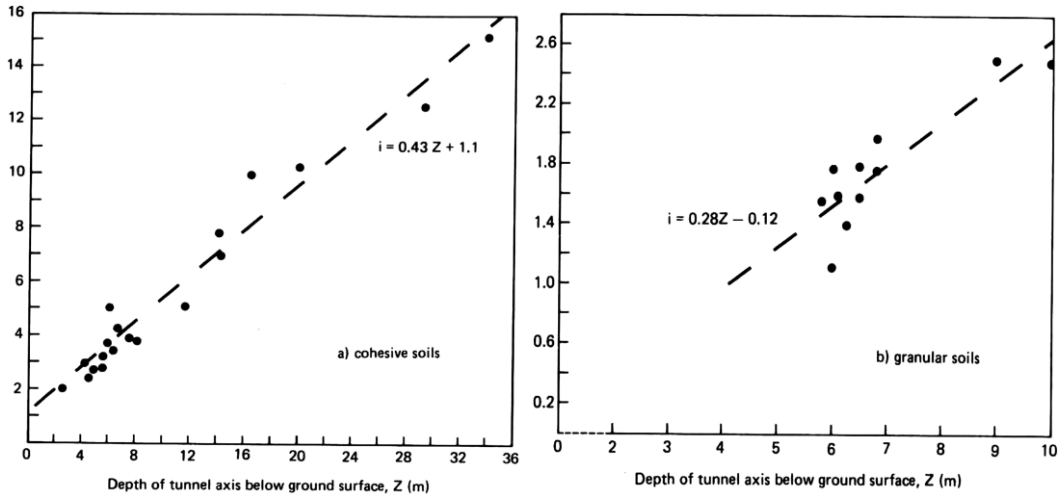

(a) (b)

Figure 2-7 Variation of Trough (channel) Width Parameter with Depth of Tunnel for: a) Cohesive Soils, and b) Granular Soils (O'Reilly and New, 1982)

A linear trend between trough (channel) width parameter and depth of tunnel was observed for both cohesive and granular soils. O'Reilly and New (1982) presented data as shown in Equation 2.8 and 2.9:

$i = 0.43Z + 1.1$ for cohesive soils Equation 2-8

$i = 0.28Z – 0.12$ for granular soils Equation 2-9

where:

i = Horizontal distance of the inflection point of the settlement trough (channel) from the tunnel centerline (m)

Z = Depth of tunnel from ground surface (m)

Coefficient of determination (R-squared or R^2) is used to determine how well data points fit the model in regression analysis. Generally, R^2 value less than 0.9 means that the model does not represent the data very well. R^2 for Equations 2-8 and 2-9 were 0.96 and 0.78 respectively and Equation 2-9, suggested for granular soils, had had its accuracy challenged. For practical purposes, the relation between settlement trough (channel) parameter, i, and depth of the tunnel was simplified and presented as Equation 2-10.

$i_z = K.Z$ Equation 2-10

where:

i_z = Trough (channel) width parameter at depth z above tunnel axis (m)

K = A parameter that depends on the soil (e.g., i = 0.4 for strong clay and sand below water level, i = 0.7 for soft clay, and i = 0.2-0.3 for sand above water table).

Z = Depth of the tunnel from ground surface (m)

Suggested equations by O'Reilly and New did not consider effect of pipe diameter, overcut size and soil properties in calculating trough (channel) parameter, i. Moreover, suggested equations for determining i parameter in granular soil with low R^2 means that their suggested model did not present data well. Equations were proposed to estimate surface settlement associated with tunneling circular pipes. Therefore, equations are not applicable for BJ method where a rectangular box is jacked.

Mair et al. (1993) performed research to evaluate subsurface movements due to tunneling in clayey soils, and they showed that the Gaussian function can be adapted to estimate subsurface settlements trough (channel) by modifying the trough (channel) width parameter. However, they suggested that parameter K does not have linear relationship with depth.

$$i = K.(z_0 - z)$$ Equation 2-11

where,

K = A function of depth

z_0 = Depth of tunnel axis from ground surface (m)

z = Depth of the specific horizon from ground surface (m)

According to field measurements of subsurface settlements, parameter K increases with depth increase of the tunnel. However, the relationship is not linear. Mair et al. (1993) suggested a nonlinear Equation 2-12 to calculate K in clay.

$$K = \frac{0.175+0.325.(1-\frac{z}{z_0})}{1-\frac{z}{z_0}} \quad \text{Equation 2-12}$$

where,

z_0 = Depth of tunnel axis from ground surface (m)

z = Depth of the specific horizon from ground surface (m)

Mair et al. (1993) made improvements by considering the nonlinear effect of depth on determining tough parameter i. However, soil parameters, pipe diameter, and overcut size were not considered in the suggested equation by Mair et al. Moreover, suggested equations are applicable for estimating surface settlement associated with tunneling in clay and its applicability was not investigated for BJ operation.

Wu and Lee (2003) investigated surface settlement due to installing unlined tunnel in clayey soil. In this study, a series of single- tunnel centrifuge tests were performed to determine the surface ground movements caused by tunneling in clayey soil prior to tunnel collapse. Tunneling was simulated by pressurizing a rubber bag with air to balance the overburden pressure. Then the air pressure was reduced to zero at the rate of 20kPa/min and surface settlement was recorded.

Sample results for one of the tests with cover (C) to depth (D) ratio of 2 is presented in Figure 2-8.

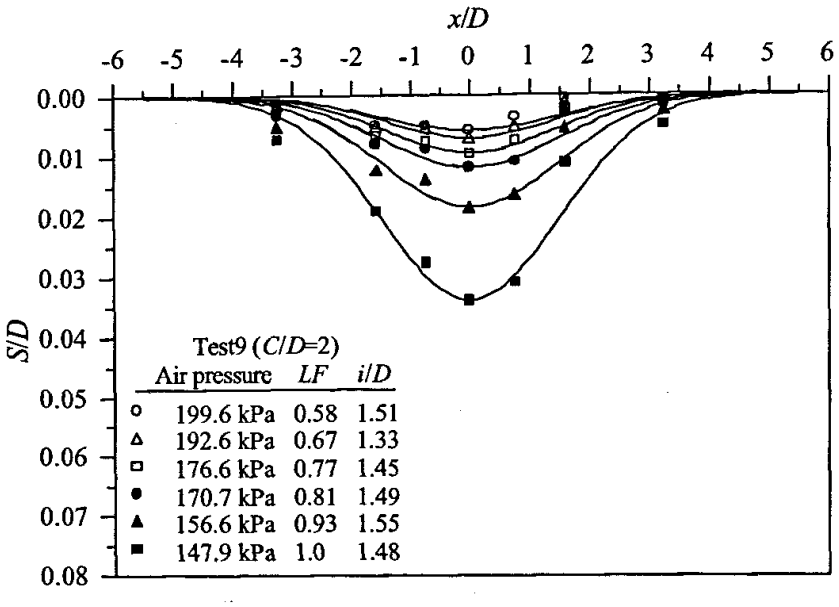

Figure 2-8 Settlement Trough (Channel) induced by Single Tunneling, C/D = 2

Wu and Lee (2003) conducted different tests with various cover to depth ratios and suggested Equation 2-13 to estimate trough (channel) parameter, i.

$$\frac{2i}{D} = 0.58\left(\frac{z}{D}\right) + 1.0 \qquad \text{Equation 2-13}$$

where:

z = depth tunnel from surface to top of the tunnel (m)

D = Tunnel diameter (m)

Research has been conducted to determine maximum surface settlement, S_{max}. Equation 2.4, suggested by Peck (1969), can be rewritten as Equation 2.14.

$$S_{max} = \frac{V_s}{2.5\, i} \qquad \text{Equation 2-14}$$

where:

V_s = Volume of surface settlement (m^3/m)

i = Horizontal distance of the inflection point of the settlement trough (channel) from the tunnel centerline (m)

Estimating volume of surface settlement is difficult since it depends on various factors such as soil properties, overcut size, etc.

Milligan and Marshall (1995) assumed that volume of surface settlement, V_s, is equal to the volume of ground loss at the tunnel, V_L, in loss soil and suggested Equation 2-15, originally proposed by Peck (1969), to calculate the volume of surface settlement.

$$V_s = V_L = \frac{\pi(d_s^2 - d_R^2)}{4}$$

Equation 2-15

Where:

d_s = Outside diameter of the jacking or shield machine

d_R = Outside diameter of the jacking pipe

Equation 2-14 can be rewritten by substituting V_s

$$S_{max} = \frac{\pi(d_s^2 - d_R^2)}{10\,i}$$ Equation 2-16

Equations suggested by Milligan and Marshall (1995) overestimate the maximum surface settlement, S_{max}, since the arching effect was not considered in their equations. Arching is a phenomenon where the interaction of the individual soil particles physically prevents the soil from collapsing completely onto the over-excavated area (e.g., overcut). Also, equations were suggested to estimate maximum surface settlement in pipe jacking projects only.

Settlements in trenchless construction projects can be evaluated using a method developed by Bennett (1998). Bennett's model assumes systematic settlements as an inverted normal probability curve, or settlement trough (channel), with maximum settlements occurring directly above the centerline of the bore, and with settlements

decreasing with distance from the bore centerline. It was assumed that the unit volume of the settlement trough (channel) is equal to volume of soil lost in due to the bore annulus. Figure 2-9 shows the schematic settlement estimation for microtunneling.

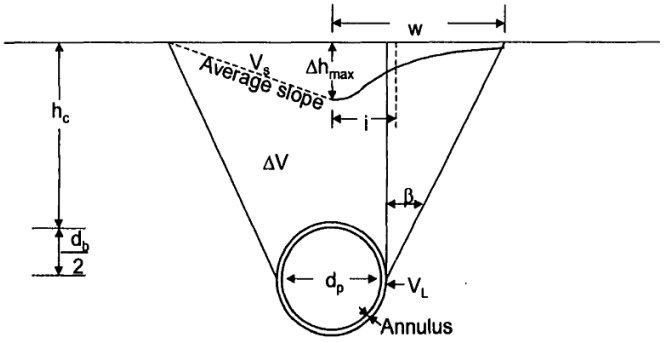

Figure 2-9 Schematic Settlement Trough (Channel) above Microtunneling

(Bennett, 1998)

where the variables are as follow:

w = Settlement trough half-width

Δh_{max} = Settlement trough (channel) depth at centerline (maximum settlement)

V_s = Settlement trough (channel) volume per unit of bore length

V_L = Volume loss around tunnel ($\pi(d_b^2 - d_p^2)/4$)

h_c = Depth of clearance above crown of bore

d_b = Diameter of the bore

d_p = Diameter of the pipe

Maximum settlement at centerline, Δh_{max}, can be calculated using Equation 2-17.

$\Delta h_{max} = V_s / w$ Equation 2-17

It was assumed that the volume of annulus is transferred directly to the surface and is equal to the settlement trough (channel) volume, ($V_a = V_s$), and w is defined as Equation 2.16.

$$w = d_b/2 + (h_c + d_b/2) \cdot \tan(45 - \phi/2) \qquad \text{Equation 2-18}$$

where:

ϕ = Friction angle of soil

It was found that settlements increase with increasing annular volume (e.g., overcut size). On the other hand, settlement decreases with increasing ground clearance from the crown of the pipe. This is because a deeper bore causes the settlement volume to spread out over a larger trough (channel) width and decreases the depth of the settlement trough (channel). Figure 2-10 shows the effect of ground clearance on the shape of the settlement trough (channel) and maximum settlement at the centerline of the pipe. However, it should be noted that the enclosed area under both plots are the same.

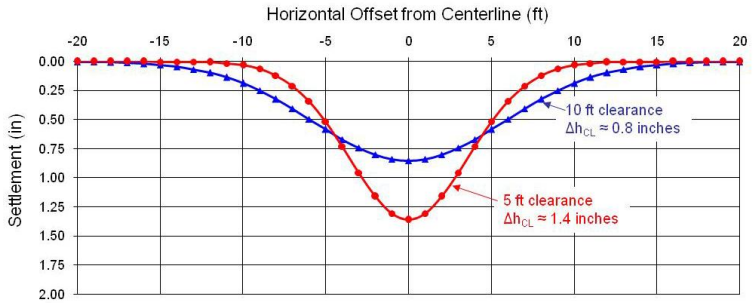

Figure 2-10 Effect of Ground Clearance on Maximum Settlement and Shape of Trough (Channel) (Wallin et al., 2008)

As mentioned before, it was assumed that the settlement volume is equal to the annular volume. However, three factors, including soil mass loosening, soil strength (arching), drilling fluid left in the annulus, and cement grouting can affect the percentage of annular volume that contributes to the settlement trough (channel) volume.

The process of losing soil density and soil dilation is called soil mass loosening which leads to increased soil volume and, therefore, a decreased volume of the settlement trough (channel) at the surface. However, soil mass loosening in very loose

soils causes a volume decrease and therefore increases the settlement magnitude at the surface.

Interaction of individual soil particles prevents the soil from collapsing completely onto the pipe and therefore only a percentage of annular space is transferred to the surface. This phenomenon is called soil arching. Arching effect is undermined by seeping groundwater toward the bore. Also, arching effect is reduced as the diameter of the pipe is increased.

Finally, drilling fluid left inside the annulus and cement grouting can prevent the soil from collapsing onto the pipe and consequently, decrease the maximum surface settlement (Wallin et al. 2008).

Moreover, the proposed equations by Bennett (1998) are for microtunneling only. Also, other soil properties such as soil unit weight, modulus of elasticity, cohesion were not studied in developing equations.

Analytical Methods

Several studies have been conducted over past 20 years to evaluate ground movement associated with pipe jacking and tunneling using numerical methods. Numerical methods have been developed based on theoretical soil mechanics and fluid mechanics. However, analytical methods applicability is limited to mathematical assumptions based on restricted geometry or boundary conditions.

Sagaseta (1987) conducted a research to obtain the strain field and soil deformation in an isotropic and homogeneous incompressible soil due to soft ground tunneling. He assumed that the surrounding soils completely collapse and fill the void area left by the soil extraction. Free surface modeling in fluid mechanics is a very difficult. Therefore, he followed three main steps to model the free surface.

Step 1) Neglect the effect of soil surface and calculate strains as the point sink will be on infinite medium.

Step 2) Since the free surface has a stress-free condition, the stress, produced by strains, at the surface are canceled by one the following methods:

2-1) Consider a negative mirror image of the actual sink that produces opposite normal stress and the same shear stresses as the actual sink. This procedure is referred to as virtual image technique.

2-2) Consider a positive image that produces the same normal stress and opposite shear stresses.

Step 2-1 is more useful since it only produces horizontal displacements which do not violate surface vertical movement estimation.

Step3) Evaluate and remove the remaining shear or normal stresses at the surface and then, add the resulting strains to those calculated in previous steps.

Sagaseta (1987) assumed that a finite volume of soil, and point sink with a radius of a, was located at the depth of h from the ground surface as shown in Figure 2-11 . Ground loss volume was $4/3\ \pi a^3$ in 3-dimensional problem and πa^2 in plane strain condition (2-dimensional).

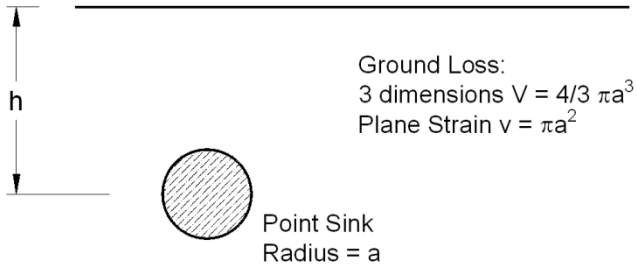

Figure 2-11 Ground loss at the Depth of h (Sagaseta, 1987)

If the free surface is ignored, as discussed in Step 1, the problem becomes symmetric about the sink and the radial displacement can be calculated as follows:

$$S_r(r) = \frac{a}{n}\left(\frac{a}{r}\right)^{n-1}$$ Equation 2-19

where:

n = 2 in plane strain condition and 3 in three dimensions

a = sink radius (m)

r = distance of a considered point from the sink as shown in Figure 2-12 (m)

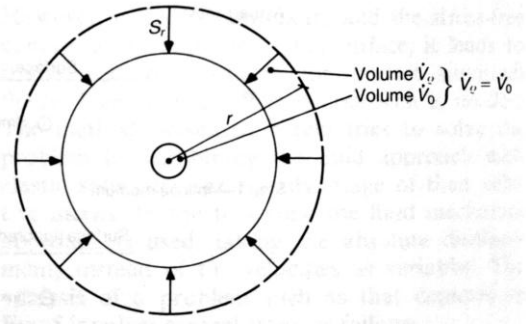

Figure 2-12 Point Sink in Infinite Medium (Sagaseta, 1987)

Equation 2.18 can be converted into a Cartesian reference frame (Figure 2-13) and rewritten as Equation 2-20 and 2-21.

$$S_x = -\frac{a^n}{n}.\frac{x-x_0}{r^n}$$ Equation 2-20

$$S_z = -\frac{a^n}{n}.\frac{z-z_0}{r^n}$$ Equation 2-21

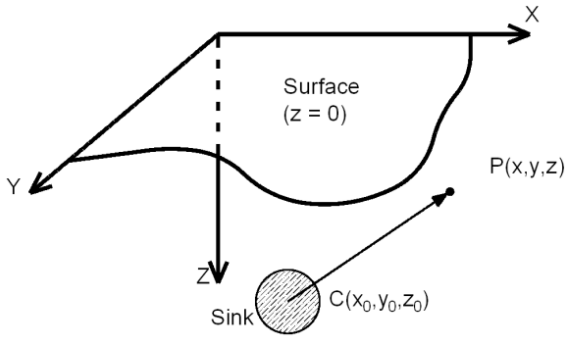

Figure 2-13 Cartesian Coordinates (Sagaseta, 1987)

Considering a flow from point P in the direction of the sink radially (Figure 2-14) and free surface conditions, Sagaseta (1987) suggested Equation 2-22 and 2-23 to estimate ground movements due to tunneling.

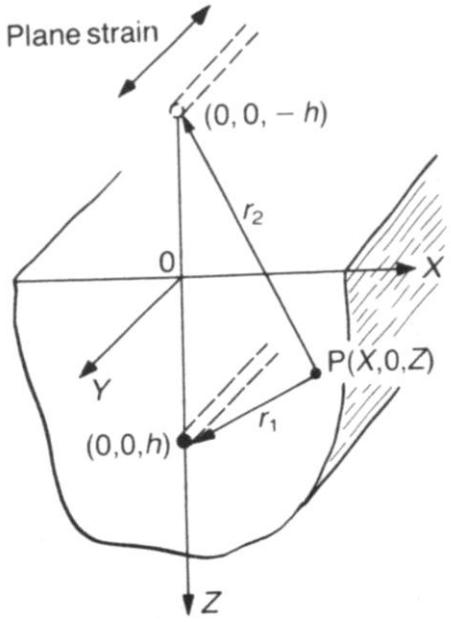

Figure 2-14 Point sink and negative image in plane strain (2D)

$$S_{x0} = S_{x(z=0)} = -2\frac{a^n}{n}.\frac{x}{(x^2+h^2)^{\frac{n}{2}}}$$ Equation 2-22

$$S_{z0} = S_{z(z=0)} = 2\frac{a^n}{n}.\frac{h}{(x^2+h^2)^{\frac{n}{2}}}$$ Equation 2-23

The disadvantage of method according to Sagaseta (1987) is the assumption of soil incompressibility. This means that the long-term soil movements due to consolidation or creep are ignored in movement calculations. Also the method is applicable for tunneling in clayey soil only.

Rogers and O'Reilly (1991) extended the method suggested by Sagaseta (1987) for pipe jacking and trenching by considering the loss of soil during pipe jacking due to overcut. They assumed the soil flow from a point P radially in the direction of a sink and

used virtual image technique, as illustrated in Figure 2-15 to suggest new questions to estimate ground movements associated with pipe jacking and trenching.

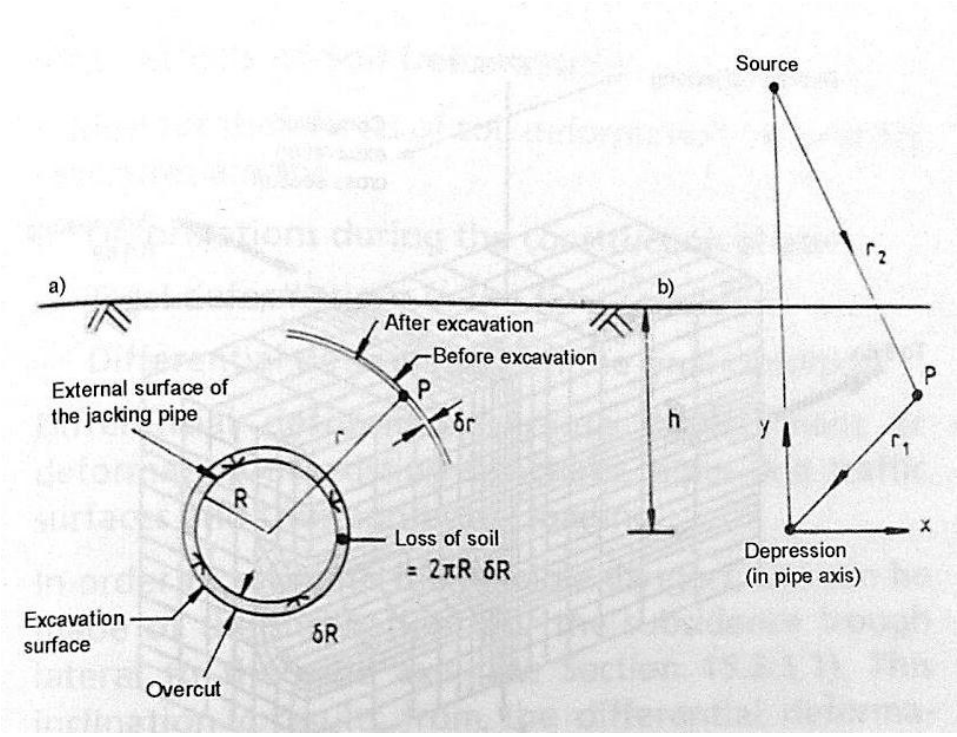

Figure 2-15 Method of Calculation Suggested by Rogers and O'Reilly (1991)

The geometric parameters r_1 and r_2, as show in Figure 2-15 can be calculated as presented in Equations 2-24 and 2-25.

$$r_1 = \sqrt{x^2 + y^2} \qquad \text{Equation 2-24}$$

$$r_2 = \sqrt{x^2 + (2h - y)^2} \qquad \text{Equation 2-25}$$

Where;

h = depth of pipe axis (m)

x, y = Considered point coordinates, whereby the origin of the coordinate system lies on the pipe axis (m)

Equations 2-26 and 2-27 were suggested by Rogers and O'Reilly (1991) to estimate ground movement due to pipe jacking.

$$S_x(x,y) = R.\delta R.x.\left(\frac{1}{r_1^2} - \frac{1}{r_2^2}\right) = R.\delta R.x.\left(\frac{1}{x^2+y^2} - \frac{1}{x^2+(2h-y)^2}\right) \quad \text{Equation 2-26}$$

$$S_y(x,y) = R.\delta R.\left(\frac{y}{r_1^2} - \frac{2h-y}{r_2^2}\right) = R.\delta R.\left(\frac{y}{x^2+y^2} - \frac{2h-y}{x^2+(2h-y)^2}\right) \quad \text{Equation 2-27}$$

where:

$S_x(x,y)$ = Horizontal displacement of considered point (e.g., point P)

$S_y(x,y)$ = Vertical displacement of considered point (e.g., point P)

R = Outside diameter of the jacking or shield machine (m)

δR = Overcut size (m)

Overcut size can be considered zero in firm stable soils or rock and annular gap size in loose sediments.

As discussed before, the method suggested by Sagaseta (1987) did not consider the long-term ground movements due to tunneling and pipe jacking. Stein (2005) introduced the factor α to consider the change of volume during pipe jacking. According to Stein (2005), factor α can be calculated using Equations 2-28 and 2-29 for densely stratified soils and loosely stratified soils respectively.

$$\alpha = \frac{1+\sin\psi'}{1-sin\psi'} \quad \text{Equation 2-28}$$

$$\alpha = \frac{1-\sin\psi'}{1+sin\psi'} \quad \text{Equation 2-29}$$

where:

ψ' = Soil strain angle (e.g., $\frac{5}{4}(\phi' - \phi'_{crit})$)(Bolton, 1986)

ϕ' = Effective angle of friction

ϕ_{crit}' = Critical angle of friction

Then, the radial deformation, S_r, in pipe jacking can be calculated as follows:

$$S_r = k.\left(\frac{\alpha}{2}\right).\left(\frac{\alpha}{r}\right)^{\alpha}$$ Equation 2-30

where:

S_r = Radial deformation

k = 1 for pure elastic deformation

The equations for horizontal and vertical soil movement calculations, suggested by Stein (2005), are as follows:

$$S_x = \left(k\left(\sqrt{2R.\delta R}\right)^{\alpha}.\frac{x}{\alpha}\right).\left(\frac{1}{r_1^{\alpha}} - \frac{1}{r_2^{\alpha}}\right)$$ Equation 2-31

$$S_y = \frac{\left(k\left(\sqrt{2R.\delta R}\right)^{\alpha}.\frac{x}{\alpha}\right)}{\alpha}.\left(\frac{y}{r_1^{\alpha}} - \frac{(2h-y)}{r_2^{\alpha}}\right)$$ Equation 2-32

Suggested equations by Rogers and O'Reilly (1991) and Stein (2005) are for estimating ground movements due to pipe jacking only and its applicability for BJ is not evaluated.

Numerical Methods

Different numerical methods such as Finite Element Methods (FEM), Finite Difference Methods (DFM), and Kinematic Element Methods (KEM) are available to study the soil behavior during jacking and tunneling (Stein, 2005).

The FEM is extensively used due to its capability of modeling stress and strain in different types of soils associated with complicated geometrics. The principle of FEM is dividing a continuous linked system into an equivalent system of smaller units which is referred as discretization. Once the main system is discretized, each of the smaller units can be solved. Finally, the solutions for each smaller unit can be combined to obtain the solution for the entire system (Desai et al., 2011).

Duan (2001) numerically analyzed ground movements associated with microtunneling. FLAC 3D, a finite element modeling software, was used to simulate microtunneling procedure. Soil behavior was modeled by Mohr-Coulomb and plain strain

condition was assumed. Since the model was symmetric, the advantage of half-symmetry geometry was taken as presented in Figure 2-16.

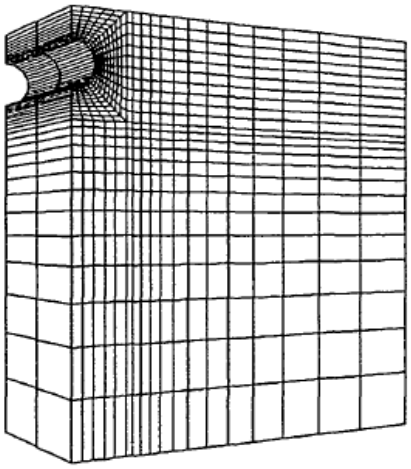

Figure 2-16 Numerical Modeling (Duan, 2001)

The numerical model results were then compared with results collected from two case studies to assure the numerical models were able to predict surface settlement. Figure 2-17 compares results obtained from a case study using numerical mode based on a case study where an 8 meter diameter subway tunnel was installed in red clay with sand and gravel.

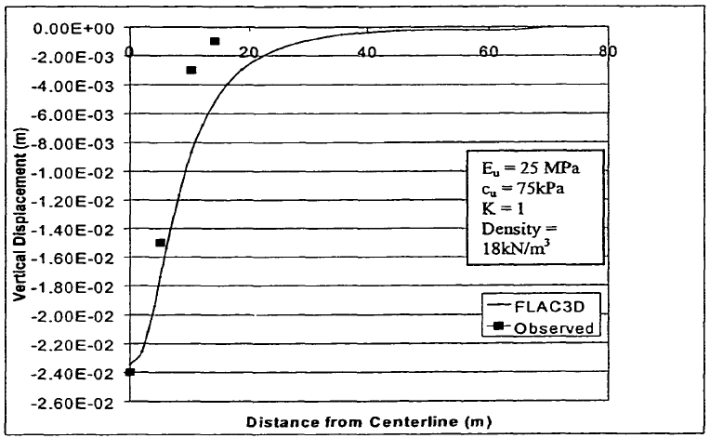

Figure 2-17 Observed and Predicted Surface Settlement (Duan, 2001)

A sensitivity analysis was done to study the effect of soil properties such as modulus of elasticity, cohesion, density, Poisson's ratio, etc. on surface vertical displacement. The procedure of sensitivity analysis was carried out by varying a considered parameter and keeping other parameters constant. Figure 2-18 illustrates the effect of changing soil modulus of elasticity on vertical soil displacement. It was assumed that the amount of Poisson's ration, cohesion and friction angle remained at 0.3, 2 kPa, and 15 degree while the amount of modulus of elasticity varied among 0.5, 1, 5, 10, 20, 30, and 40 MPa.

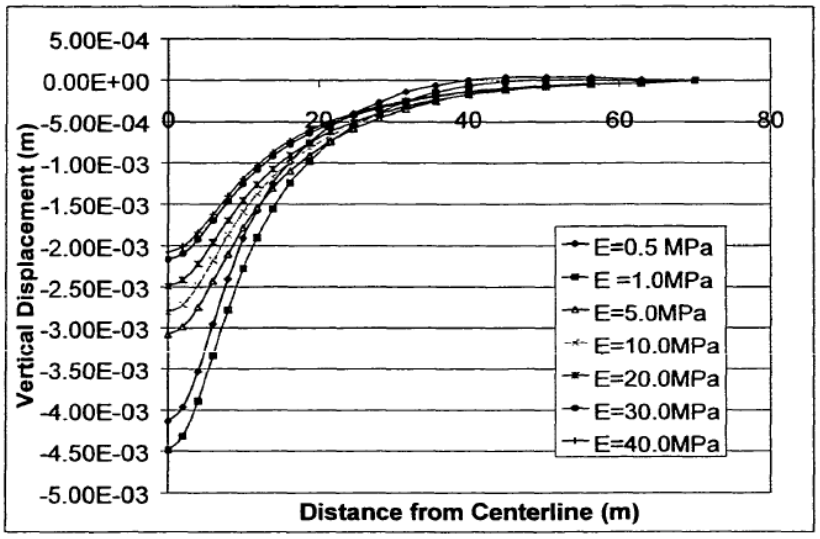

Figure 2-18 Effect of Modulus of Elasticity on Surface Vertical Displacement

(Duan, 2001)

The proposed procedure and related results are appropriate for microtunneling where a TBM machine is used for excavation. Also, the effect of soil properties changes on surface vertical displacement was not justified and explained.

Research was conducted by Shou and Chang (2006) to study surface settlement and pipe-soil interaction due to pipe jacking in loose and dense sands. They used ABAQUS to develop finite element models and then calibrated models with physical

models. Physical models consisted of a sand box (1.8m x 1.2m x 1.5m) and pipe jacking module to simulate pipe jacking procedure on a small-scale as presented in Figure 2-19.

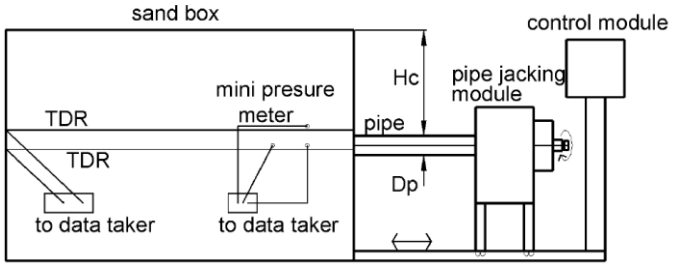

Figure 2-19 Physical Model (Shou and Chang, 2006)

ABAQUS results showed reasonable agreement with those collected from physical models as shown in Figure 2-20.

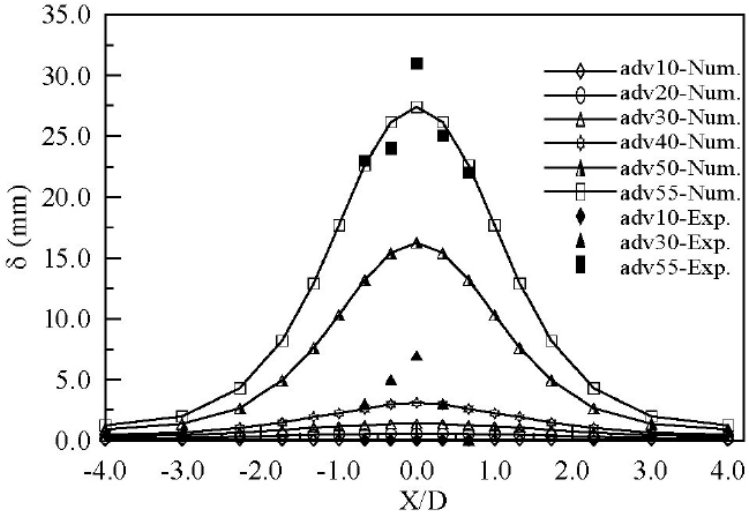

Figure 2-20 Surface Settlement during Pipe Jacking (Shou and Chang, 2006)

They concluded that surface settlement mainly occurs due to the lack of driving force. Moreover, results showed that the depth of the pipe had a critical effect on determining a proper driving force to stabilize the tunneling face.

The research conducted by Shou and Chang (2006) evaluated the advance settlement in pipe jacking but not settlement due to soil collapse into the overcut area.

Also, only two types of soils were considered in the study and the effect of soil properties were not fully studied.

Liu and Lu (2012) conducted a 3D numerical analysis of soil structure interaction behaviors of a pipe jacking construction (PJ) with hand mining excavation. The procedure was simulated using a finite element method program of Plaxis-3D Tunnel (Figure 2-21) to evaluate the effect of advancement distance, and contraction ratio (CR). Advancement distance was defined as soil excavation in front of jacking pipe. Three advancement distances of 0.3, 0.5 and 1 m were assumed. The contraction ratio was expressed as a percentage, representing the ratio of the area reduction and the original outer tunnel cross section area. CR of 0.5, 1.5, 2.0, 2.5, 2.75, and 3% was used to simulate the gap between pipe segments and bore.

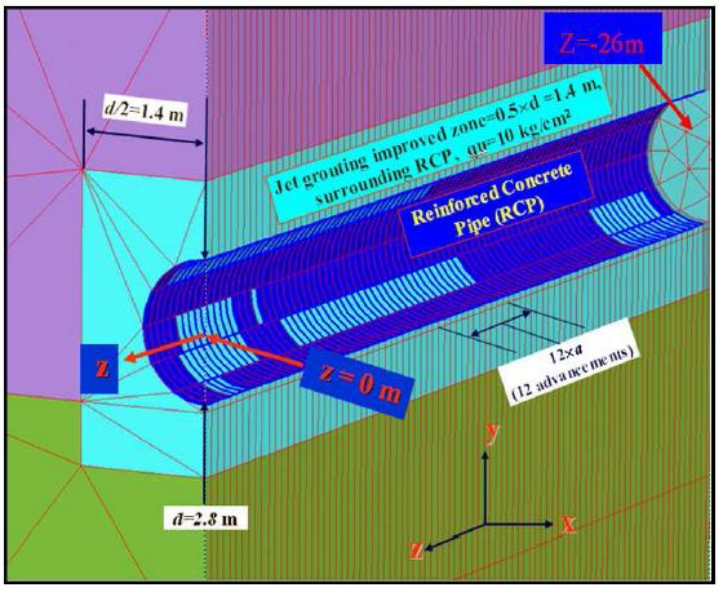

Figure 2-21 Finite Element Modeling of Project (Liu and Lu, 2012)

The scope of the project was to install a reinforced concrete pipe (RCP) with a diameter of 2.4 m and length of 23.85 m under a highway. The underground soils

consisted of eight different soil layers, simulated by the Mohr-Coulomb model, as presented in Figure 2-22.

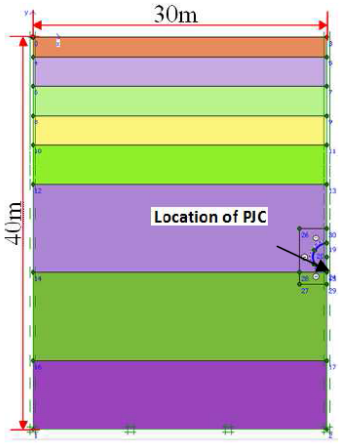

Figure 2-22 Soil Layers (Lui and Lu, 2012)

Jet grouting with pressure of 5, and 10 kgf/cm^2 were used in the project to control soil movements. It was concluded that the pipe can safely be installed with jacking distance of less than 0.3m and contraction ratio of less than 2.5% (e.g., gap size of less than 3.8 cm). Also to prevent any movements due to pipe jacking a grout pressure higher than 10 kgf/cm^2 was needed. The research did not study the effect of soil properties on final results and was limited to a specific project condition.

Hosseini et al. (2012) conducted a research to study the relationship between twin tunnel distance (pillar width) and surface subsidence in soft ground. The scope of the project was installing a new metro tunnel near an existing tunnel. A finite element model using ANSYS program was developed to study interaction between circular parallel twin tunnels excavated by Earth Pressure Balance (EBP) machine. To eliminate the effect of tunnel construction on the lateral border of the model, the boundary of the model was extended to a distance of 5.5D which is equal to 38 m from each tunnel's

centerline. Figure 2-23 shows the finite element model used for analysis of twin horizontally aligned tunnels with diameter of 6.88 m and width of 7 m.

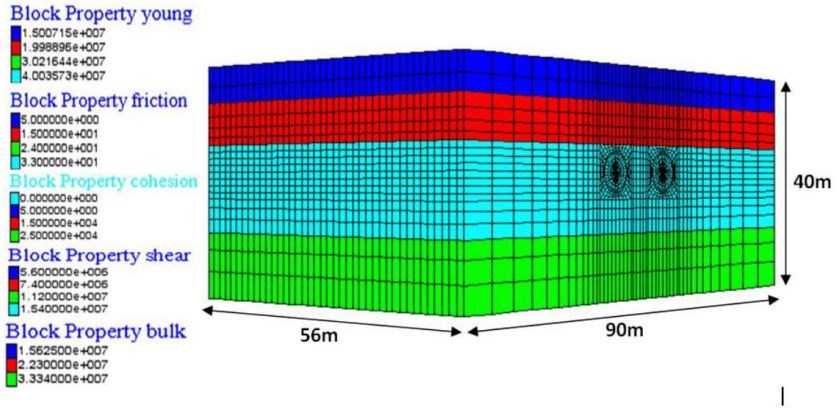

Figure 2-23 Finite Element Model (Hosseini et al., 2012)

Initial vertical stress is considered as the weight of the soil layers at the top of the tunnels. The soil behavior was assumed to be elastic perfectly plastic according to the Mohr-Coulomb criterion. Effects of distance between tunnels on the surface subsidence, bending moment and axial forces were investigated. Results showed that the maximum surface settlement increased with decrease in pillar width. Figure 2-24 shows the surface settlement variation with changes in pillar width.

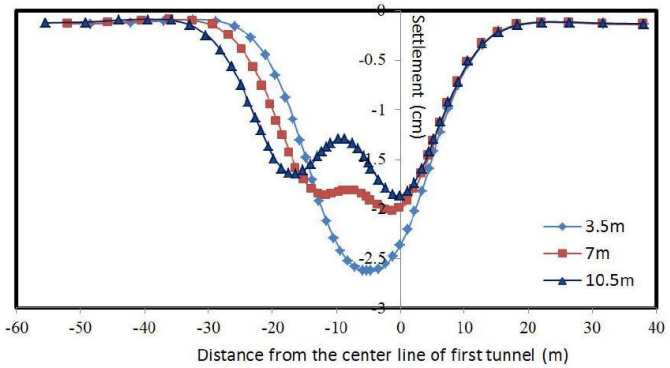

Figure 2-24 Surface Settlement for Different Pillar Widths between Twin Tunnels (Hosseini et al., 2012)

Also, results showed that the location of the maximum surface subsidence was offset from the centerline of the first tunnel. The offset increased with decrease in the distance between tunnels. Figure 2-25 presents the offset of maximum surface settlement from the centerline of the first tunnel due to changes in pillar width.

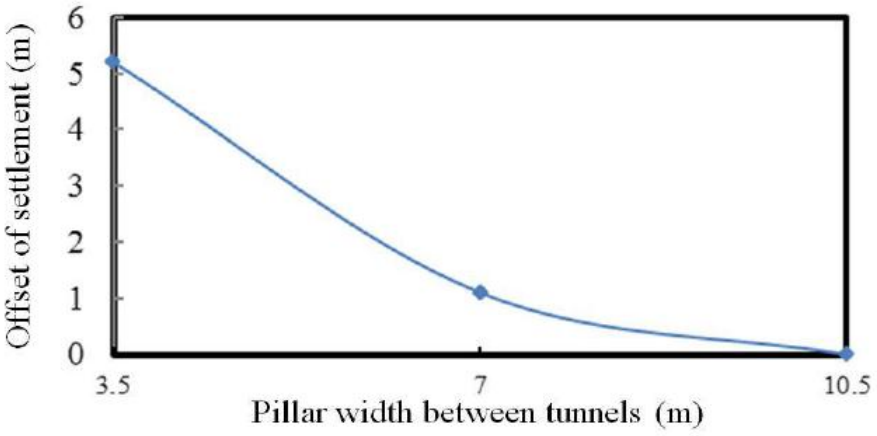

Figure 2-25 Maximum Surface Settlement Offset from the Centerline of the First Tunnel (Hosseini et al., 2012)

Artificial Neural Network (ANN)

The human brain is a complex network that consists of hundreds of billions of special cells called neurons. Neurons send information back and forth to other neurons and provide the capability of learning, analysis, prediction, and recognition. A real neuron in the brain consists of four parts:

1. body
2. Incoming channel
3. Outgoing channel
4. Synapse

Synapses allot specific weights to incoming signals so that each of the signals has a different effect on the receiving neuron (Lawrence, 1994). Figure 2-26 illustrates brain neuron and synapse area.

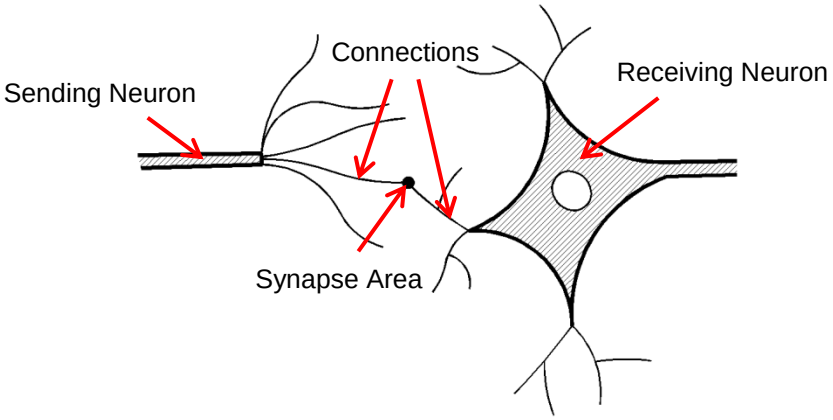

Figure 2-26 Brain Neuron and Synapse Area (Lawrence, 1994)

Artificial Neural Network (ANN) uses the same concept to simulate human brain network. Different ANN can be described in terms of its individual neurons, the connection between neurons, and its learning rule. Neurons are also called processing elements, nodes, or cells. Figure 2-27 shows an artificial neuron receiving inputs and transferring them to outputs.

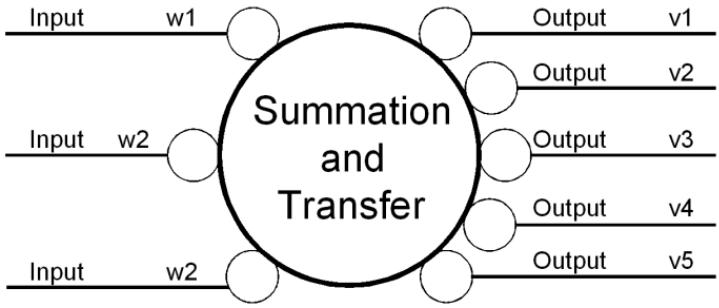

Figure 2-27 Artificial Neuron (Lawrence, 1994)

Each neuron receives the output signal from other neurons and calculates its own output by finding the weighted sum of its inputs and then by the use of a function

called activation or transfer function. The calculated output is then transferred to other neurons by connection links. Each connection link associates with a specific weight. The way in which neurons are connected has a high impact on the operation of the network and determining the type of processing (Lawrence, 1994).

A neural network consists of layers of neurons which are connected to each other as presented in Figure 2-28. Some of the neurons communicate with outside world and are placed in the input layer and some of the neurons are placed in output layer and present results. There are some neurons which are placed between input and output layers and communicate with other neurons. This layer is called hidden layer. The number of neurons in hidden layer depends on the number of parameters (neurons) in input layer. Increasing the number of neurons in hidden layers result in a more accurate model sometimes but, increases require calculation and convergence time. It is recommended to consider 1.5 times the number of parameters in input layer to have accurate model and optimum calculation time.

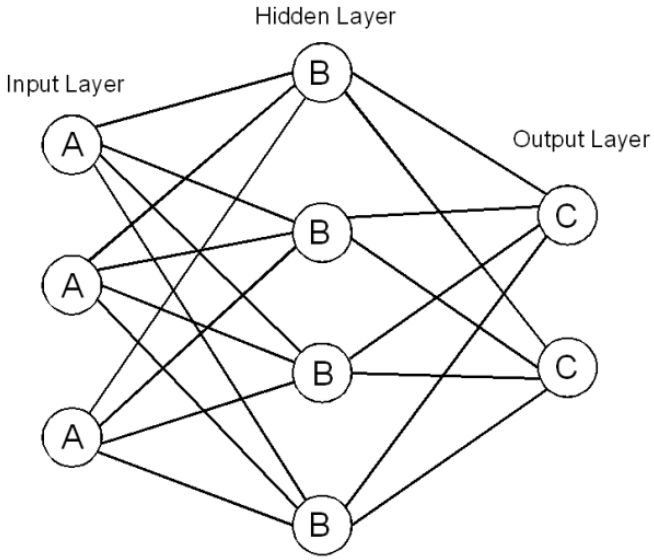

Figure 2-28 A Simple Neural Network

Activation and Transfer Functions

Once signals from other neurons are transferred to a neuron, the weighted signals are summed to a net value. Equation 2-33 shows a basic of all artificial neural networks (Lawrence, 1994).

$$net_i = \sum_{j=1}^{n}(w_{ij} * o_j) \qquad \text{Equation 2-33}$$

where:

net_1 = Net output signal of neuron i

n = Total number of receiving

j = Number of receiving

w_{ij} = weight if connections from neuron j to neuron i

o_j = Input signal from neuron j

Once the weighted inputs are summed, an activation or transfer function converts the net output signal of the neuron to produce the actual neuron outputs. Basically, activation or transfer function specifies what the neuron does after summing weighted signals. Activation or transfer function can be written as a_i (t), where i is the neuron and (t) is a particular time (Lawrence, 1994). Figure 2-29 illustrates artificial neuron functions as introduced by Equation 2-33.

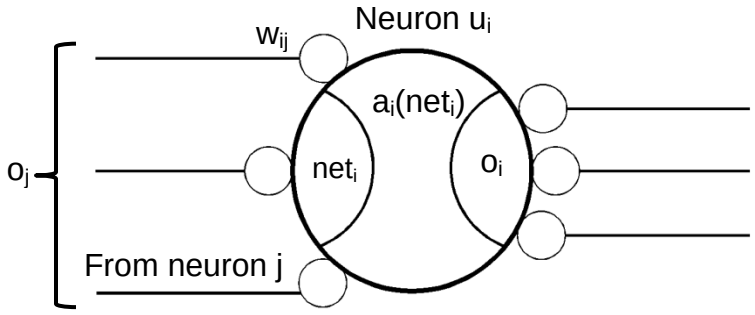

Figure 2-29 Artificial Neuron Functions (Lawrence, 1994)

Several transfer functions are available for neurons. Some of the widely used transfer functions are:

1) Linear
2) Linear threshold
3) Step
4) Sigmoid

Linear function has a constant slop output as presented in Figure 2-30. Linear function can be express as Equation 2-34.

$$a(x) = x \qquad \text{Equation 2-34}$$

where:

a (x) = activation or transfer function

x = input values

Center of the function is located where the input has zero value output (Figure 2-30). Linear transfer function is not applicable for most applications (Lawrence, 1994).

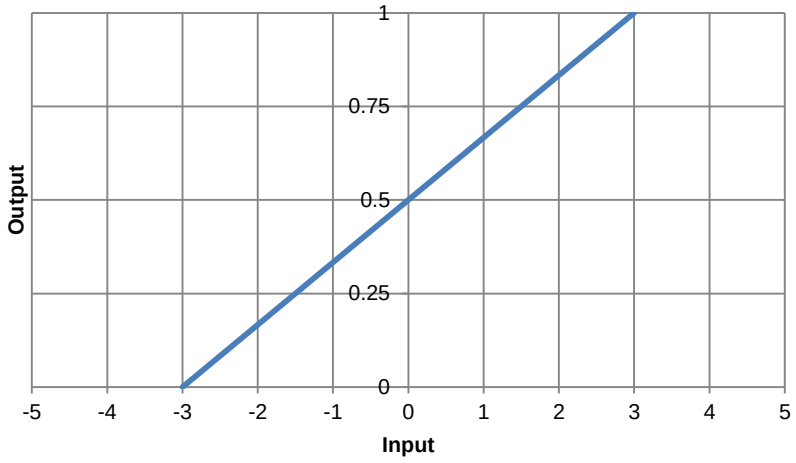

Figure 2-30 Linear Transfer Function

Linear threshold transfer function is a linear function which is trimmed to a high and a low value as presented in Figure 2-31 and expressed in the following equation:

$$a(x) = \begin{cases} 1 & if \quad x > n \\ x & if \quad -n \leq x \leq n \\ 0 & if \quad x < -n \end{cases}$$ Equation 2-35

The center of the function is located at (High+Low)/2. Linear threshold function is considered as a non-linear function because of the thresholds and results in more accurate outputs compared to linear function (Lawrence, 1994).

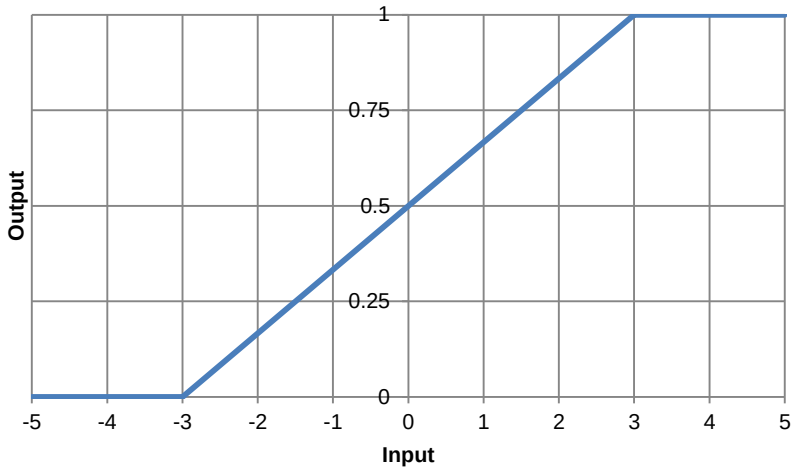

Figure 2-31 Linear Threshold Transfer Function

A step transfer function limit the output to two possible values (thresholds). Step transfer function can be shown as Equation 2-36.

$$a(x) = \begin{cases} 1 & if \quad x \geq 0 \\ 0 & if \quad x < 0 \end{cases}$$ Equation 2-36

Step transfer function is considered as nonlinear function because of the discontinuity. This function show much more accurate results than partially or entirely

linear function (Lawrence, 1994). Figure 2-32 illustrates step transfer function with two possible values of 0 and 1.

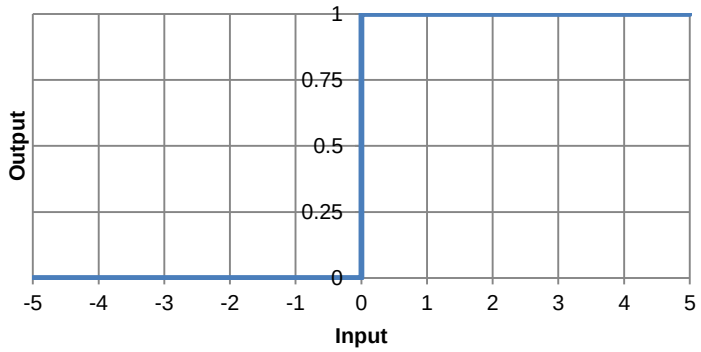

Figure 2-32 Step Transfer Function

Sigmoid transfer function or S-shaped function, as shown in Figure 2-33, has a continuous, monotonic shape and can be expressed as follows (Lawrence, 1994):

$$a(x) = \frac{1}{(1+e^{-x})}$$ Equation 2-37

The function gradually approaches the low and high values with center located at (High+Low)/2. Because sigmoid function is non-linear and continuously differentiable, it shows extremely accurate results when used to construct neural networks (Lawrence, 1994).

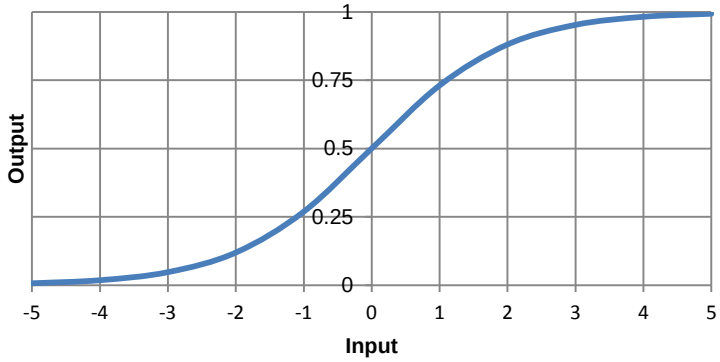

Figure 2-33 Sigmoid Transfer Function

Learning Methods

Learning methods are divided into two main categories

1) Feedback

2) Feed forward

The names of feedback and feed forward methods refer to the ways that neurons are connected in each method. In feedback neural networks, output signals form neurons that are directly sent back to neurons in the same or proceeding layers to be used as input signals as presented in Figure 2-34. Once the weight matrix is created by adding the outer signal of each input pattern vector with itself or with an associated input, an inaccurate input pattern can be presented to the network. Then, the network can converge to one of the original input Feedback network patterns. Since the model has some random elements, it usually does not provide identical results with the same inputs. Hopfield and BAM are two well-known feedback models. Also, a feedback model must cycle through the network until the final outputs stop changing and this causes a slow computation speed (Lawrence, 1994).

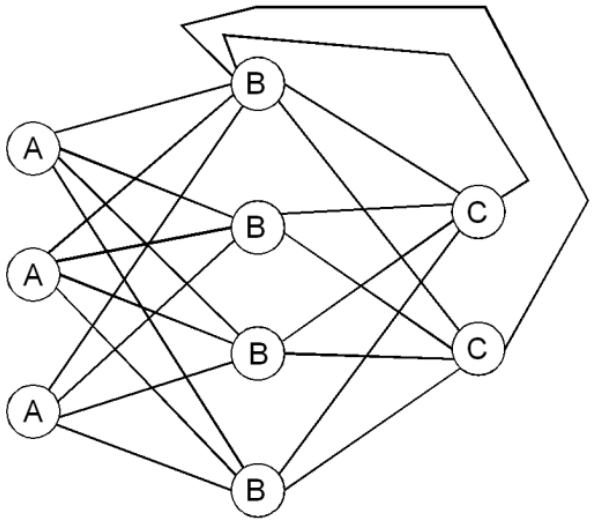

Figure 2-34 A Simple Feedback Network (Adapted from Lawrence, 1994)

As the name of the feed forward network implies, output signals from neurons are used as input signals for neurons in the proceeding layers as presented in Figure 2-35. Therefore, no loops clutter the network unlike the feedback method. Feed forward method is faster than feedback method, since only one pass through the network is needed to find a solution. Some of the feed forward methods are Perseptron, the Linear Associator, Kohonen's Network, Neocognitron, and back propagation. Among all feed forward models, back propagation is the most popular model (Lawrence, 1994).

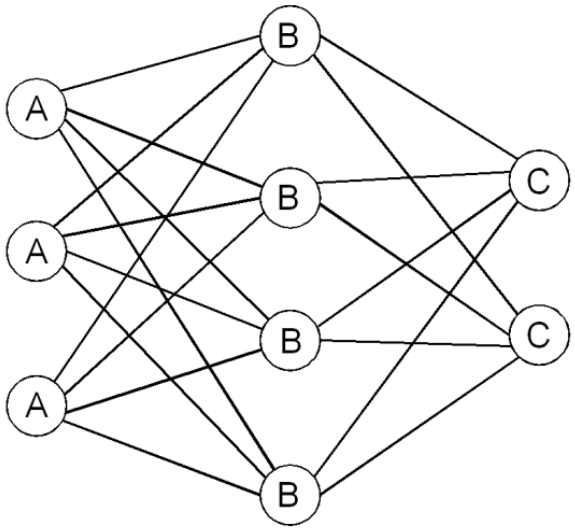

Figure 2-35 Sample Feed Forward Network

In back propagation model, the error at the final layer (output) is fed back through the network to alter weights and prevent the same error from happening again. Each cycle of feeding forward and backward is called an epoch. This procedure continues until matching output pattern is produced by the given corresponding input and the amount of error is minimized (Lawrence, 1994).

Data Sets

The first step in developing an optimal neural network is dividing the data into three subsets:

1) Training data set

2) Validation data set

3) Testing data set

Training data set, as the name implies, is used to train the ANN model and adjust the weights. Validation data set is used to verify that any increase in accuracy over the training data set results in an increase in accuracy over a data set which is not used during the training process (e.g., validation data set). Also, the validation data set is used to determine the performance of the trained ANN model. Mean Squared Error (MSE) is one the available methods to quantify the difference between estimated and exact values. The performance of the ANN model is determined by calculating the mean squared error using Equation 2-37.

$$Mean\ Squared\ Error\ (MSE) = \frac{1}{n}\sum_{i=1}^{n}(\hat{Y}_i - Y_i)^2 \qquad \text{Equation 2-38}$$

where:

n = number of data

$\hat{Y}_i$ = Vector of n predictions

Y_i = Vector of the true values

Testing data set is used after the final model is developed to confirm the actual predictive power of the ANN model.

Model Validation

First step in validating the final ANN model is evaluating the best validation performance. Performance of a neural network model represents the MSE of the model. The lower validation performance means that the model's error is lower and the model is able to predict outputs more accurately.

The performance (or MSE) is decreased as the model is being trained and it reaches its minimum (e.g., 0.70) after nine epochs. However, the analysis is continued

for six more epochs (iteration) before the training stops to assure that validation performance remains minimum. The ANN model developer should assure that the performance of an ANN model is within an acceptable range before the model is used for new data. If the performance is not acceptable, the developer can change the number of hidden layers and/or transfer functions in input and output layers to decrease the performance and develop a more accurate model. Figure 2-36 illustrates a sample performance plot of an ANN model.

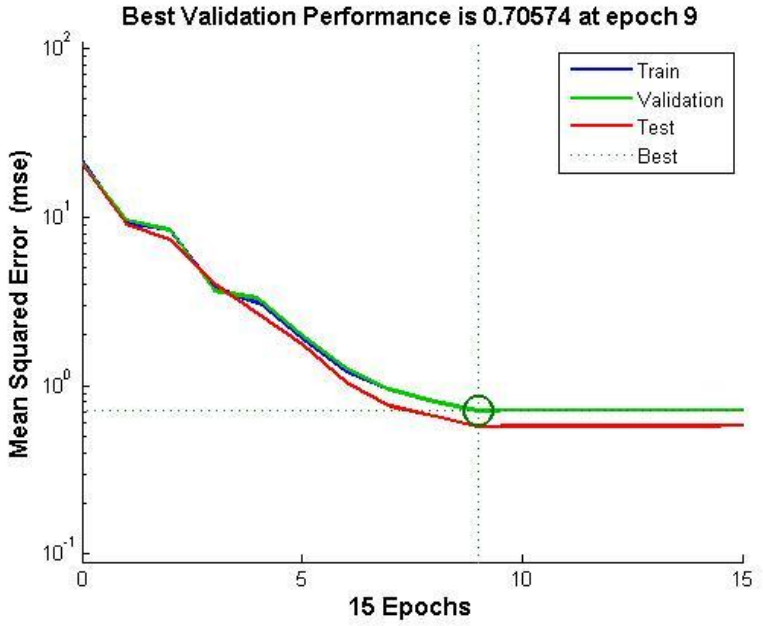

Figure 2-36 Sample Performance Plot of an ANN Model

Creating regression plots which show the relationships between the outputs (training, validation, and test) and the targets for training is the next step in validating the ANN model. In a perfect training, the outputs are exactly equal the targets. However, this situation rarely happens in practice. The dashed line in the plot represents the perfect targets (result – outputs). The best fit linear regression lines between outputs and targets are represented by solid lines. The R value at the top of each regression plots indicates

the relationships between outputs and targets. An R value close to 1 indicates that there is a linear relationship between outputs and targets while an R value close to zero indicates non-linear relationships. Figure 2-37 illustrates sample regression plots for an ANN model.

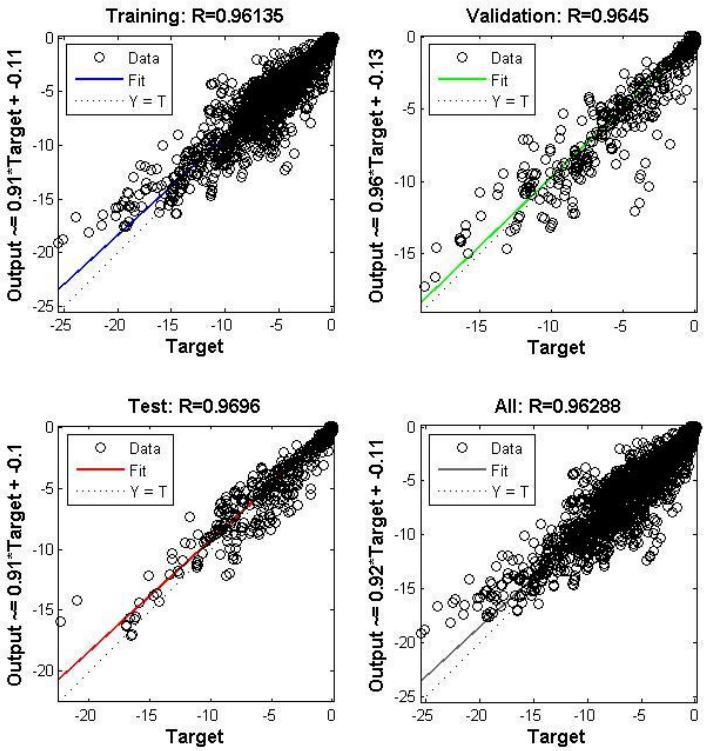

Figure 2-37 Sample Regression Plots for an ANN Model

Artificial Neural Network (ANN) versus Regression Analysis

As discussed before, ANN method is a technique to relate input data to an output data using weights and transfer functions. The ANN model is able to predict outputs based on new inputs. The accuracy of the ANN model can be further improved by adding new data to the model. Regression analysis method is used to derive a specific equation to relate input to output data. Deriving an equation in complicated nonlinear data is

sometimes difficult and transformation is required to establish a linear relation between input and output data. On the other hand, ANN method is mainly used to model complicated nonlinear data. Moreover, while increasing the number of parameters in the regression analysis method may increase nonlinearity and consequently decrease the accuracy of the model, more parameters in ANN results in a more accurate model.

Standard Penetration Tests (SPT)

Standard Penetration Test (SPT) was developed in 1970 and it is one of the most popular field tests. The SPT is conducted by driving a sampler into the ground by use of a drop hammer with mass of 63.5 kg (140 lb) falling 760 mm (30 in.) (Figure 2-38). The sampler is driven 152 mm (6 in.) into the ground and then a number of blows (N) required to penetrate an additional 304 mm (12 in.) is counted. The number of blows (N) is called standard penetration number (Budhu, 2011).

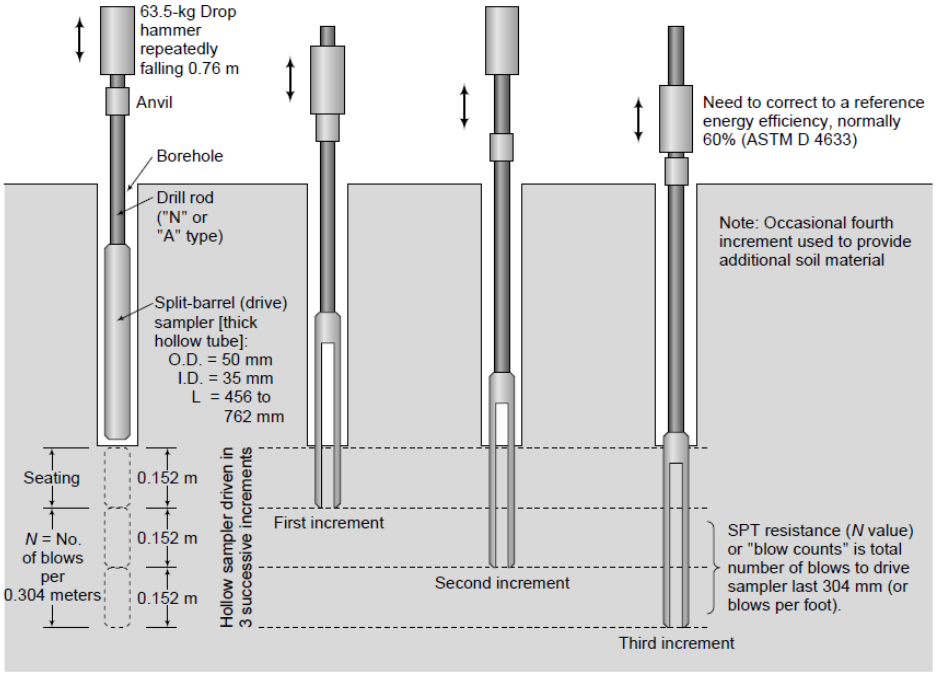

Figure 2-38 Standard Penetration Test (SPT) (Budhu, 2011)

Several methods are used to perform SPT and different correction factors are introduced to correct N. However, for most geotechnical applications the N value is corrected to a rod energy ratio of 60% and is denoted as N_{60}. N_{60} can then calculated as follows (Budhu, 2011):

$$N_{60} = N\left(\frac{ER_r}{60}\right) = NC_E \qquad \text{Equation 2-39}$$

where:

ER_r = Energy ratio

C_E = 60% rod energy ratio correction factor

The value of C_E is presented in Table 2-2 for different hammer types.

Table 2-2 Energy Correction Factor (C_E) (Budhu, 2011)

Hammer Type	**C_E**
Donut	0.5-1.4
Safety	0.7-1.2
Trip	0.8-1.4

SPT Relationships with Soil Properties

Several studies have been conducted to find the relationships between N_{60} and soil properties such as E,ϕ andγ. Tan et al. (1991) suggested Table 2-3 to estimate the modulus of elasticity, E, for cohesionless soils using N_{60}.

Table 2-3 Relationships among Modulus of Elasticity and N_{60} (Tan et al., 1991)

Soil	**Modulus of Elasticity (kPa)**
Normally Consolidated Sand	$E = 500(N_{60} + 15)$
Over-consolidated Sand	$E = 18000 + 750\ N_{60}$
Gravelly Sand and Gravel	$E = 600\ (N_{60} + 60)$ for $N_{60} < 15$ $E = 600\ (N_{60} + 6) + 2000$ for $N_{60} > 15$
Clayey Sand	$E = 320\ (N_{60} + 15)$
Silty Sand	$E = 300\ (N_{60} + 6)$

Duncan and Buchignani (1976) offered Table 2-4 to estimate friction angle and dry unit weight of cohesionless soils.

Table 2-4 Relationships among Descriptive Relative Density, N_{60}, Friction Angle, and Dry Unit Weight of Cohesionless Soils (Duncan and Buchignani, 1976)

Descriptive Relative Density	**N_{60}**	**Friction Angle, ϕ (degree)**	**Dry Unit Weight, γ (kN/m^3)**
Very loose	< 4	< 30	< 14
Loose	4 – 10	30 – 32	14 – 16
Medium Dense	10 – 30	32 – 35	16 – 18
Dense	30 – 50	35 – 38	18 – 20
Very Dense	> 50	> 38	> 20

Chapter Summary

This chapter discussed different trenchless technology (TT) methods, and then presented a literature survey for ground movement analysis of tunneling and pipe jacking (PJ). Three main methods were reviewed: empirical, analytical and numerical. A literature review of studies on PLAXIS 2D and Artificial Neural Network (ANN) was also presented. Finally, Standard Penetration Test (SPT) was thoroughly discussed and its relation with soil properties such as soil unit weight, modulus of elasticity and friction angle were presented.

Chapter 3

Methodology

Introduction

Previous chapter presented trenchless technology methods and discussed available ground movement analysis for tunneling and pipe jacking. As discussed in Chapter 2, three calculation methods, namely empirical, analytical, and numerical, are used to analyze settlement associated with PJ and tunneling. Numerical method is becoming more popular due to its capability to model different types of projects with complicated geometries and conditions. In this study, the numerical method is used to analyze settlement due to BJ operation. Chapter 3 discusses adopted numerical method to simulate box jacking operation. In this research, Finite Element Modeling (FEM) using PLAXIS 2D was used for simulation. One of the main disadvantages of the numerical method is its restriction to specific project conditions as presented in Chapter 2. This research considers the Artificial Neural Network (ANN) method to correlate FEM inputs and outputs and overcome the restrictions of the numerical method. The combination of these two methods, FEM and ANN, results in a model that can be used in variety of BJ projects within the considered assumptions.

Main Scenarios and Analysis Procedure

Main Scenarios

Eight parameters, as listed below, were changed to generate unique BJ projects. These parameters were classified as soil related, box related and miscellaneous parameters.

A) Box related parameters

   1) box culvert height (h)

   2) box culvert width (w)

B) Soil related parameters

1) modulus of elasticity (E)

2) friction angle (ϕ)

3) unit weight (γ)

4) cohesion (c)

C) Miscellaneous parameters

1) overcut size (s)

2) depth of box culvert from surface to top of the box culvert (H_1)

Box Related Parameters

In this research, six box dimensions, as listed in Table 3-1, are considered to generate BJ projects. Box dimensions are selected so that hand mining is feasible and cover a different range of available standard box dimensions. According to manufacture standards, modulus of elasticity and unit weight of boxes are 2.50×10^7 kN/m^2 (36,260 ksi) and 24 kN/m^3 (152 lb/ft^3) respectively.

Table 3-1 Considered Box Dimensions

No.	Width (w), m (ft)	Height (h), m (ft)	Thickness, mm (in.)
1	1.8 (6)	1.2 (4)	20 (0.79)
2	1.8 (6)	1.8 (6)	20 (0.79)
3	2.4 (8)	1.2 (4)	30.5 (1.2)
4	2.4 (8)	2.4 (8)	30.5 (1.2)
5	3.0 (10)	1.5 (5)	30.5 (1.2)
6	3.0 (10)	3.0 (10)	30.5 (1.2)

Soil Related Parameters

Soil related parameters include E, ϕ, γ and c. Soil properties are interrelated and a parameter cannot be assumed without considering the effect of other soil properties. Since SPT values (N_{60}) relationships with soil properties such as E, ϕ, and γ are developed, as discussed in Chapter 2, N_{60} is considered to generate appropriate E, ϕ and

γ. N_{60} random values between 4 and 60, where N_{60} = 4 corresponds with very loose sand and N_{60} = 60 corresponds with very stiff sand, were assumed and then corresponding E, ϕ and γ were calculated based on available relationships. Usually, sandy soils contain small amount of clay and silt that make the soil cohesive. According to interviews with geotechnical professors and engineers, cohesion (c) values between 0 to 24 kN/m^2 (0 to 3.5 psi) were considered and randomly assigned to each set of soil properties. Maximum and minimum values for different soil properties, considered in the research, is presented in Table 1-5. A total of 50 soil properties data sets were generated for each box culverts. With 6 box culverts considered in this research, exactly 300 scenarios were generated representing different BJ projects, as presented in Appendix C.

Miscellaneous Parameters

Miscellaneous parameters include overcut size and depth of box from the ground surface to the top of the box (H_1). As discussed in Chapter 1, minimum overcut size for pipe jacking and BJ was 25 to 50 mm (1 to 2 in.): therefore, three overcut sizes of 30, 40, and 50 mm (1.18, 1.57, and 1.97 in.) were randomly generated and assigned to data sets.

Depth of box from the ground surface to the top of the box (H_1) is defined as a function of box height (h). Five possible depths (H_1) namely 2h, 3h, 4h, 5h, and 6h were considered and randomly generated for each box and added to the data sets.

Finite Element Modeling (FEM)

PLAXIS 2D, geotechnical finite element modeling software, was used to simulate BJ operation. This is because PLAXIS includes important soil behavior criteria such as Mohr-Coulomb. Moreover, discontinuities and complicated geometries can be modeled easier than other finite element modeling software such as ABAQUS or ANSYS.

A comprehensive literature survey, as presented in Appendix B, was conducted to assure an appropriate procedure was followed in modeling. For modeling purposes, the problem was defined by a geometry illustrated in Figure 3-1. Since the problem was symmetric, half of the geometry was simulated. Moreover, it was assumed that the strain in z-direction (perpendicular to the geometry) is negligible and plane strain condition can be adopted. The origin of reference axis was located at the bottom of the domain.

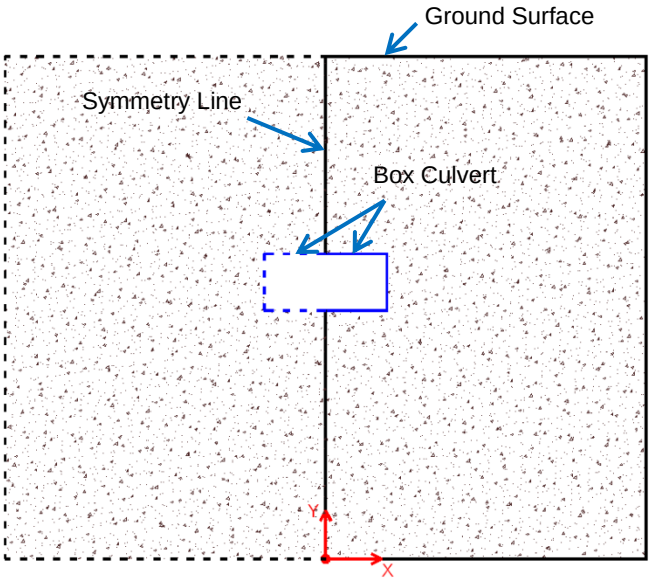

Figure 3-1 General PLAXIS 2D Simulation Geometry

Standard boundary conditions, roller supports at both sides and pinned supports at the bottom of the geometry, were considered for modeling as illustrated in Figure 3-2. Roller supports were free to rotate and move along the surface but restricted movements in perpendicular direction of the surface (e.g., X-direction in this study). Pinned supports were only free to rotate but restricted movements on directions (e.g., X- and Y-direction in this study). W, H_1 and H_2 represented the model width, depth of box culvert from surface to top of the box, and depth of box culvert from bottom of the model to the bottom of the

model respectively. Moreover, w/2 and h are half of box culvert width and height respectively. Figure 3-2 boundary conditions and parameters.

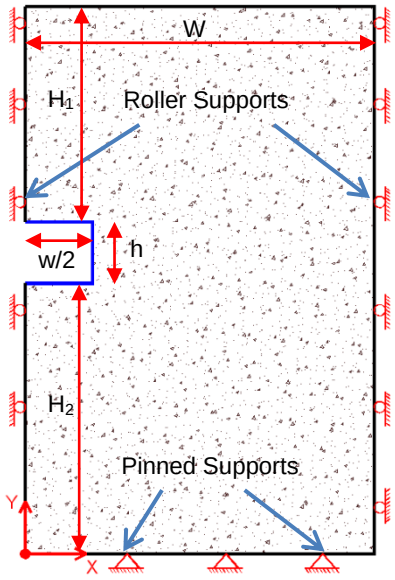

Figure 3-2 Boundary Conditions

Overcut (s) were simulated by creating a cavity around the box culvert. It was assumed that the soil was homogenous and could be modeled using the Mohr-Coulomb criteria. Mohr-Coulomb criteria is able to model sandy soils with common soil properties such as soil friction angle, cohesion, soil density and modulus of elasticity. The box culvert was assumed to be an elastic type material.

To simulate a real BJ project procedure, stage construction feature was adopted. First stage of model analysis was generating initial stress due to soil weight. Since the PLAXIS models in this research had a horizontal surface with parallel soil layers, the initial stress was generated in the modeling procedure by use of K_0 procedure. In the first stage, the initial stress was generated due to soil weight while the box culvert was not activated. Second stage of analysis, which was plastic analysis, was generated by activating box culvert and annular space, and deactivating soil inside the annular space

and soils inside the box culvert. Deactivating annular space soil allows the soil to collapse into the annular space. Once the soil contacts the box culvert, the box stops further movement. To calculate the displacements associated with BJ operation, displacement due to initial stress generation reset to zero. Therefore, only displacements due to soil collapse into the annular space was captured. Figure 3-3 a and b illustrates analysis stages.

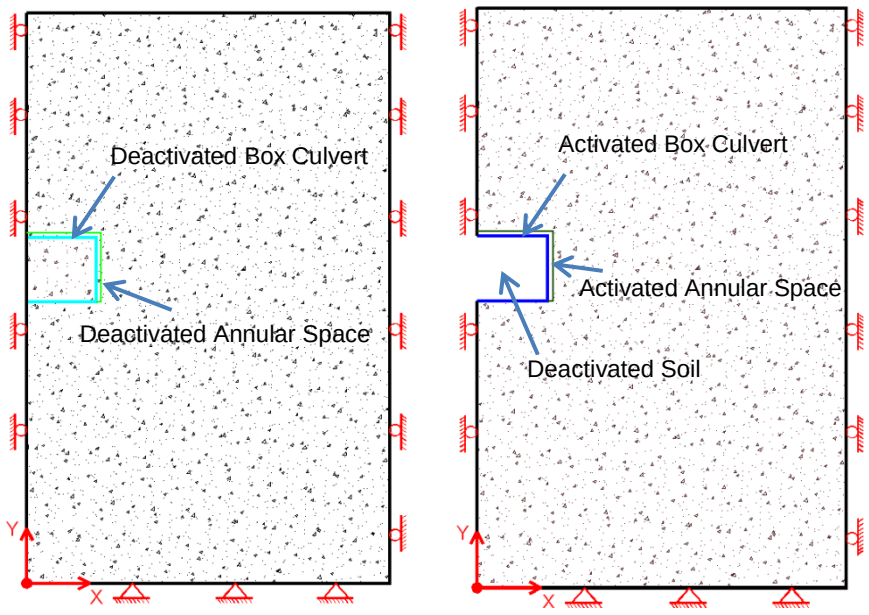

(a) (b)

Figure 3-3 Analysis Stages: a) First Stage Analysis Model, b) Second Stage Analysis

Initial Scenario

An initial scenario was considered in this research to conduct sensitivity analysis and study the effect of different parameters on surface vertical displacement. Moreover, the initial scenario was used to determine appropriate model dimensions and mesh size.

The initial scenario was a 1.8 m x 0.9 m (6ft x 3 ft) box culvert, installed at the depth of H_1 = 4h =3.6 m (11.8 ft) from the ground surface. It was assumed that the

overcut size was 50 mm (1.96 in.). The soil properties of the initial scenario are presented in Table 3-2.

Table 3-2 Initial Scenario Soil Properties

Soil Properties	Unit Weight kN/m^3 (lb/ft^3)	Cohesion kPa (psi)	Friction Angle (degree)	Modulus of Elasticity MPa (psi)
Value	17.4 (110.8)	20 (2.9)	34	12 (1740)

Model Dimensions

One of the concerns in building finite element models is selecting appropriate model sizes so that boundary conditions do not affect results. In this research, model width (W) was determined based on depth of the box from the surface (H_1) by conducting a sensitivity analysis on initial scenario.

Four scenarios with width (W) of $5H_1$, $6H_1$, $7H_1$, and $8H_1$ were generated in PLAXIS 2D and surface vertical displacement were compared. Figure 3-4 shows surface vertical displacement comparisons obtained from different scenario widths (W).

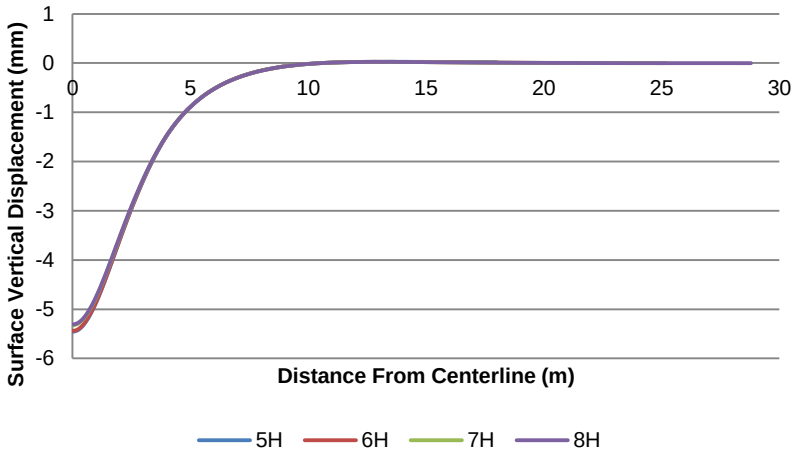

Figure 3-4 Surface Vertical Settlement in Scenarios with Different Widths

Maximum surface vertical displacements in scenarios are presented in Table 3-3. Results showed that boundary conditions affect the magnitude of surface vertical

displacement. It was observed that surface vertical displacement remains constant after width of $7H_1$. This indicated that minimum width (W) of $7H_1$ was required to prevent the effect of boundary conditions on results.

Table 3-3 Maxim Surface Displacements in Different Scenarios

Model Width (W)	**$5H_1$**	**$6H_1$**	**$7H_1$**	**$8H_1$**
Maximum Surface Displacement mm (in.)	-5.5 (-0.216)	-5.4 (-0.212)	-5.3 (-0.208)	-5.3 (-0208)

Mesh Size

Selecting an optimum mesh size is another concern in finite element modeling. Very coarse mesh size may not be able to calculate results accurately while very fine mesh size may take too long to converge and calculate results. A sensitivity analysis was conducted on the initial scenario to determine optimum mesh size.

Five mesh sizes including very coarse, coarse, medium, fine and very fine were considered in mesh size sensitivity analysis. Figure 3-5 shows comparison of surface vertical displacement results obtained from scenarios with different mesh sizes.

Figure 3-5 Surface Vertical Displacement Comparison with Different Mesh Sizes

Maximum surface vertical displacements for different mesh sizes and analysis times are presented in Table 3-4. Results showed that mesh size affects maximum surface vertical displacement and shape of the trough (channel). It was observed that surface displacement in model with fine mesh size was similar to the model with very fine mesh size. However, less analysis time was required for a model with fine mesh size than very fine size. This indicated that fine mesh size was the appropriate mesh size and can lead to accurate results and fast calculation.

Table 3-4 Maxim Surface Displacements for Different Mesh Sizes and Analysis Time

Mesh Size	Very Coarse	Coarse	Medium	Fine	Very Fine
Maximum Surface Vertical Displacement mm (in.)	-5.0 (-0.196)	-5.1 (-0.200)	-5.2 (-0.204)	-5.3 (-0.208)	-5.3 (-0.208)
Analysis time (sec)	63	70	82	104	146

Considering results, the final initial scenario was a model with width of $7H_1$ (25.2 m or 11.8 ft) with fine mesh sizes. Figure 3-6 illustrates initial scenario geometry and meshing. The width of $7H_1$ with fine mesh size was used to generate all models in this research.

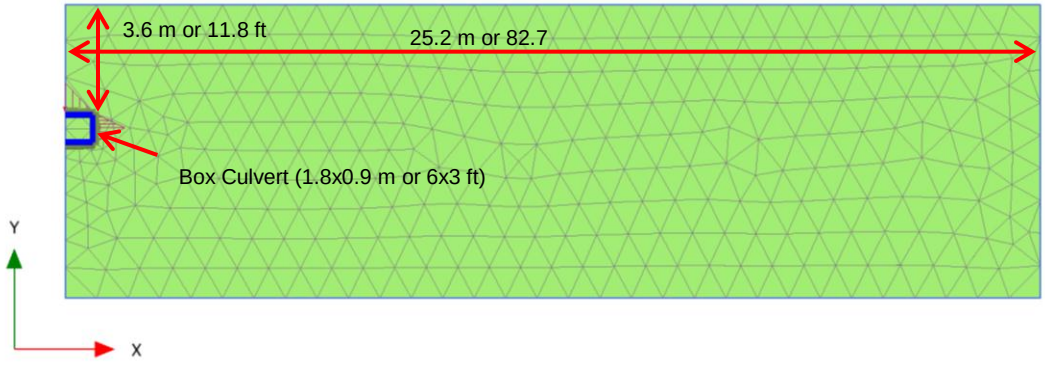

Figure 3-6 Final Initial Scenario Geometry and Meshing

Adopted Artificial Neural Network (ANN)

The feed forward back propagation method was adopted in this research to construct the neural network. Neural network code was written in MATLAB program. The code is presented in Appendix D. Three layers including input, hidden and output layers were considered to generate the network. Since the number of parameters in the input layer is eight, the number of neurons in hidden layer was assumed to be 1.5 x 8 = 12. A schematic figure of the artificial neural network is presented in Figure 3-7.

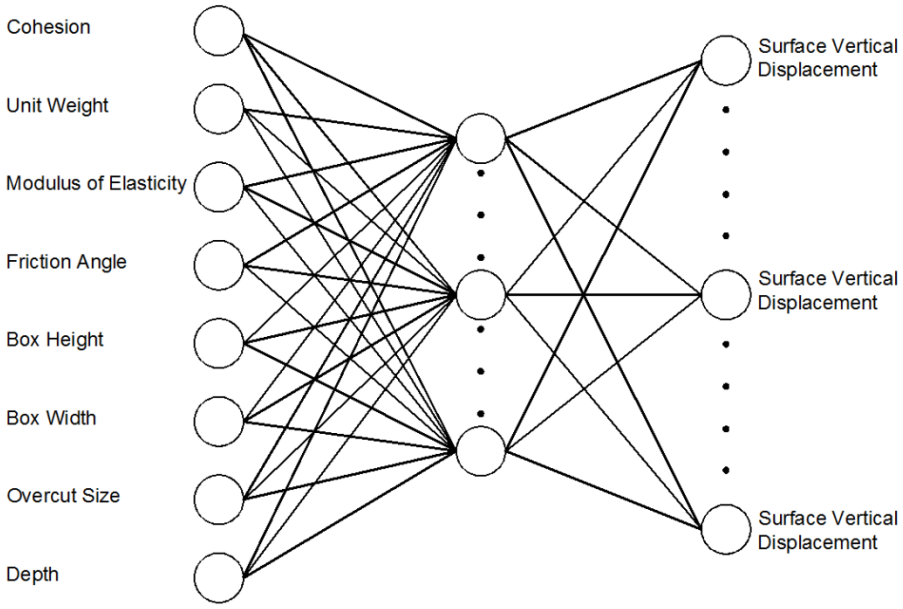

Figure 3-7 Schematic Neural Network in This Research

To train the neural network, all input and corresponding output values were stored in separate Excel files. Input values included cohesion, unit weight, modulus of elasticity, friction angle, box height, box width, overcut size, and depth of box values which were used to generate finite element models by PLAXIS 2D. Output values were calculated surface vertical displacements by PLAXIS 2D. Both input and output files contained 300 set of data. Since input layer had 8 parameters, 1.5x8 = 12 neurons were considered in the hidden layer.

As discussed in Chapter 2, all input data was divided into three categories including training, validation, and testing. After conducting a literature review, the data were determined to represent training, validation and testing at 70%, 15%, and 15% respectively.

To find the best transfer function in this research, four combinations of linear and sigmoid functions for input and output layers were considered in this research as follows:

1- Linear – Linear

2- Linear – Sigmoid

3- Sigmoid – Linear

4- Sigmoid – Sigmoid

The performance plots of each model were compared to find the most accurate model.

As discussed in Chapter 2, creating regression plots were the next step in validating the ANN model. Regression plots of all models were developed and compared to assure that the final ANN model was the most accurate model.

Verification Procedure

Two methods were considered in this research to verify the final ANN model:

1. New finite element models

2. Case Studies

New Finite Element Models

A similar procedure for generating main scenarios was followed to generate 22 new BJ projects. First 12 scenarios had the same box culvert sizes as the main scenarios but different soil properties, depths and overcut sizes. The rest of scenarios have completely different specifications. New scenarios were used to verify the final ANN model to assure that the model was able to predict the surface vertical displacement

accurately in other BJ projects where soil properties, box dimensions, depth and overcut size are different from training data sets. Table 3-5 presents new scenarios specifications

Table 3-5 New Scenarios Specifications

No.	Width x Height m (ft)	Overcut mm (in.)	Depth m (ft)	E MPa (psi)	ϕ (Degree)	γ kN/m^3(lb/ft^3)	c kPa (psi)
1	1.8X1.2 (6X4)	30 (1.18)	4.2 (13.8)	17 (2,465)	33	16.9 (108)	14.0 (2)
2	1.8X1.2 (6X4)	40 (1.57)	3.5 (11.5)	28.5 (4,132)	37	19.2 (122)	10.4 (1.5)
3	1.8X1.8 (6X6)	30 (1.18)	5.0 (16.4)	13 (1.185)	32	16.1 (102)	16.7 (2.4)
4	1.8X1.8 (6X6)	50 (1.97)	6.5 (21.3)	25.5 (3,697)	36	18.6 (118)	4.8 (0.7)
5	2.4X1.2 (8X4)	40 (1.57)	3.0 (9.8)	30.5 (4,422)	37	19.6 (125)	23.6 (3.4)
6	2.4X1.2 (8X4)	50 (1.97)	4.1 (13.5)	26.5 (3,842)	36	18.8 (120)	3.0 (0.4)
7	2.4X2.4 (8X8)	30 (1.18)	10.3 (33.8)	22 (3,190)	35	17.9 (114)	8.6 (1.2)
8	2.4X2.4 (8X8)	50 (1.97)	5.4 (17.7)	15 (2,175)	33	16.5 (105)	5.1 (0.7)
9	3X1.5 (10X5)	40 (1.57)	4.0 (13.1)	27 (3,915)	36	18.9 (120)	6.6 (1.0)
10	3X1.5 (10X5)	40 (1.57)	6.3 (20.7)	31.5 (4,567)	38	19.8 (126)	10.0 (1.6)
11	3X3 (10X10)	30 (1.18)	11.0 (36)	29.5 (4,277)	37	19.4 (124)	10.7 (1.6)
12	3X3 (10X10)	50 (1.97)	6.9 (22.6)	16.5 (2,392)	33	16.8 (107)	23.6 (3.4)
13	1.8X1.5 (6X5)	50 (1.97)	4.7 (15.4)	16.5 (2,392)	33	16.8 (107)	23.6 (3.4)
14	2X1.2 (7X4)	30 (1.18)	5.1 (16.7)	28.5 (4,132)	37	19.2 (122)	22.0 (3.2)
15	2X2.1 (7X7)	50 (1.97)	10.0 (32.8)	20 (2,900)	34	17.5 (111)	20.5 (3.0)
16	2.4X1.5 (8X5)	50 (1.97)	4.8 (15.7)	13.5 (1,957)	32	16.2 (103)	14.9 (2.2)
17	2.4X2.1 (8X7)	40 (1.57)	7.9 (25.9)	28 (4,060)	37	19.1 (122)	11.4 (1.7)
18	2.8X1.5 (9X5)	30 (1.18)	5.4 (17.7)	10.5 (1,522)	31	14.7 (94)	11.3 (1.6)
19	2.8X2.4 (9X8)	40 (1.57)	10.5 (34.4)	14 (2,030)	32	16.3 (104)	13.2 (1.9)
20	2.8X2.7 (9X9)	50 (1.97)	8.0 (26.2)	14.5 (2,102)	33	16.4 (104)	18.0 (2.6)
21	3X1.8 (10X6)	30 (1.18)	6.0 (19.7)	29.5 (4,277)	37	19.4 (124)	6.7 (1.0)
22	3X2.4 (10X8)	30 (1.18)	8.1 (26.6)	20.5 (2,972)	34	17.6 (112)	12.1 (1.8)

New scenarios were simulated using PLAXIS 2D and results were recorded. Then, inputs from new finite element models, Table 3-5, were given to the final ANN model to predict surface vertical displacement. Results obtained from the final ANN model and PLAXIS 2D were compared to assure that the results were in a good agreement with each other.

Case Studies

Two case studies were considered in this research to verify final ANN model. Project specifications, data collection procedure and collected data are fully discussed in Chapter 4. Required parameters (inputs) from case studies were given to the final ANN model to predict surface vertical displacement. Then results obtained from the model and case studies were compared.

Applicability of Empirical Method for BJ Project

Empirical method, suggested by Milligan and Marshall (1995), was adopted to calculate surface displacement associated with box jacking. Figure 3-8 shows ground loss (V_s) due to overcut in BJ project.

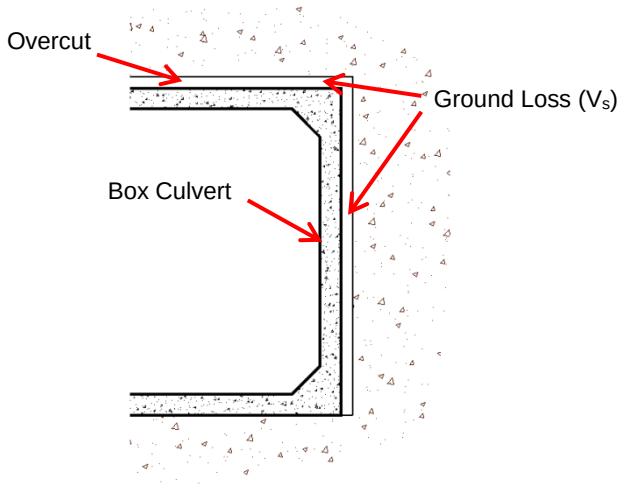

Figure 3-8 Ground Loss in BJ Projects

Generally, ground loss is defined as the area of the annular space around the pipe or box culvert. Although Equation 2-15 was originally suggested for circular pipe culverts, the same concept was adopted to calculate the ground loss in rectangular shape culvert (box culvert).

Table 3-6 presents empirical method parameters for new finite element models. Empirical method parameters for two case studies are presented in Chapter 4.

Table 3-6 Empirical Method Parameters for New Finite Element Models

Scenario #	Ground loss (V_s) m^2 (ft^2)	i, m (ft)	S_{max} mm (in.)
1	0.0621 (0.67)	1.2 (3.9)	-20.3 (-0.8)
2	0.0824 (0.89)	1.0 (3.2)	-32.1 (-1.3)
3	0.0801 (0.86)	1.5 (4.9)	-20.9 (-0.8)
4	0.1325 (1.43)	2.0 (6.4)	-27.2 (-1.1)
5	0.0944 (1.02)	0.9 (2.9)	-42.5 (-1.7)
6	0.1175 (1.26)	1.2 (3.9)	-39.3 (-1.5)
7	0.1071 (0.15)	3.1 (10.2)	-13.8 (-0.5)
8	0.1775 (1.91)	1.7 (5.6)	-41.1 (-1.6)
9	0.1184 (1.27)	1.2 (3.9)	-39.1 (-1.5)
10	0.1184 (1.27)	1.9 (6.2)	-25.5 (-1.0)
11	0.1341 (1.44)	3.4 (11.1)	-15.9 (-0.6)
12	0.2225 (2.39)	2.2 (7.2)	-39.9 (-1.6)
13	0.1175 (1.26)	1.4 (4.6)	-33.4 (-1.3)
14	0.0651 (0.70)	1.5 (4.9)	-17.6 (-0.7)
15	0.1525 (1.64)	3.0 (9.8)	-20.5 (-0.8)
16	0.1325 (1.43)	1.4 (4.6)	-37.0 (-1.5)
17	0.1304 (1.40)	2.4 (7.9)	-21.9 (-0.9)
18	0.0861 (0.93)	1.6 (5.2)	-21.5 (-0.8)
19	0.1504 (1.62)	3.2 (10.5)	-19.1 (-0.8)
20	0.2025 (2.18)	2.5 (8.2)	-32.4 (-1.3)
21	0.0981 (1.06)	1.8 (5.9)	-21.7 (-0.9)
22	0.1161 (1.25)	2.5 (8.2)	-18.7 (-0.7)

Inflection point, i, was calculated using Equation 2-9 suggested by O'Reilly and New (1982) for granular soils. The maximum surface settlement, S_{max}, was calculated using Equation 2.16, suggested by Marshall and Milligan (1995).

Chapter Summary

This chapter discussed the methodology of the research and presented Finite Element Modeling (FEM) procedure adopted in this research to simulate box jacking operation. An investigation was conducted to determine the minimum width of model and optimum mesh size. Artificial Neural Network (ANN) model parameters and details were presented at the end of the chapter. Verification procedure, adopted in this research, was discussed. At the end, the methodology used to calculate surface displacement using available empirical methods was presented.

Chapter 4

Case Studies

Introduction

In this chapter, specifications of two box jacking projects are presented. One of the projects was located in Vernon, TX and the other one was in Navarro County, TX. Soil tests and their results for each project are discussed. Data collection procedures and equipment are presented. Ground movements data collected from two projects are used to verify final model in this research.

Case Study 1: Vernon Project

The location of the Vernon project was in the City of Vernon, northwest of Wichita Falls, Texas, under US Highway 287 (Figure 4-1). The purpose of this project was to alleviate the flood problem on the upstream side of the highway facility. TxDOT's Wichita Falls District decided to install a 1.8 m × 1.2 m (6 ft x 4 ft) box culvert to improve channel capacity at the depth of 6.7 m (22 ft) from the surface to top of the box.

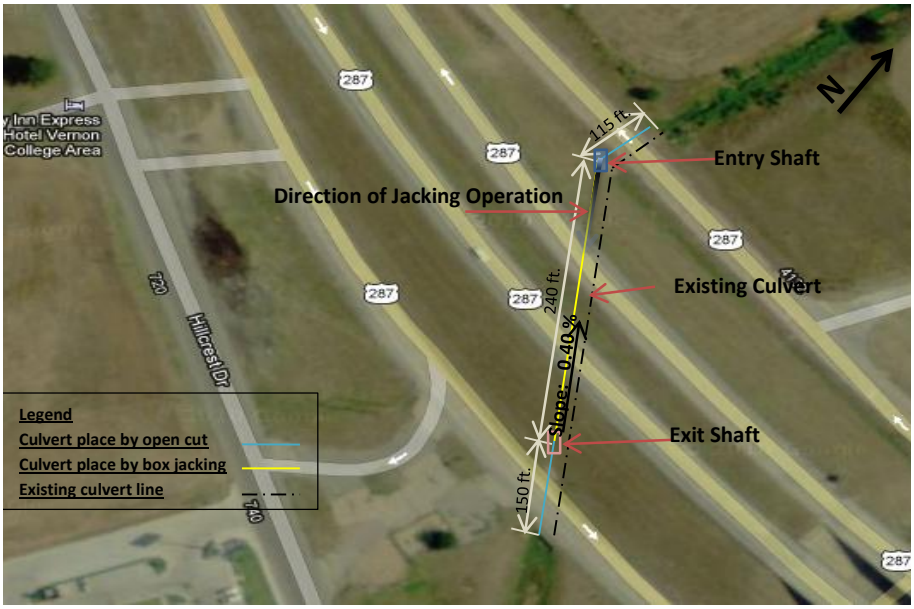

Figure 4-1 Vernon Project Location (Tavakoli, 2012)

Box Jacking (BJ) Operation

Before starting the jacking operation, the contractor made two reinforced concrete columns and a reinforced concrete wall behind the launch shaft to stabilize the existing soil and prevent soil movement during the jacking operation. Then the launch shaft was excavated and jacks were placed into it. The size of the launch shaft was 5.2 m x 3.96 m (17 ft x 13 ft) with a 3.66 m (12 ft) depth.

Before the main jacking operation began, a leveling pad was placed under the new box lower level to prevent boxes from sinking. First, a 1.2 m x 1.2 m (4 ft x 4 ft) hole was excavated and then a 1.2 m x 122 mm (4 ft x 4.8 in) leveling pad was placed as a support for the new box culvert as shown in Figure 4-2. The number of leveling pads needed depends on the size of the box culverts as large boxes require up to two pilot holes.

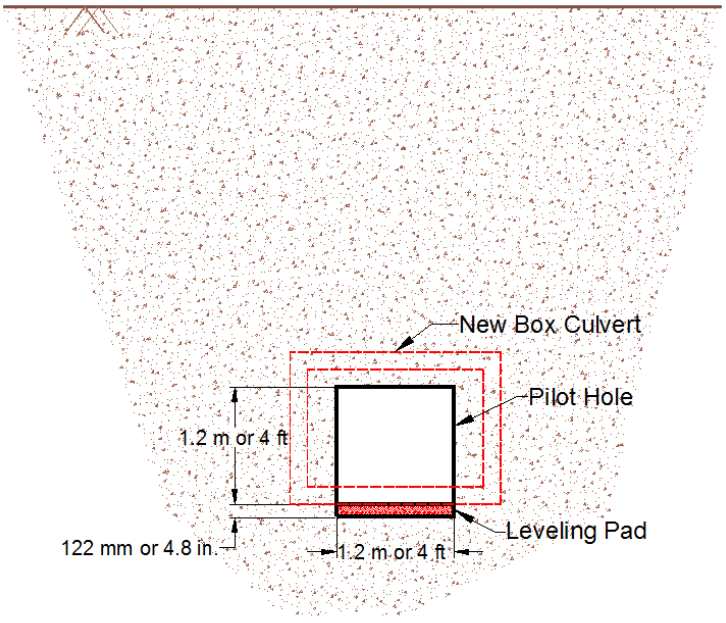

Figure 4-2 Pilot Hole and Leveling Pad for New Box Culverts

Geotechnical Investigation

A geotechnical investigation was conducted in connection with the design and construction of a new box culvert at US 287 Vernon project locations. This study included drilling and sampling three (3) borings (B-1, B-2 & B-3) of 7.62 m, 15.24 m, and 6 m (25 ft, 50 ft and 20 ft) respectively for the Vernon project location.

A minimum of one boring is recommended per 30.5 m (100 ft) interval for linear projects with minor width and volume. Borings for soil investigation should extend a minimum of 4.5 m (15 ft) below the invert level of culvert (U.S. Army Corps of Engineers, 2003). Hence, a minimum of three sampling points were recommended for the U.S. 287 project locations in Vernon. Figure 4-3 illustrates boring locations of the project.

Figure 4-3 Borehole Locations at Vernon Project

Sieve Analysis

Sieve analysis was conducted on the samples collected in SPT. Soil was classified using Unified Soil Classification System (USCS). Table 4-1 presents soil gradation results obtained by sieve analysis and corresponding USCS classifications.

Table 4-1 Sieve Analysis Results for Vernon Project

Sample ID	Soil Depth, m (ft)	Soil Gradation %				USCS Classification	
		Gravel	Sand	Silt	Clay	Group Name	Group Symbol
B1	0.15-1.2 (0.5-4)	0	53	47	0	Silty Sand	SM
	1.5-1.98 (5-6.5)	0	43	56	2	Sandy Silt	ML
	5.6-6.1 (18.5-20)	0	95	5	0	Poorly Graded Sand	SP
B2	0.76-1.2 (2.5-4)	0	40	49	11	Sandy Lean Clay	CL
	1.5-2 (5.0-6.5)	0	72	26	2	Silty Sand	SM
	2.6-3 (8.5-10)	0	90	10	0	Poorly Graded Sand with Silt	SP-SM
	10.2-10.7 (33.5-35)	5	75	19	1	Silty Sand	SM
	13.2-13.7 (43.5-45)	9	73	17	1	Silty Sand	SM
	14.8-15.2 (48.5-50)	18	62	19	1	Silty Sand with Gravel	SM
B3	0.15-0.6 (0.5-2.0)	19	60	20	1	Silty Sand with Gravel	SM
	0.76-1.2 (2.5-4)	0	66	33	1	Silty Sand	SM
	5.6-6.1 (18.5-20)	0	70	28	2	Silty Sand	SM

As sieve analysis results shows in Table 4-1, the dominant soil was sandy soil that contains silt, and gravel at some locations.

Standard Penetration Test (SPT)

SPT was conducted in the field to determine N_{60} at different depths. The size of the borehole in the test was 4 in. and a split-spoon sampler was used to collect samples. Safety hammer-type equipment was used during the test. Considering the conducted SPT specifications and available correction factors discussed in previous section, the SPT values obtained from the field can be used without any corrections. Table 4-2 presents SPT values (N_{60}) obtained in Vernon project.

Table 4-2 SPT Results Obtained for Vernon Project

Sample ID	**Soil Depth, m (ft)**	**N_{60}**
B1	0.15-1.2 (0.5-4.0)	50
	1.2-4.9 (4.0-16.0)	35
	4.9-6.1 (16-20)	24
B2	0.15-0.3 (0.5-1)	50
	0.3-1.5 (1-5)	29
	1.5-2 (5-6.5)	33
	2-10.5 (6.5-34.5)	25
	10.7-11.9 (35-39)	50
	12.2-13.4 (40-44)	35
	13.4-14.9 (44-49)	25
	14.9-15.2 (49-50)	43
B3	0.15-5.5 (0.5-18.0)	38
	5.5-6.1 (18-20)	42

Unconfined Compressive Strength (UCS) Test

UCS test was conducted to determine undrained cohesion values. Table 4-3 presents unconfined compressive strength and undrained cohesion.

Table 4-3 UCS Test Results for Vernon Project

Sample ID	Soil Depth, m (ft)	Unconfined Compressive Strength (q_u), kPa (psi)	Undrained Cohesion (c_u), kPa (psi)
B1	2.4-3 (8.0-10)	121.7 (17.6)	61 (8.8)
	3.9-4.6 (13-15)	135.5 (19.6)	68 (9.8)
B2	1.5-2.1 (5-7)	89.5 (13)	45 (6.5)
	2.4-3 (8-10)	87.5 (12.7)	44 (6.4)
	4.1-4.6 (13.5-15)	100 (14.5)	50 (7.3)
	5.6-6.1 (18.5-20)	114 (16.5)	57 (8.3)
	7.2-7.6 (23.5-25)	260 (37.7)	130 (18.9)
	8.5-9.1 (28-30)	86 (12.5)	43 (6.3)

Soil Properties

Considering geotechnical reports and soil tests results, soil properties was calculated using SPT relationships as presented in Table 4-4.

Table 4-4 Soil Properties of Vernon Project

ID	Depth m (ft)	Soil Type	N_{60}	Friction Angle (Degree)	Modulus of Elasticity, MPa (psi)	Unit Weight, kN/m^3 (lb/ft^3)	Cohesion, kPa (psi)
B1	0-1.2 (0-4)	SM	50	38	16.8 (2,436)	20 (127)	23 (3.3)
	1.2-4.8(4-16)	ML	35	30	80 (11,600)	19 (121)	64 (9.3)
	4.8-12.2(16-40)	SP	24	34	19.5 (2,827)	17.5 (111)	2 (0.3)
B2	0-1.2(0-4)	CL	29	20	20 (2,900)	20 (127)	45 (6.5)
	1.2-12.2(4-40)	SM	30	35	10.8 (1,566)	18 (114)	10 (14.5)
B3	0-12.2(0-40)	SM	40	37	13.8 (2,001)	19 (121)	15 (2.2)

Project Instrumentation

A Pressure Transducer was used to record the jacking loads applied during the box culvert installation process. A Total Station survey instrument and Horizontal Inclinometers (HI) were used to record the movement of the overlying pavement and adjoining soil around the box culvert.

Pressure Transducer

A Geokon Model 4500H pressure transducer, illustrated in Figure 4-4, was used for measurement of the jacking loads applied to the box culvert during the installation process. It was coupled directly into the hydraulic line of the jacking machine. This device basically converts an applied pressure into an electrical signal that was recorded into a laptop computer that was onsite. The data sheet of the pressure transducer is presented in Appendix E.

Figure 4-4 Geokon Model 4500H Pressure Transducer (GEOKON, 2014)

Total Station and Survey Points

A Total Station TC407 survey instrument was used to measure the existing pavement surface to record settlement and/or heave. Four shoulder points (Points A, B, C and D) were selected as shown in Figure 4-5.

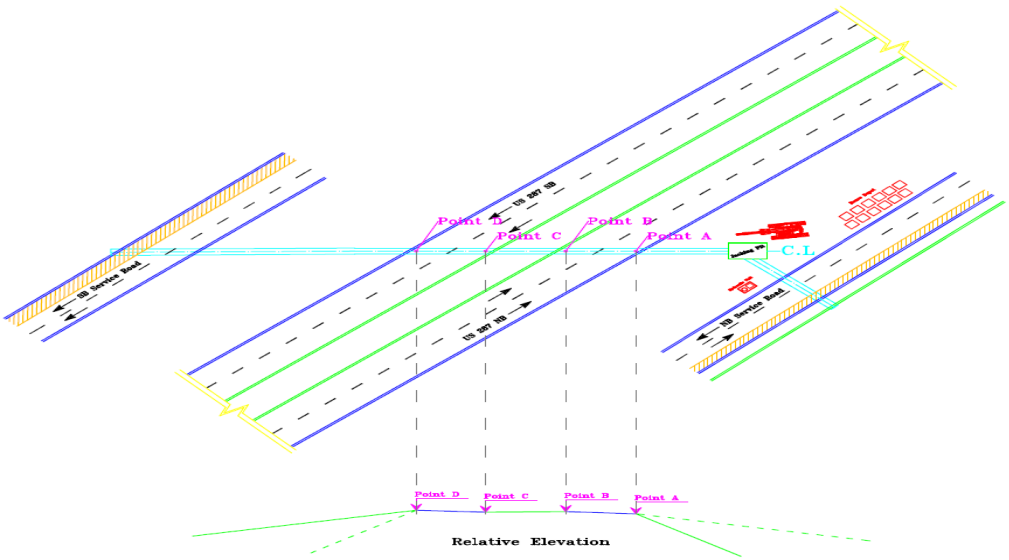

Figure 4-5 Total Station Points (Tavakoli, 2012)

Horizontal Inclinometer (HI)

Durham Geo Enterprises, Inc.'s Horizontal Inclinometer (HI) system was used to monitor settlement and/or heave around existing and new culverts. Typical applications of HI include monitoring settlement and heave under storage tanks, embankments, dams, and landfills. The HI employs a force-balanced servo-accelerometer that measures inclination from horizontal (vertical) in the plane of the probe wheels. A change in inclination indicates that movement has occurred. The amount of movement is calculated by finding the difference between the current inclination reading and the initial reading and converting the result to a vertical distance (DGSI, 2013). This system consisted of

inclinometer casings, a horizontal probe, control cable, and a readout unit (Figure 4-6). HI's data sheet containing more information is presented in Appendix F.

Figure 4-6 Horizontal Inclinometer Data Collection System (DGSI, 2013)

To measure the soil movement in the vicinity of the box jacking operation, three 85 mm (3.34 in.) casings were installed on each side of the highway for inclinometer testing. Figure 4-7 illustrates casings locations on north side of the project.

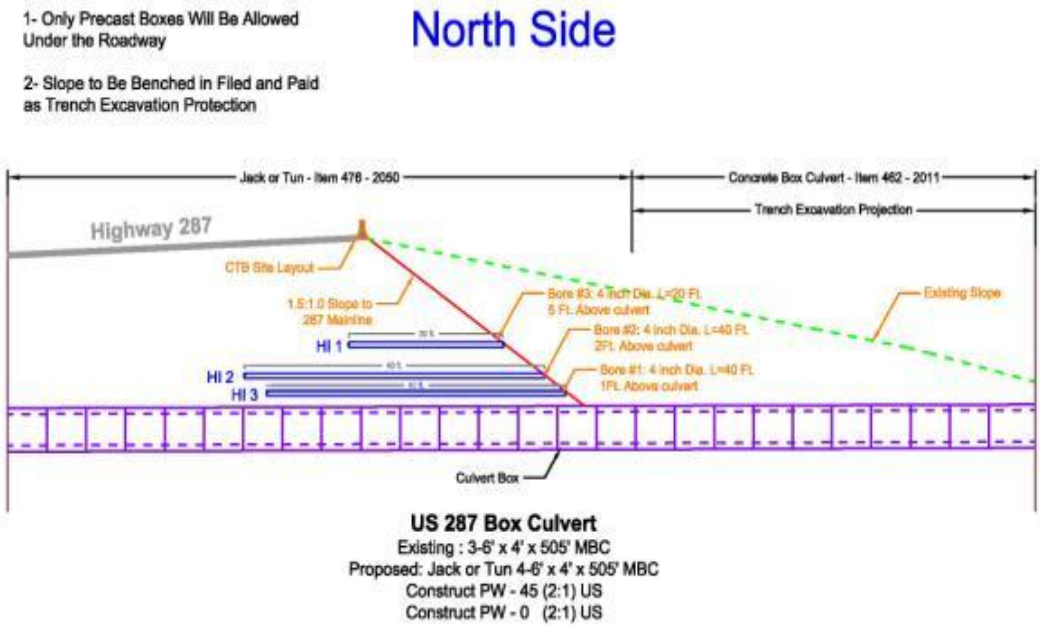

Figure 4-7 Inclinometer Installation Plan North Side (Tavakoli, 2012)

Figure 4-8 illustrates casings locations on south side of the project.

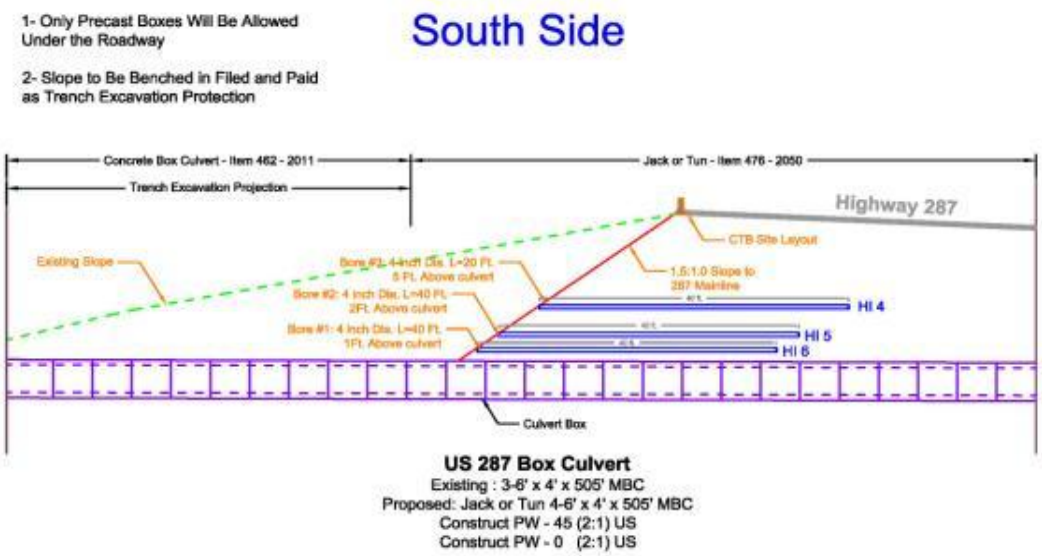

Figure 4-8 Inclinometer Installation Plan South Side (Tavakoli, 2012)

To place casings, a Horizontal Directional Drilling (HDD) rig was used as shown in Figure 4-9.

Figure 4-9 HDD Rig Set to Drill Hole (Tavakoli, 2012)

After the casings were installed, grout slurry was injected around the casings and allowed to harden, and then a survey was conducted by pushing the horizontal probe using PVC pipe to the far end embedded in the embankment and then drawing it back to the open end of the casing. The location of each casing in both the North and South sides are presented in Figure 4-10 and Figure 4-11 respectively.

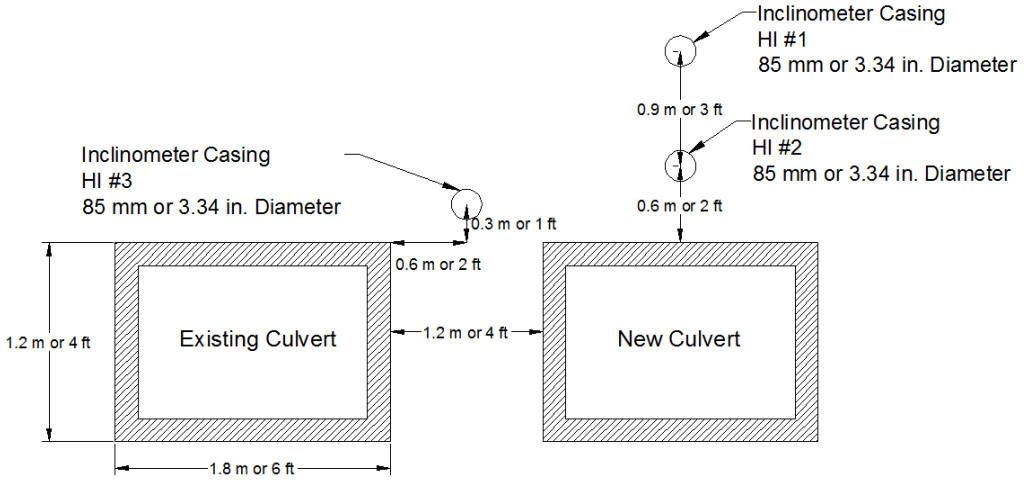

Figure 4-10 North Side Casings

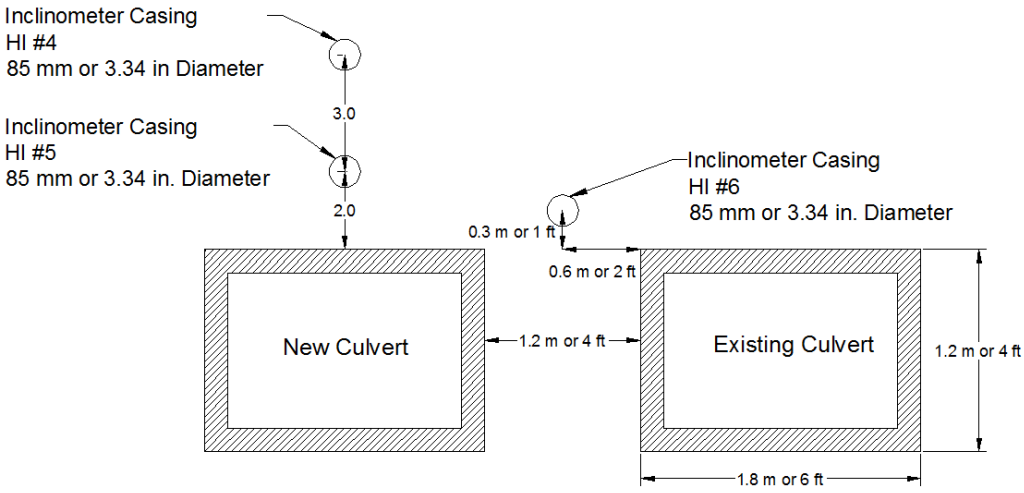

Figure 4-11 South Side Casings

Data was recorded each 2 ft (0.61 m) starting at the far end and proceeding until exposed at the opening. The number of data collected from each casing was dependent on its length. For example, for a casing with a length of 40 ft (12.2 m), and data at 20 points was recorded. Once the probe was extracted, it was rotated and inserted again to take readings at the same 2 ft (0.61 m) increments. Two additional repetitions were performed to establish a baseline for future collected data. This process was used per the manufacturer's instructions. This was termed as one survey. The first survey established the initial profile of the casing. Subsequent surveys revealed changes in the profile (vertical direction) if ground movement occurred. The length of each casing is shown in Table 4-5.

Table 4-5 Length of Casings

HI #	**During Construction m (ft)**	**After Completion m (ft)**
1	6.1(20)	12.2 (40)
2	12.2 (40)	12.2 (40)
3	12.2 (40)	18.3 (60)
4	12.2 (40)	18.3 (60)
5	12.2 (40)	18.3 (60)
6	12.2 (40)	18.3 (60)

Collected Data and Measures

Pressure Transducer

The intermediate jacking station was a fabricated steel cylinder fitted with hydraulic jacks that was incorporated between two pipe/ box segments. Its function was to distribute the jacking load over the box string on long drives to decrease the total jacking forces exerted on the thrust block and box sections near the shaft opening (Najafi, 2013). The maximum applied force was 574 tons (510 metric tons). The jacking

force was increased with length of the BJ and then was reduced significantly due to use of intermediate jacking station. Figure 4-12 readings from the transducer.

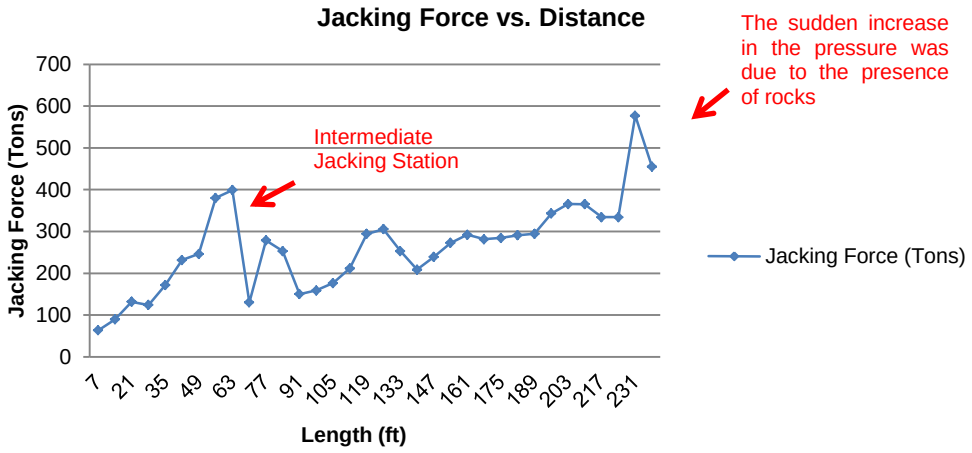

Figure 4-12 Jacking Pressure vs. Distance (Tavakoli, 2012)

Surface Displacements

Surface displacements were collected by Total Station during construction. Table 4-6 presents

Table 4-6 Total Station Readings

Date	Relative Elevations, mm (in.)			
	Point A	Point B	Point C	Point D
August 29, 2012	30 (1.20)	173 (6.84)	289 (11.40)	34 (1.32)
September 12, 2012	34 (1.32)	176 (6.96)	289 (11.40)	36 (1.44)
September 18, 2012	34 (1.32)	176 (6.96)	290 (11.40)	39 (1.56)
September 20, 2012	37 (1.44)	176.8 (6.96)	292 (11.52)	39 (1.56)
September 22, 2012	37 (1.44)	179 (7.08)	292 (11.52)	39 (1.56)
September 24, 2012	40 (1.56)	179.8 (7.08)	292 (11.52)	42 (1.68)
September 26, 2012	40 (1.56)	183 (7.20)	296 (11.64)	42 (1.68)

Underground Soil Displacements

Underground soil displacements due to BJ process were measured by Horizontal Inclinometer (HI). Table 4-7 shows the maximum displacements in all of the casings during project execution.

Table 4-7 Maximum Displacements

Location	HI #	Maximum Displacements, mm(in.)
North Side	1	13.2 (0.5)
	2	27.6 (1.1)
	3	13 (0.5)
South Side	4	8.9 (0.4)
	5	20.1 (0.8)
	6	8.2 (0.3)

According to Table 4-7, the maximum displacement in the horizontal casings on the North and South sides of the highway occurred in HI #2 and HI #5 respectively. HIs #2 and #5 were located 2 ft (0.61 m) above the new box culvert on the North and South side respectively.

Finite Element Modeling (FEM)

As discussed before, three (3) bore samples (B1, B2, and B3) were collected from the Vernon Project. Therefore, three (3) corresponding scenarios (Scenario 1, Scenario 2, and Scenario 3) were generated in PLAXIS 2D. Finite element models were generated to simulate jacking a 1.8 m x 1.2 m (6 ft x 4 ft) box underground. The depth of box culvert (H_1) was 6.7 m (22 ft).

As discussed before, the width of the finite element model (W) should be $7H_1$. Therefore, the width of scenario #1 through #3 was $7H_1 = 7 * 6.7 \approx 47$ m (154 ft). The overcut size in Vernon project was 50 mm (1.97 in.).

Figure 4-13 (a) through (c) shows finite element modeling of Scenario 1, Scenario 2, and Scenario 3.

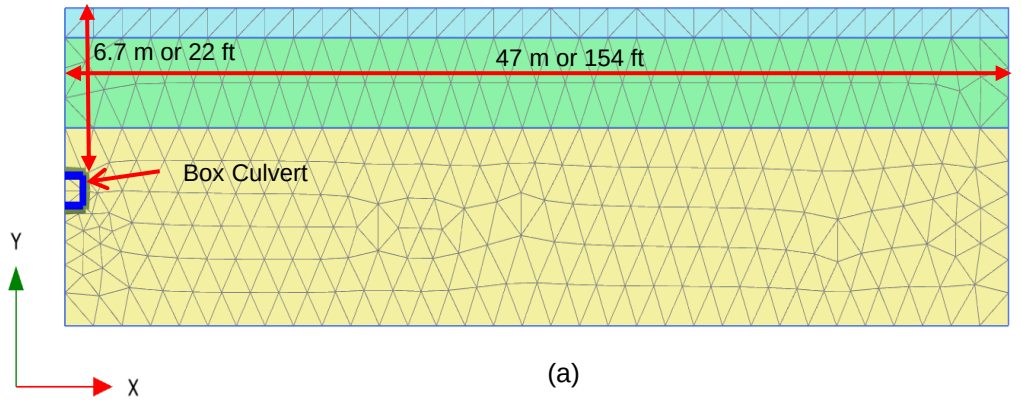

(a)

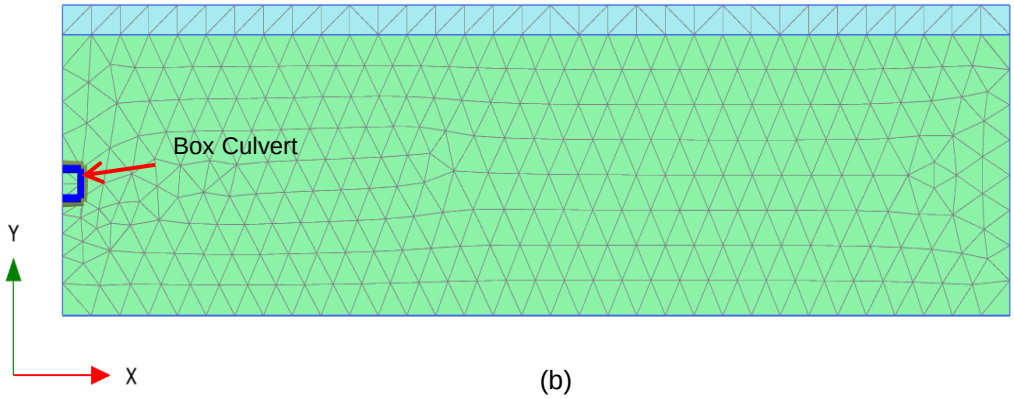

(b)

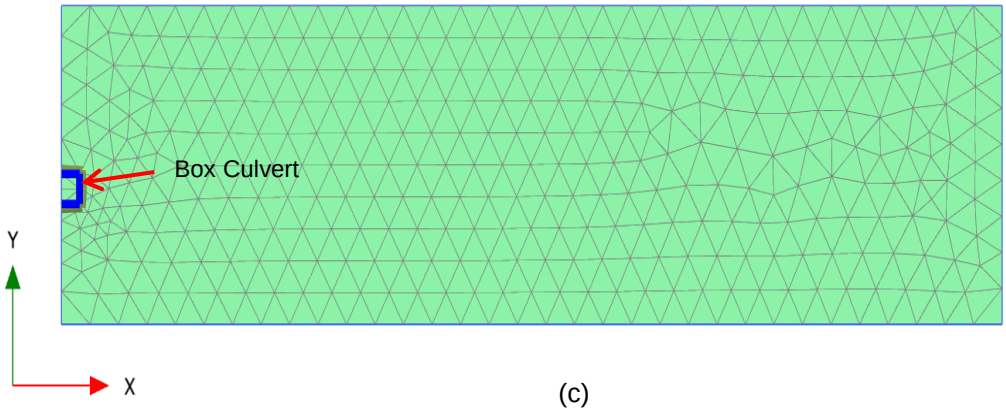

(c)

Figure 4-13 Finite Element Modeling a) Scenario 1, b) Scenario 2, and c) Scenario 3

Soil layers in all scenarios settled because of ground loss due to soil collapse into the annular space around the box as presented in Figure 4-14.

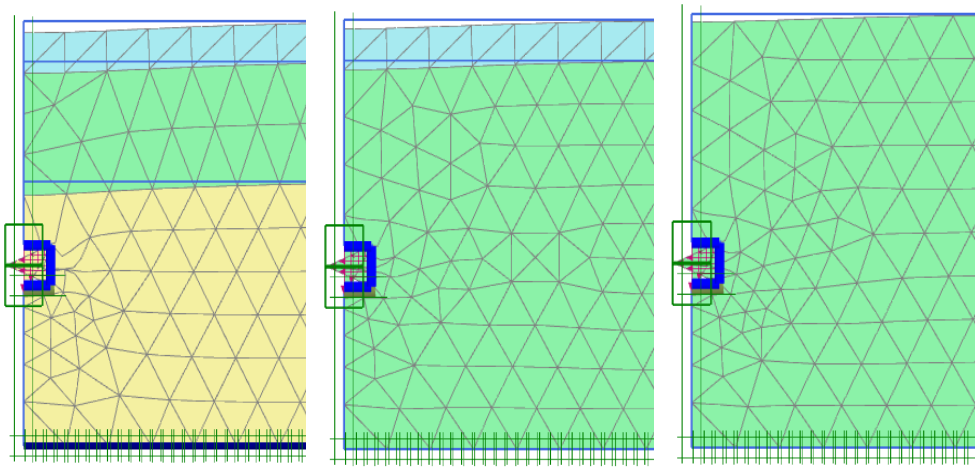

(a) (b) (c)

Figure 4-14 Soil Displacement a) Scenario 1, b) Scenario 2, and 3) Scenario 3

Table 4-8 shows vertical displacements at different locations

Table 4-8 Results Obtained from PLAXIS and Field Measurements

Project Locations	**Point Location**	**Vertical Displacements mm (in.)**	
		PLAXIS	**Field**
North Side (Scenario 1)	Surface	-12.03 (-0.5)	-10 (-0.4)
	HI #1	-14.65 (-0.6)	- 13.2 (-0.5)
	HI #2	-31.64 (-1.2)	-27.6 (-1.1)
	HI #3	-14.42 (-0.6)	- 13 (-0.5)
Middle (Scenario 2)	Surface (Point B)	-8.82 (-0.3)	-10 (-0.4)
	Surface (Point C)	-8.82 (-0.3)	-7 (-0.3)
South Side (Scenario 3)	Surface	-6.77 (-0.3)	-8.5 (-0.3)
	HI #4	-11.67 (-0.5)	-8.9 (-0.4)
	HI #5	-15.6 (-0.6)	-20.1 (-0.8)
	HI #6	-6.51 (-0.3)	-8.2 (-0.3)

It is observed that ground movements obtained from PLAXIS model in north side are higher than collected data from the field. This is probably due to injecting bentonite slurry during the project execution. Bentonite slurry is injected into the annular space to reduce the friction force between the box culvert and surrounding soils. However, the pressure of the slurry can prevent the soil from fully collapsing into the annular space and consequently reduce associated ground movements.

Vertical displacement at HI #3, which was located 0.3 m (1 ft) above the box culvert, was less than the one at HI #2, which was located 0.61 m (2 ft) above the box culvert. This indicates that vertical displacement not only decreases vertically away from the top of the box culvert, but also decreases away horizontally from box culvert centerline. The same trend is observed for HI #6 and HI #5 which are located at south side of the project as well. This confirms that the vertical displacement dependency on depth suggested by Martos (1958) for pipe jacking and tunneling and illustrated in Figure 2-3 can be applied for BJ projects.

Empirical Method Parameters

To examine the applicability of empirical method for BJ project, as discussed in Chapter 3, empirical method parameters were calculated for Vernon project.

Ground loss (V_s), maximum surface displacement and inflection point were 0.0825 m^2 (0.89 ft^2), 16.9 mm (0.67 in.), and 1.952 m (6.4 ft) respectively

Case Study 2: Navarro County Project

Another BJ project was conducted in Navarro County, TX. The work scope was to install a 2.7 m x 1.2 m (9 ft x 4 ft) box under an existing railroad. The depth of the box culvert from the ground surface to top of the box culvert was 1.8 m (6 ft).

Due to small size of box culvert, hand mining method was used to excavate the bore. The overcut size was 50 mm (1.98 in.) Figure 4-15 shows a box culvert used in the project.

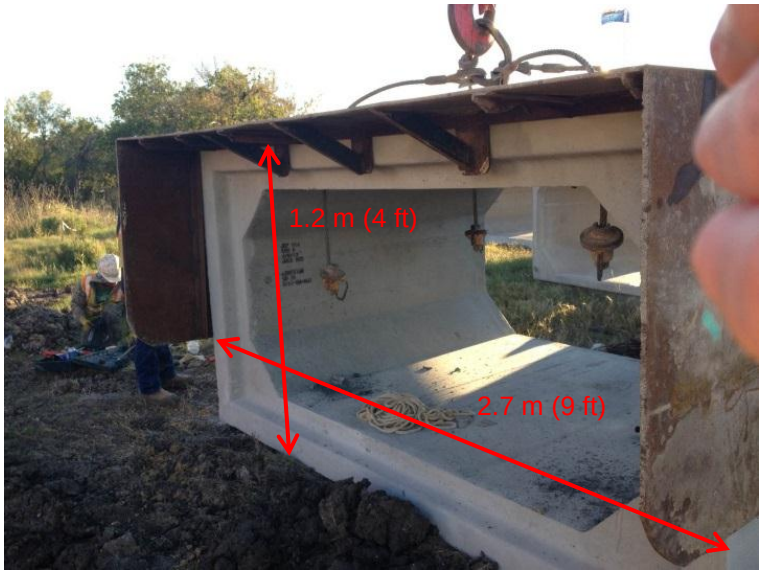

Figure 4-15 Schematic Box Cross Section of Navarro County Project

The size of the overcut was 50 mm (1.97 in.). In situ SPT using safety hammer type was conducted to determine N value. Atterberg limits were determined. Table 4-9 presents SPT results and Atterberg limits in Navarro Country project.

Table 4-9 SPT Results and Atterberg Limits for Navarro County Project

Depth, m (ft)	Material Description	USCS Symbol	N-Value	Atterberg Limits			Fines Content (%)
				Liquid Limit	Plastic Limit	Plastic Index	
0-1.2 (0-4)	Poorly Graded Sand with Clay and Gravel	SC-SM	26	18	12	6	28
1.2-2.4 (4-8)			10	-	-	-	28
2.4-4.3 (8-14)			45	22	16	6	28

Soil properties were calculated using available relationships between SPT results and soil properties. Since the hammer type was safety, C_E value was 1, therefore, SPT values used to derive soil properties without any modification. Table 4-10 presents calculated soil properties for Navarro project.

Table 4-10 Soil Properties for Navarro County Project

Depth, m (ft)	N_{60}	Friction Angle, Degree	Unit Weight kN/m^3 (lb/ft^3)	Modulus of Elasticity MPa (psi)	Cohesion kPa (psi)
0-1.2 (0-4)	26	34.5	17.6 (112)	13.12 (1,902)	7 (1)
1.2-2.4 (4-8)	10	32	16 (102)	8 (1,160)	7 (1)
2.4-4.3 (8-14)	42	37.2	19.5 (124)	19.2 (2,784)	10 (1.45)

To monitor surface settlement during project execution, 15 points (six sets) were selected and marked along the BJ alignment (Figure 4-16). Distance between points in each set was 1.2 m (4 ft). A total station was used to collect surface displacement data from control points.

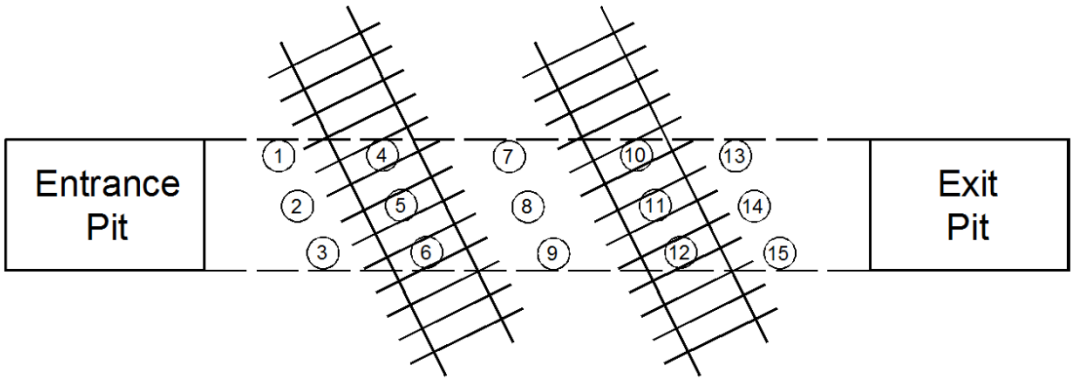

Figure 4-16 Location of Control Points

Table 4-11 presents control points displacement in Navarro County project. Figure 4-17 illustrates surface vertical displacement at control points.

Table 4-11 Surface Vertical displacement in Navarro County Project

Set #	Point #	Distance from Centerline m (ft)	Vertical Displacement mm (in.)
Set 1	1	-1.2 (-3.3)	-11.2 (-0.44)
	2	0	-24.5 (-0.96)
	3	1.2 (3.3)	-9.5 (-0.37)
Set 2	4	-1.2 (-3.3)	-9.3 (-0.36)
	5	0	-23.4 (-0.92)
	6	1.2 (3.3)	-10.2 (-0.4)
Set 3	7	-1.2 (-3.3)	-12.1 (-0.48)
	8	0	-30.2 (-1.19)
	9	1.2 (3.3)	-9.4 (-0.37)
Set 4	10	-1.2 (-3.3)	-11.3 (-0.44)
	11	0	-20.3 (-0.8)
	12	1.2 (3.3)	-10.8 (-0.43)
Set 5	13	-1.2 (-3.3)	-12.1 (-0.48)
	14	0	-22.4 (-0.88)
	15	1.2 (3.3)	-9.4 (-0.37)

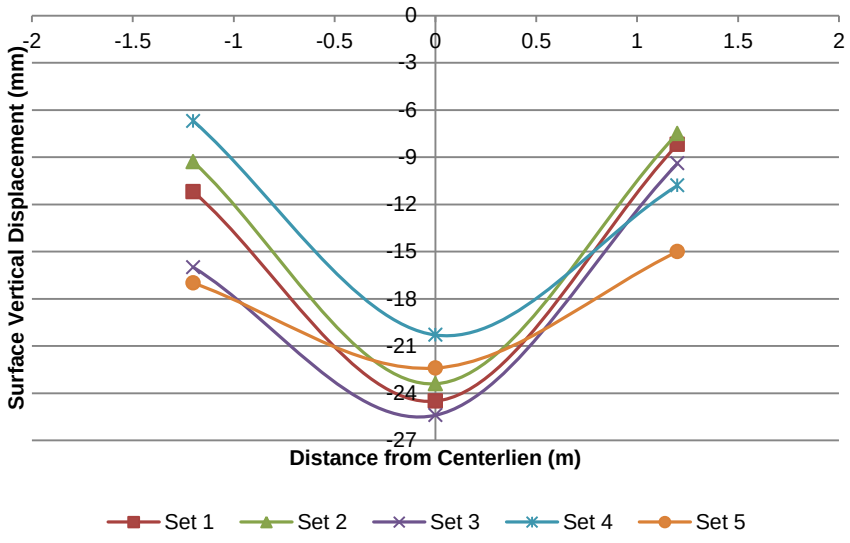

Figure 4-17 Surface Vertical Displacement at Control Points

Finite Element Modeling (FEM)

Three soil layers and their properties were used to generate finite element model of Navarro County project. The length of the model (W) was considered $7H_1$ = 7x1.8 m (5.9 ft) ≈ 13 m (42.7 ft). Since the whole project was modeled in PLAXIS, total length of model was 13 m x 2 = 26 m (85.3 ft). Figure 4-18 shows generated model and associated soil layers in PLAXIS.

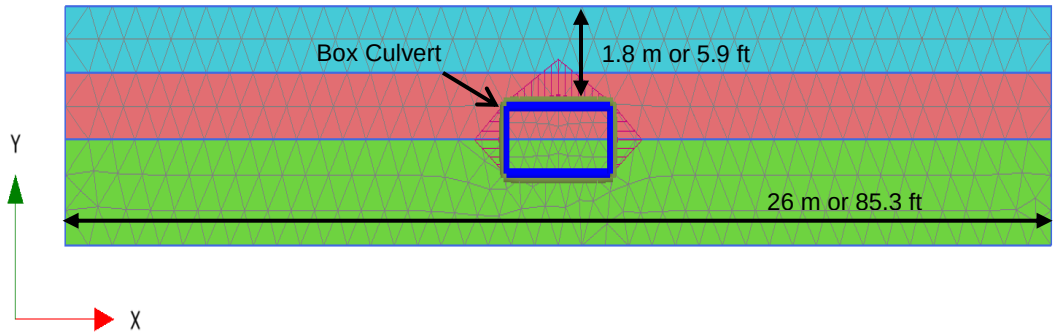

Figure 4-18 Navarro County Project Finite Element Model

Soil layers were settled due to collapsing soil into the annular space. Figure 4-19 illustrates soil deformation in different soil layers.

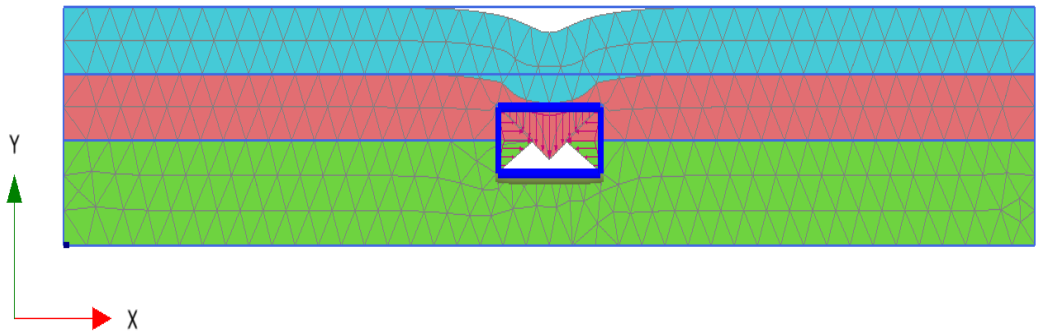

Figure 4-19 Soil Deformation in Navarro County Project

Results obtained from PLAXIS were compared with collected data from the project. Since 5 sets of data were collected from the field, PLAXIS results were compared

with average collected data. Figure 4-20 illustrates comparison of surface vertical displacement obtained from PLAXIS 2D model with collected data from the project.

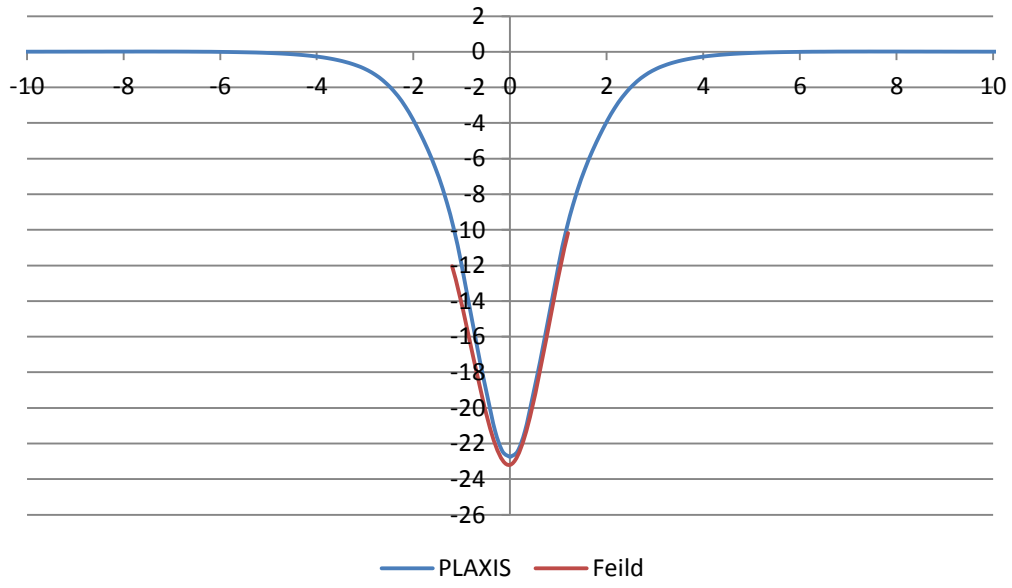

Figure 4-20 Comparison of Surface Vertical Displacement

Empirical Method Parameters

V_s, i, and S_{max} needed to be determined to obtain results using empirical method. Ground loss (V_s), inflection point (i), and maximum surface displacement was 0.131 m^2 (1.41 ft^2), 0.552 m (1.8 ft), and 94.9 mm (3.7 in).

Chapter Summary

This chapter presented details of two box jacking projects. Ground movements' data and soil tests results were discussed for both projects. Adopted Finite Element Modeling (FEM) procedures to simulate BJ process were presented. Finally, the methodologies to calculate empirical methods parameters were discussed.

Chapter 5

Results and Discussion of Results

Introduction

Two box jacking projects to verify final ANN model were presented in previous chapter. This chapter presents sensitivity analysis results, discusses arching effect in BJ projects and evaluates the applicability of suggested method in this research for different BJ projects.

Arching Effect in BJ Projects

Stress measurement on top of box culvert indicted that vertical stresses changed after box installation. This is because the surrounding soils collapsed into the annular space (overcut). According to Marston's theory presented in Chapter 1, all types of scenarios in this research are classified as positive project box culverts since box culverts were installed above the ground surface level. Collapsing of soil into the annular space creates an active arching since the annular space is compressible compared to the surrounding soils. Therefore, arching effect causes the load, due to soil prism weight above the culvert, to reduce.

According to Terzaghi's theory, the arching effect extends to the ground surface in all scenarios since the depth of the box culvert from ground surface to the top of box (H_1) in all models and case studies were less than 5 times of half of yielding strip width ($5B_1$),.

New Finite Element Models

Scenario #3 from new finite element models was selected to investigate arching effects in BJ projects. Scenario #3 was a 1.8 m x 1.2 m (6 ft x 4 ft) box culvert located at the depth of 5 m (16.4 ft) from the ground surface. Overcut size in the scenario was 30 mm (1.2 in.). It was observed that the stress was redistributed and changed due to soil

collapsing into the annular space. Figure 5-1 illustrates principle stress redistribution at top of box culvert in scenario #3.

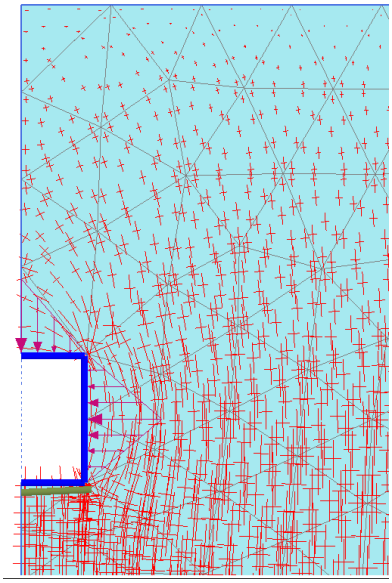

Figure 5-1 Stress Redistributions in Scenario #3

According to soil mechanics, the stress at the depth of H from surface in a soil with density of γ is γH. Considering soil density and depth of box culverts (H_1) in scenario #3, it was expected that stress would be as follows:

$$\sigma_{exp,\#3} = \gamma_{\#22}.H_{1,\#22} = 16.1 \times 5 = 80.5 \frac{kN}{m^2} or\ 11.67\ psi$$

According to Terzaghi and Marston's theories, the stress above the box culvert is changed due to arching effect. The vertical stress can be calculated using Equations 1-2 and 1-3, suggested by Terzaghi, and Equation 1-7, suggested by Marston, as follows:

Terzaghi's Theory:

$$2B_1 = 2\left[B_0 + H.\tan\left(45 - \frac{\phi}{2}\right)\right] = 2\left[0.9 + 1.8 * \tan\left(45 - \frac{32}{2}\right)\right] = 3.8\ m\ or\ 12.46\ ft$$

$$k = 1 - \sin\phi = 1 - \sin 32 = 0.47$$

$$\sigma_v = \frac{B_1\left(\gamma - {}^{c}/_{B_1}\right)}{K.\tan\phi}.\left(1 - e^{-\frac{k.D.\tan\phi}{B_1}}\right) = \frac{1.89\left(16.1 - {}^{16.7}/_{1.89}\right)}{0.47 * \tan 32}.\left(1 - e^{-\frac{0.47*5*\tan 32}{1.89}}\right)$$

$$= 25\frac{kN}{m^2} or\ 3.6\ psi$$

Marston's Theory:

$$k = \tan^2\left(45 - \frac{\phi}{2}\right) = \tan^2\left(45 - \frac{32}{2}\right) = \ 0.305$$

$$C_c = \frac{e^{-2K\mu'({}^{H}/_{B_c})} - 1}{2K\mu} = \frac{e^{-2*0.305({}^{5}/_{1.8})} - 1}{2 * 0.305 * 1} = -1.34$$

$$W_c = C_c.\gamma.B_c^2 = 1.58 * 16.1 * 1.8^2 = 17\frac{kN}{m^2} or\ 2.47\ psi$$

As illustrated in Figure 5-2, the vertical stress exactly at top of the box culvert in Scenario #3, obtained from PLAXIS model, is 44 kN/m^2. The stress is increased away from box culvert centerline and reaches its maximum value, 150 kN/m^2 (21.7 psi), at the distance of 0.9 m (3 ft) from the box centerline. Then, the stress decreases until it reaches the expected stress, 80.5 kN/m^2.

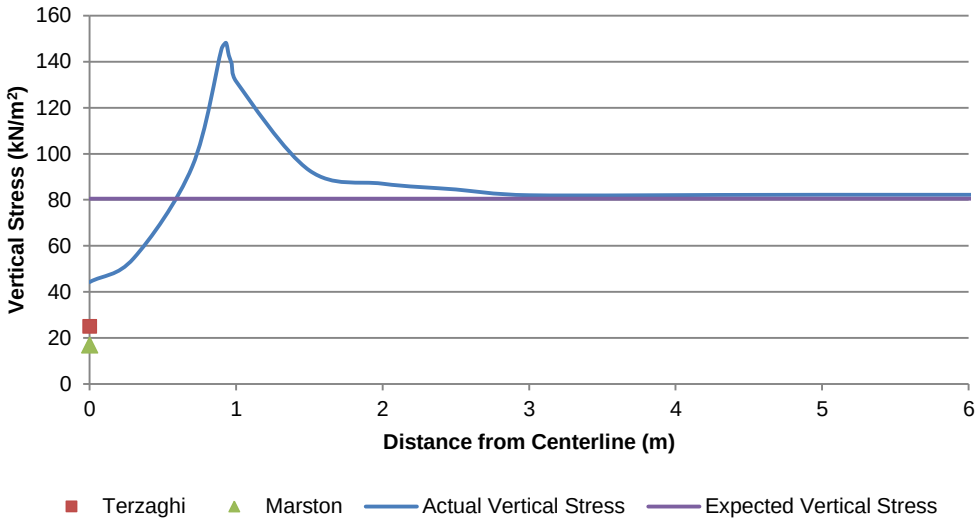

Figure 5-2 Vertical Stress Magnitude at Top of the Box Culvert in Scenario #3

It was observed that both Terzaghi and Marston's theories underestimated the stress at top of the box culvert in Scenario #3.

Table 5-1 presents expected, estimated and actual vertical stress at top of the box culverts in new finite element models.

Table 5-1 Expected, Estimated and Actual Vertical Stress at Top of Box Culverts in New Finite Element Models

Scenario	Vertical Stress kN/m^2 (psi)			
	Expected	**Terzaghi**	**Marston**	**Actual**
1	71 (10)	23 (3)	17 (2)	41 (6)
2	67 (10)	31 (4)	19 (3)	48 (7)
3	81 (12)	25 (4)	17 (2)	44 (6)
4	121 (18)	64 (9)	24(3)	84 (12)
5	59 (9)	15 (2)	26 (4)	31 (4)
6	77 (11)	51 (7)	31 (4)	69 (10)
7	184 (27)	84 (12)	43 (6)	138 (20)
8	89 (13)	58 (8)	29 (4)	66 (10)
9	76 (11)	50 (7)	41 (6)	65 (9)
10	125 (18)	65 (9)	59 (9)	109 (16)
11	213 (31)	106 (15)	74 (11)	156 (23)
12	116 (17)	47 (7)	48 (7)	85 (12)
13	79 (11)	10 (1)	18 (3)	43 (6)
14	98 (14)	18 (3)	28 (4)	55 (8)
15	175 (25)	42 (6)	29 (4)	122 (18)
16	78 (11)	31 (4)	27 (4)	52 (8)
17	151 (22)	69 (10)	44 (6)	115 (17)
18	79 (11)	38 (6)	32 (5)	51 (7)
19	171 (25)	72 (10)	47 (7)	120 (17)
20	131 (19)	55 (8)	44 (6)	84 (12)
21	116 (17)	70 (10)	55 (8)	91 (13)
22	143 (21)	71 (10)	55 (8)	95 (14)

Results showed that actual vertical stress at top of box culverts were less than expected values which was due to arching effect. It was observed that both Terzaghi and

Marston's theories underestimated stresses at top of box culverts. This is because both theories were developed for installing a new pipe or box underground using open-cut (OC) method. These results proved that arching effect happens regardless of the rectangular shape of box culverts.

According to Terzaghi's theory, the arching effect can only extend to a zone with a height of $5B_1$ above the tunnel where B_1 is the half width of the yielding strip. Since the depths of box culverts are less than $5B_1$ (H_1/B_1 ratio is less than 5), as presented in Table 5-2, ground loss due to BJ reaches ground surface and causes settlement.

Table 5-2 H_1/B_1 Ratio in New Finite Element Models

Scenario	H_1 m (ft)	B_1 m (ft)	H_1/B_1
1	4.2 (14)	1.5 (5)	2.7
2	3.5 (11)	1.5 (5)	2.3
3	5.0 (16)	1.9 (6)	2.6
4	6.5 (21)	1.8 (6)	3.6
5	3.0 (10)	1.8 (6)	1.7
6	4.1 (13)	1.8 (6)	2.3
7	10.3 (34)	2.5 (8)	4.2
8	5.4 (18)	2.5 (8)	2.2
9	4.0 (13)	2.3 (8)	1.8
10	6.3 (21)	2.2 (7)	2.8
11	11.0 (36)	3.0 (10)	3.7
12	6.9 (23)	3.1 (10)	2.2
13	4.7 (15)	1.7 (6)	2.7
14	5.1 (17)	1.6 (5)	3.2
15	10.0 (33)	2.1 (7)	4.7
16	4.8 (16)	2.0 (7)	2.4
17	7.9 (26)	2.3 (8)	3.5
18	5.4 (18)	2.3 (8)	2.4
19	10.5 (34)	2.7 (9)	3.9
20	8.0 (26)	2.9 (10)	2.8
21	6.0 (20)	2.4 (8)	2.5
22	8.1 (27)	2.8 (9)	2.9

Arching effect causes less ground loss to be transferred to the surface and consequently less displacement occurred than on top of the box culvert at the ground surface.

Vertical displacements at top of box culverts in new finite element models were recorded to evaluate its distribution. It was observed that the vertical displacement was significantly reduced in a zone above the box with the height of h, where h is the box height.

Figure 5-3 illustrates vertical displacement on top of the box culvert in Scenario #3. It is observed that the maximum vertical displacement occurred exactly on top of the box culvert then, significantly reduced in almost 2 m (6.5 ft) above the box culvert and gradually decreased to reach its minimum at the ground surface.

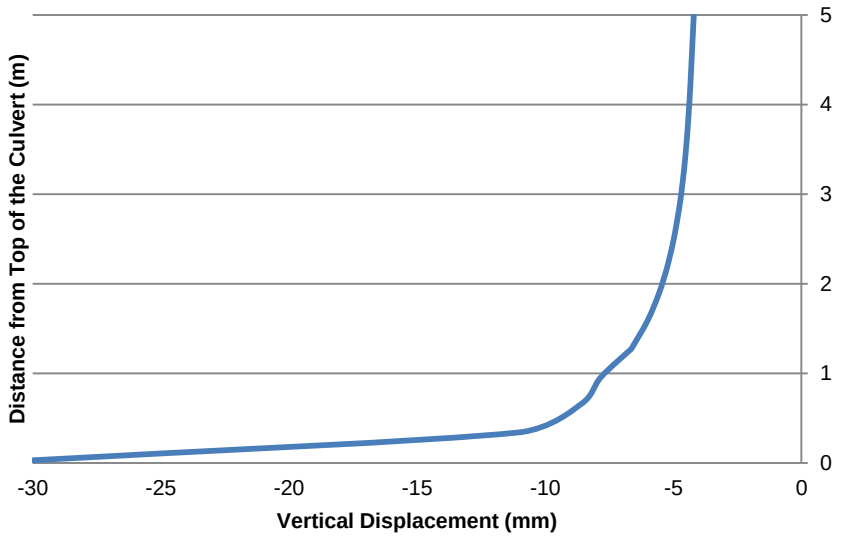

Figure 5-3 Vertical Displacements at Top of the Box Culvert in Scenario #3

Case Studies

Vernon BJ Project

FEM analysis was conducted to simulate the Vernon box jacking project as explained in Chapter 4. Figure 5-4 (a, b, and c) illustrates stress redistribution and shows how stresses were redistributed around the excavated area in all layers.

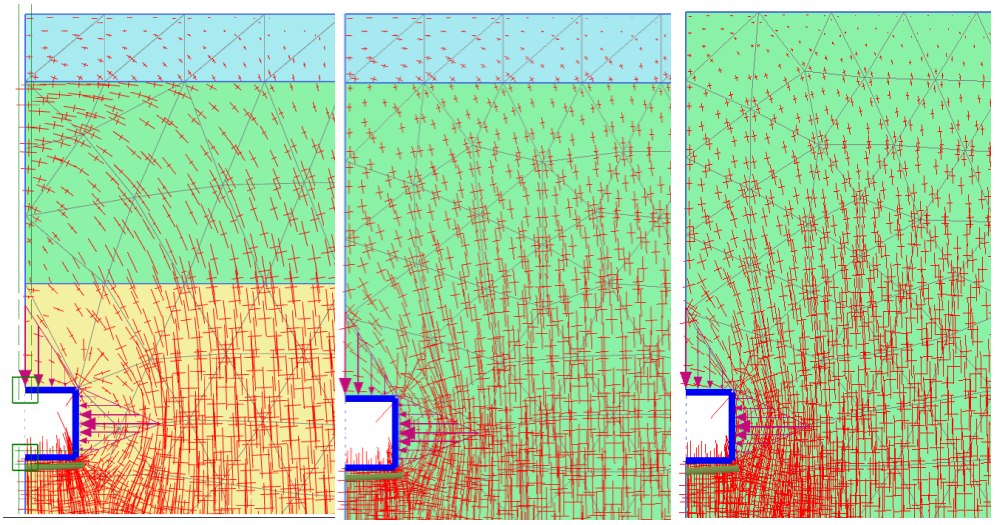

(a) (b) (c)

Figure 5-4 Effective Stress Distribution a) Scenario 1, b) Scenario 2, and c) Scenario 3

Table 5-3 presents expected, estimated and actual stress at top of box culverts in Scenarios 1-3.

Table 5-3 Expected, Estimated and Actual Stresses at Top of Box Culverts in Vernon Project

Scenario	Vertical Stress kN/m^2 (psi)			
	Expected	Terzaghi	Marston	Actual
1	117 (17)	61 (8.8)	22 (3.2)	84 (12.2)
2	121 (17.5)	43 (6.2)	23 (3.3)	58 (8.4)
3	127 (18.4)	33 (4.8)	26 (3.8)	67 (9.7)

The depth of box culverts (H_1) in Vernon project was 6.7 m (22 ft) and the value of B_1 was calculated as 1.5 m (4.9 ft). Since the H_1/B_1 was less than 5, the arching effect was extended to the ground surface.

Underground displacement data were collected using horizontal inclinometer (HI) from north and south side of the Vernon project. Figure 5-5 (a) and (b) show vertical displacements results obtained from PLAXIS model and field data collected from the project.

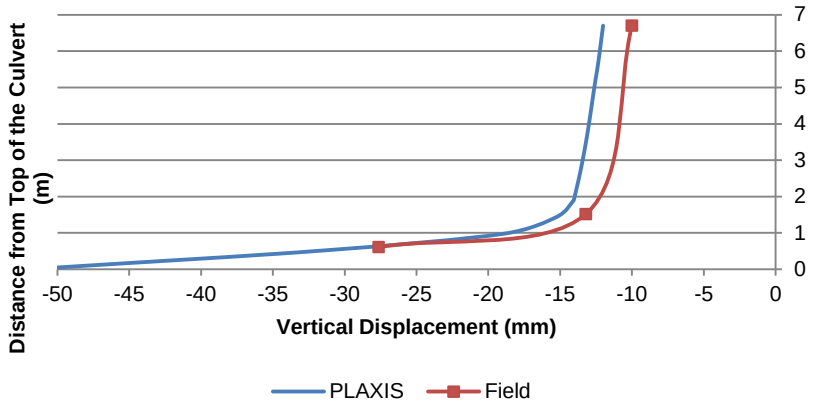

(a)

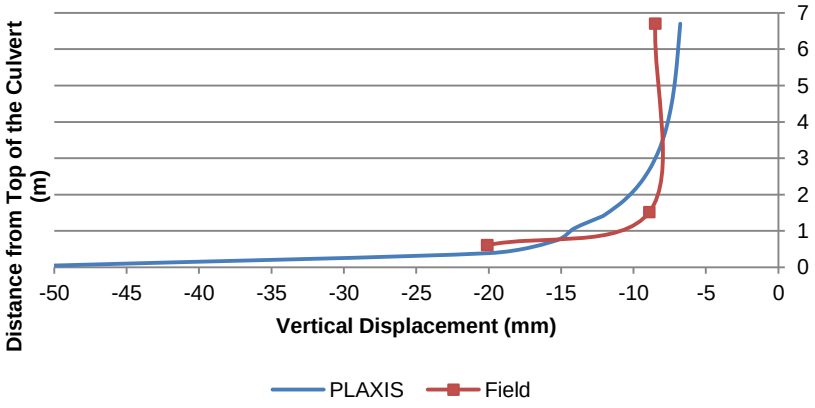

(b)

Figure 5-5 Vertical Displacements Comparison between PLAXIS and Field a) Scenario 1, and b) Scenario 3

It was observed that vertical displacement decreases away from the top of the box culvert until it reaches its minimum value on the surface. Vertical displacement was diminished immediately in almost 1.8 m (6 ft) above the box culvert and then it continued to decrease gradually to the surface.

Navarro County BJ Project

Figure 5-6 illustrates stress redistribution in the Navarro Country BJ project and shows how stresses are transferred around the excavated area in all layers.

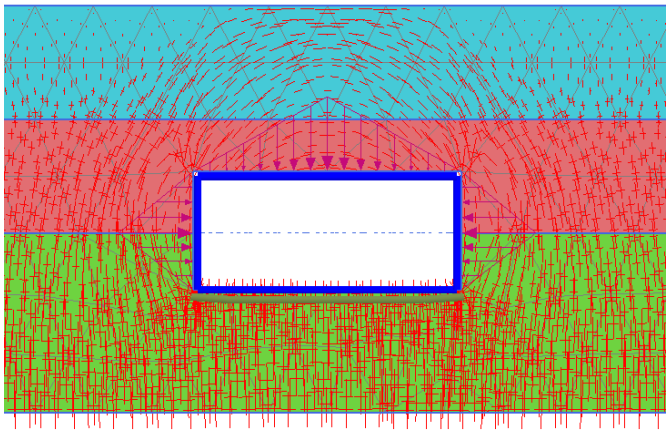

Figure 5-6 Effective Stress Distribution

Table 5-4 presents expected, estimated and actual stress at top of box culverts in the Navarro BJ project. Similar to previous finings in the Vernon project, it was observed that the actual stresses at top of box culverts are less than expected values but higher than estimated values by Terzaghi and Marston's theories.

Table 5-4 Expected, Estimated and Actual Stresses at Top of Box Culverts in the Vernon Project

Scenario	**Vertical Stress kN/m^2 (psi)**			
	Expected	**Terzaghi**	**Marston**	**Actual**
Navarro	30 (4.3)	21 (3)	17 (4.5)	25 (3.6)

The depth of box culverts (H_1) in Navarro County project was 1.8 m (5.9 ft) and the value of B_1 was calculated as 2 m (6.6 ft). Since the H_1/B_1 was less than 5, the arching effect extended to the ground surface.

Figure 5-7 presents vertical displacement at top of the box culvert in the Navarro County project. It was observed that the vertical displacement was significantly decreased at 1.2 m (4 ft) above the box culvert.

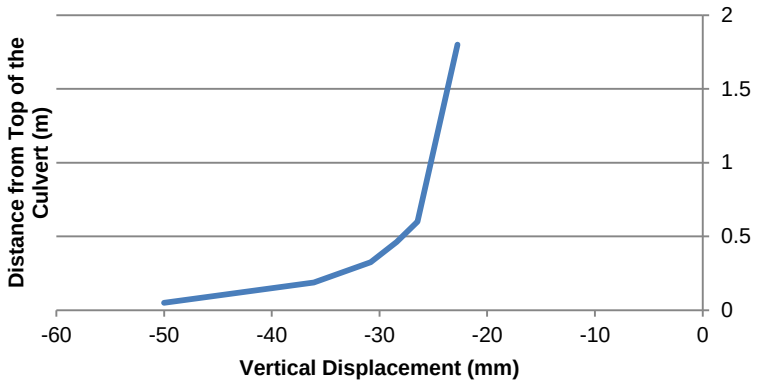

Figure 5-7 Vertical Displacement at Top of the Box Culvert

Sensitivity Analysis

A sensitivity analysis was conducted on initial scenario to study the effect of varying soil properties, box dimensions, overcut size and depth of box from the surface on surface vertical displacement.

Effect of Cohesion

To study the effect of varying cohesion on surface vertical displacement, the cohesion of the initial scenario was increased from 0 to 25 kPa. Figure 5-8 and Figure 5-9 presents surface vertical displacement variation and maximum surface vertical displacement due to change in soil cohesion respectively.

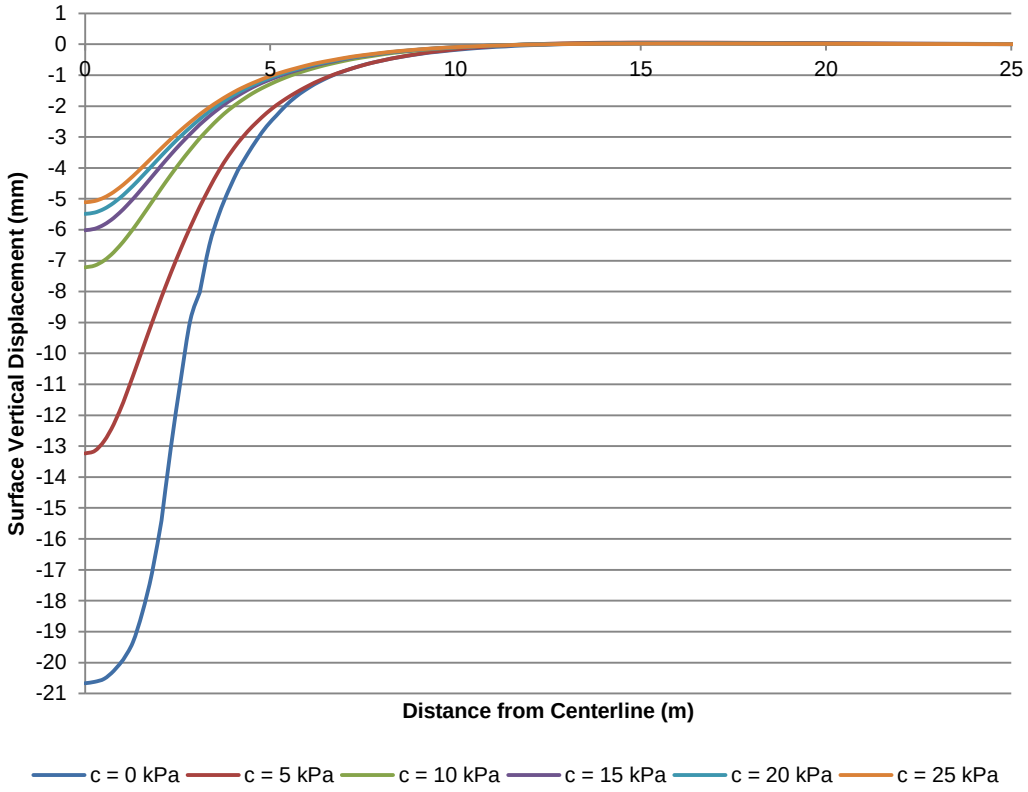

Figure 5-8 Variation of Surface Vertical Displacement with Cohesion

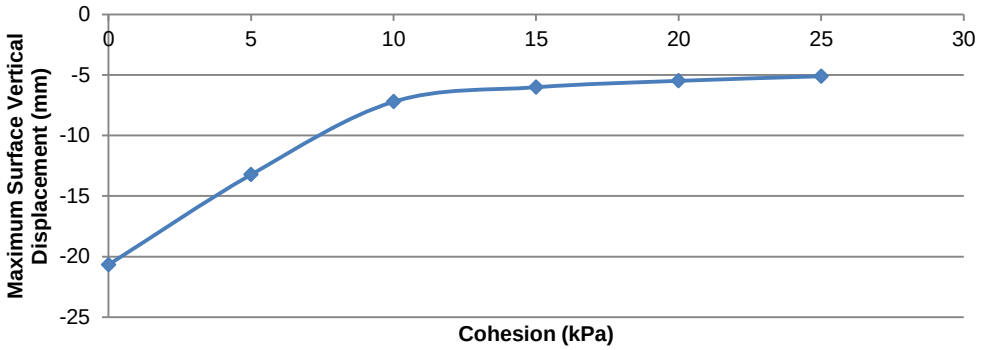

Figure 5-9 Variation of Maximum Surface Vertical Displacement with Cohesion

It is observed that the higher soil cohesion results in less maximum surface vertical displacement. These results agree with Terzaghi's vertical stress equation in Chapter 1 (Equation 1-1). According to Equation 1-1, any increase in cohesion results in

decrease in vertical stress at the top of the box culvert. This means that the effect of arching increases and causes less displacement to be transferred to the surface. The maximum surface vertical displacement decreases significantly as the cohesion increases from 0 to 10 kPa. Then, the maximum surface vertical displacement continues to decrease gradually. This means that even a small amount of cohesion in sandy soils can significantly prevent excessive settlement on the surface.

Effect of Friction Angle

The Friction angle of the initial scenario was changed, as presented in Figure 5-10, to study its effect on surface vertical displacement.

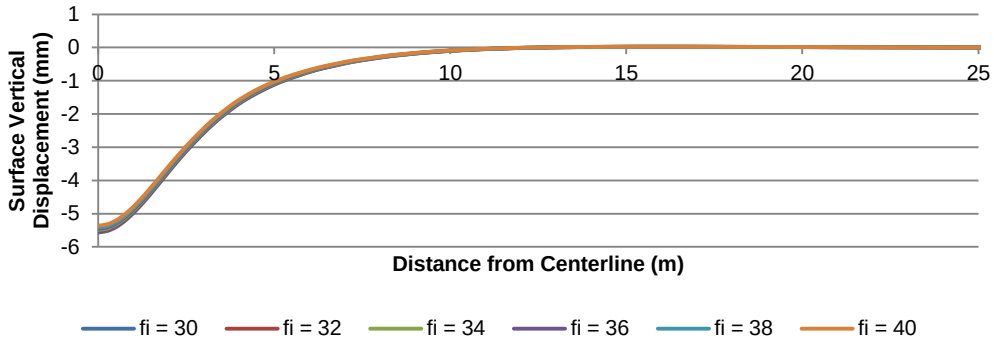

Figure 5-10 Variation of Surface Vertical Displacement with Friction Angle

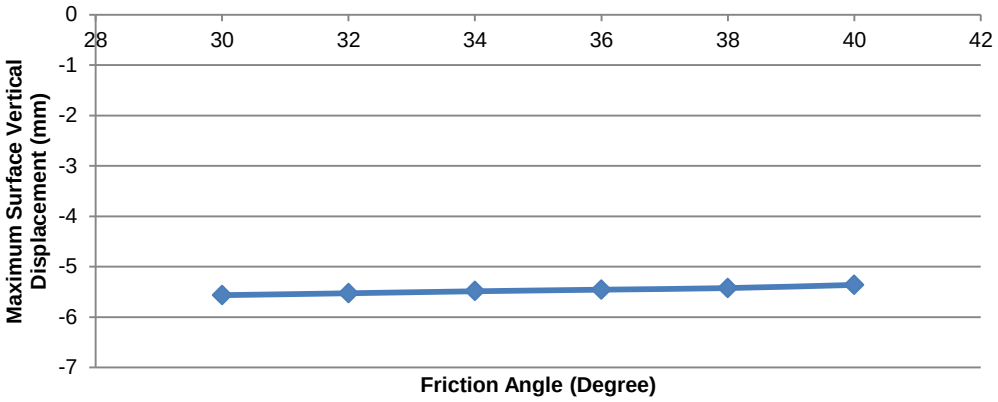

Figure 5-11 Variation of Maximum Surface Vertical Displacement with Friction Angle

Results showed that maximum surface vertical displacement decreases as friction angle increases. According to Equation 1-1, suggested by Terzaghi, an increase in friction angle results in an increase in arching effect. Therefore, less displacement is transferred through the body of the soil to the ground surface. However, the effect of the friction angle on surface vertical displacement is not significant.

Effect of Dilation Angle

Effect of dilation angle on surface vertical displacement was studied by changing it from 0 to 10 degrees. Results showed that as dilation angle increases, the maximum surface displacement decreases. However, it was observed that the effect of dilation angle is negligible as illustrated in Figure 5-12 and Figure 5-13.

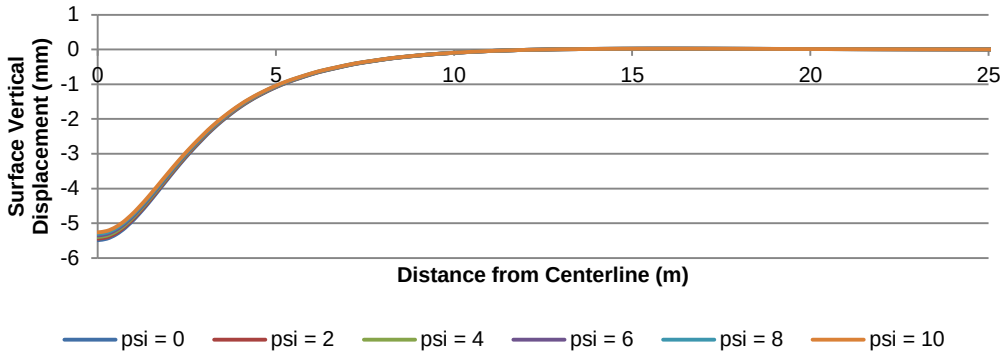

Figure 5-12 Variation of Surface Vertical Displacement with Dilation Angle

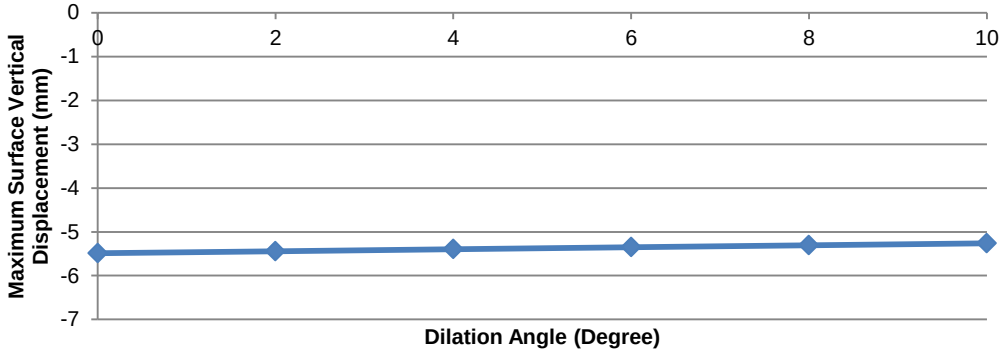

Figure 5-13 Variation of Maximum Surface Vertical Displacement with Dilation Angle

Effect of Soil Unit Weight

Soil unit weight was increased from 14 kN/m^3 (89 lb/ft^3) to 20 kN/m^3 (127 lb/ft^3) to study its effect on surface displacement. As Figure 5-15 illustrates, soil unit weight has significant impact on maximum surface vertical displacement.

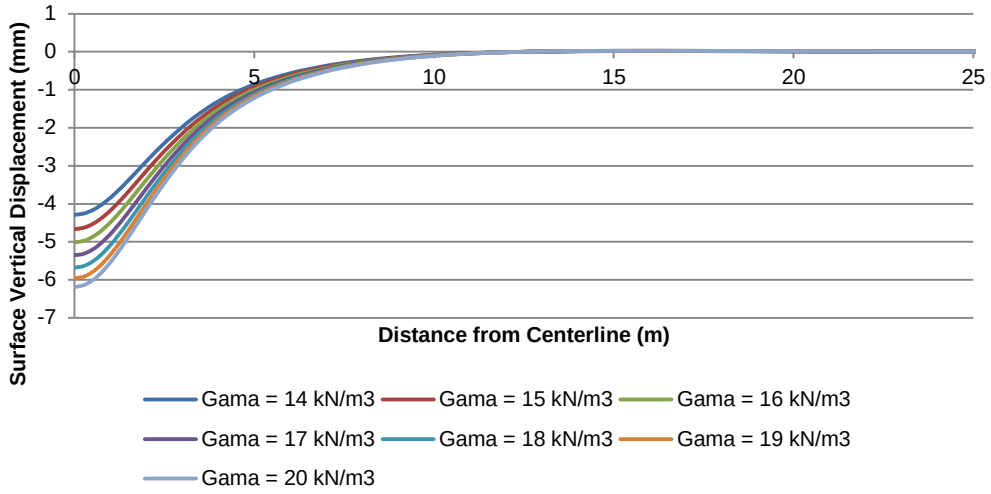

Figure 5-14 Variation of Surface Vertical Displacement with Soil Unit Weight

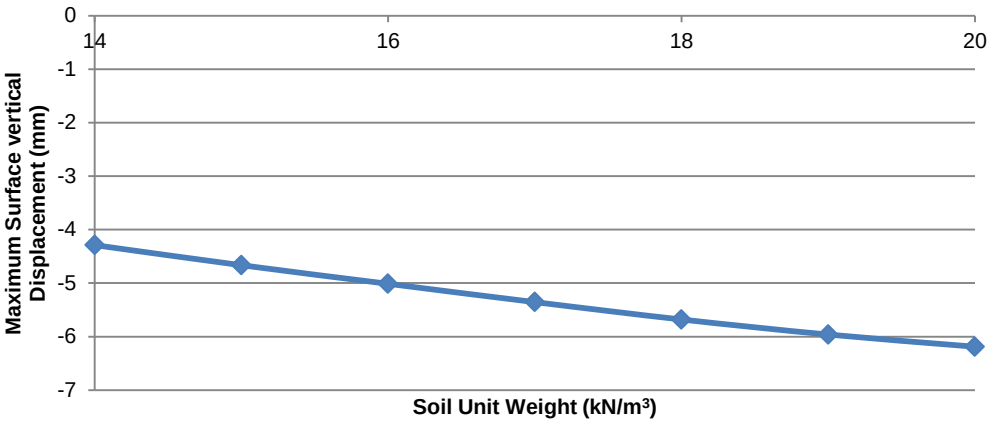

Figure 5-15 Variation of Maximum Surface Vertical Displacement with Unit Weight

Results showed that higher soil unit weight corresponds with higher maximum surface settlement. This is because higher soil unit weight increases the weight of soil

prism above the box culvert and causes the soil to collapse above the box culvert and consequently more displacement is transferred to the surface.

Effect of Modulus of Elasticity

To study the effect of changing modulus of elasticity on surface vertical displacement, an analysis was conducted by modulus of elasticity changing from 10 MPa (1,450 psi) to 40 MPa (5,801 psi) as presented in Figure 5-16 and Figure 5-17.

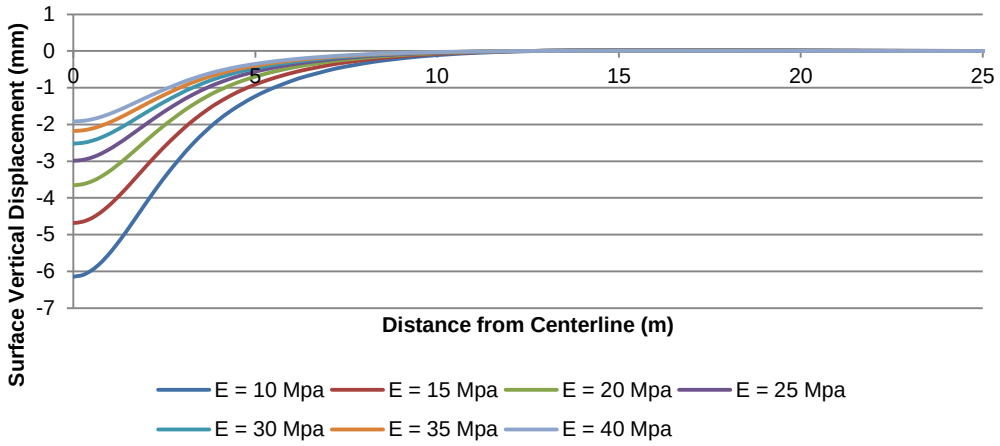

Figure 5-16 Variation of Surface Vertical Displacement with Modulus of Elasticity

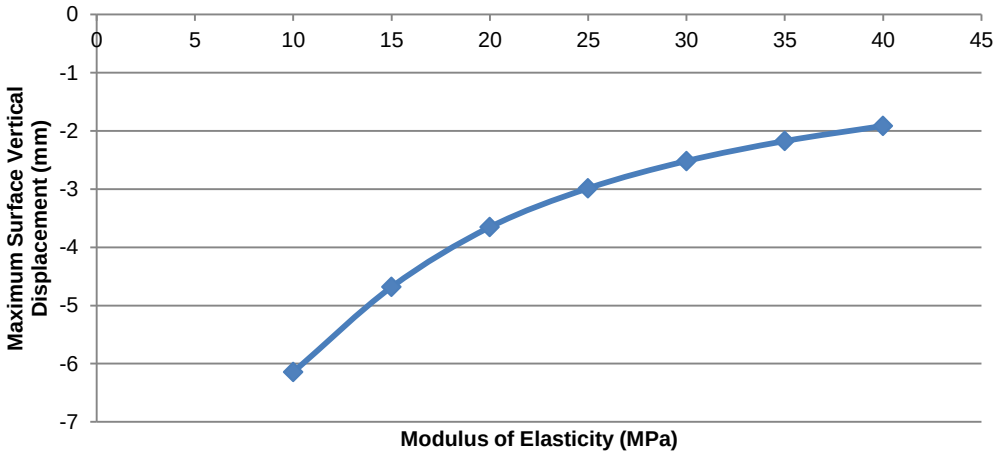

Figure 5-17 Variation of Maximum Surface Vertical Displacement with Soil Modulus of Elasticity

It was observed that the maximum surface vertical displacement was significantly decreased as soil modulus of elasticity was increased. This is because the higher modulus of elasticity increases stiffness of soil and consequently prevents the soil from settling. Therefore, less displacement is transferred to the ground surface.

Effect of Overcut Size

To study the effect of overcut size on surface vertical displacement, five overcut sizes from 30 mm to 50 mm (1.18 in to 1.97 in.) were considered. Figure 5-18 and Figure 5-19 presents variation of surface vertical displacement and the maximum surface vertical displacement with overcut size respectively.

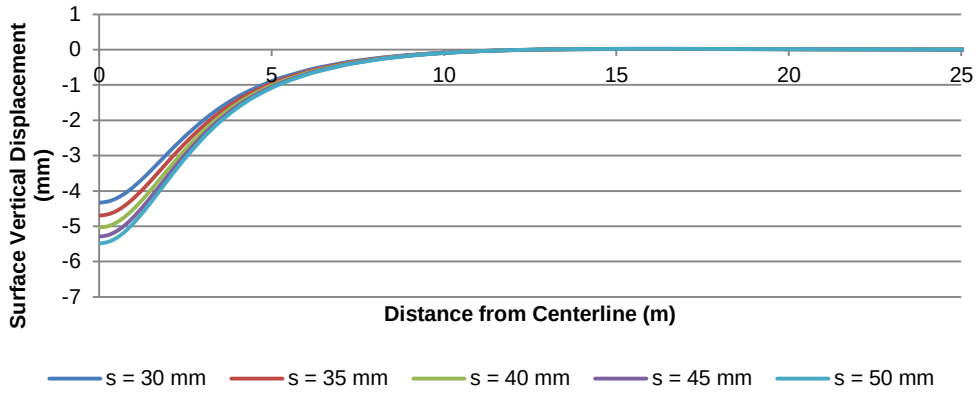

Figure 5-18 Variation of Surface Vertical Displacement with Overcut Size

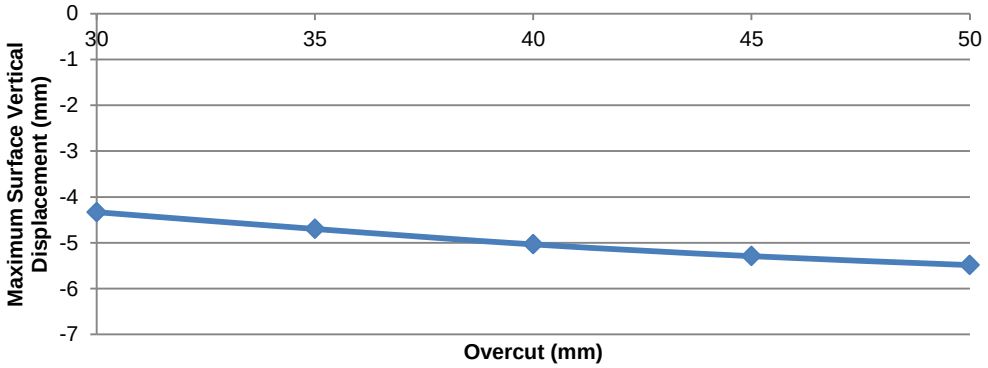

Figure 5-19 Variation of Maximum Surface Vertical Displacement with Overcut

It was observed that higher overcut size corresponds with higher surface displacement. This is because more soil collapses into the annular space in bigger overcut sizes and consequently more displacement occurs in the body of soil.

Effect of Box Culvert Width

Four box widths including 1.8 m (6 ft), 2.1 m (7 ft), 2.4 m (8 ft), 2.7 m (9 ft), and 3 m (10 ft) were studied to determine their effects on surface vertical displacement as illustrated Figure 5-20 and Figure 5-21.

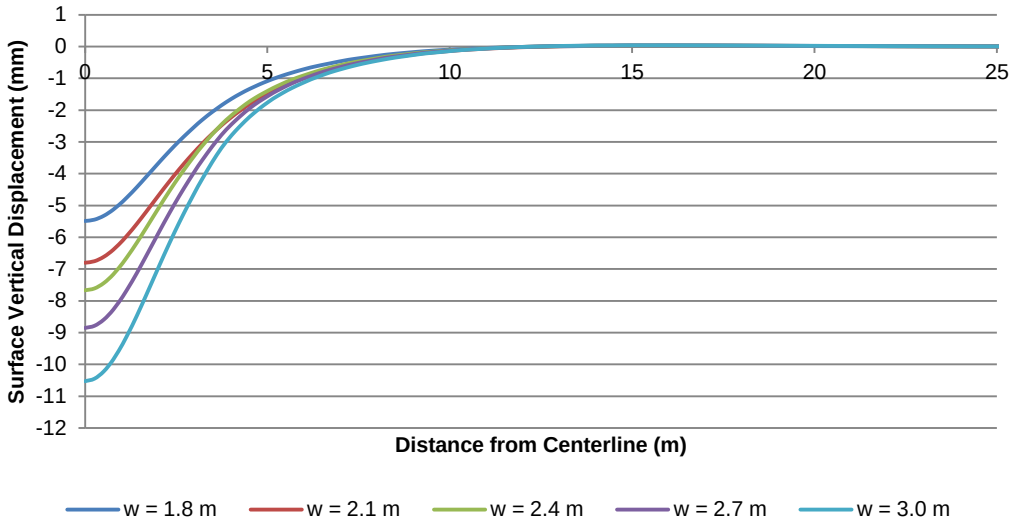

Figure 5-20 Variation of Surface Vertical Displacement with Box Width

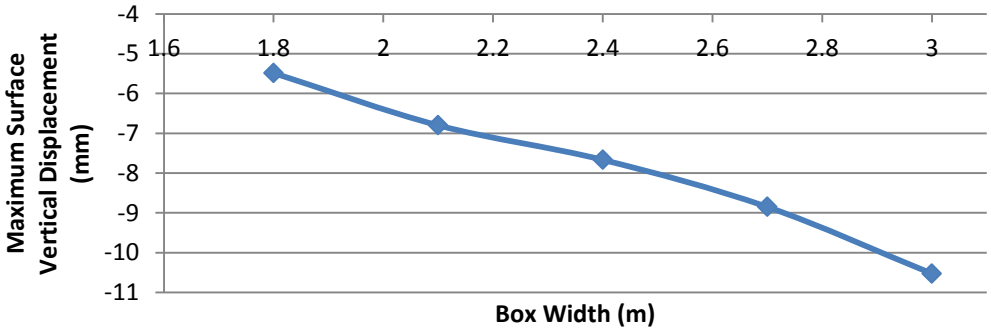

Figure 5-21 Variation of Maximum Surface Vertical Displacement with Box Width

Maximum surface displacement increases as the box culvert width (w) increases. According to Terzaghi's equation, increase in opening width decreases the effect of arching on top of the opening and consequently more displacement is transferred to the surface. Moreover, wider box culverts increase the volume of ground loss and increase the amount of soil displacement in the body of the soil consequently.

Effect of Box Culvert Height

Box culvert height (h) was changed to study its effect of surface vertical displacement as illustrated in Figure 5-22 and Figure 5-23.

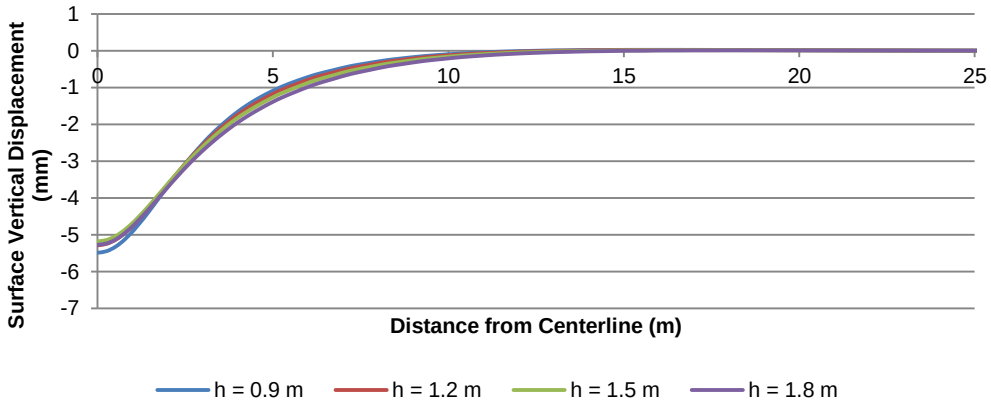

Figure 5-22 Variation of Surface Vertical Displacement with Box Height

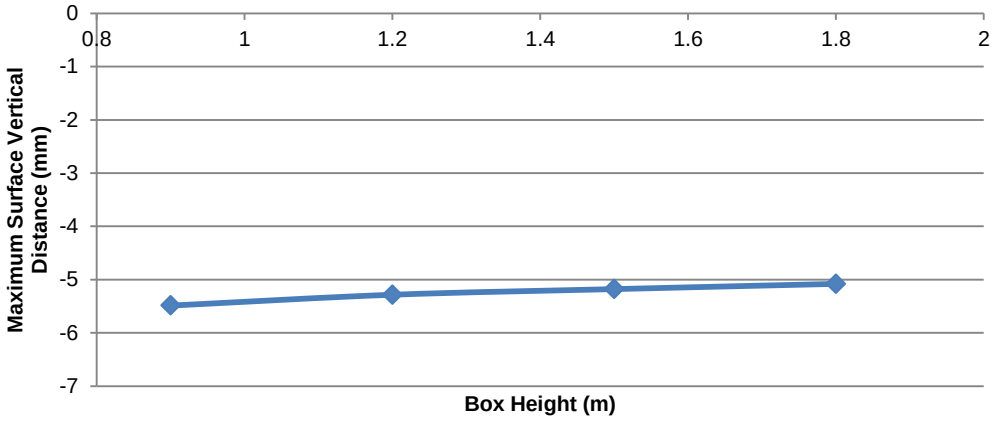

Figure 5-23 Variation of Maximum Surface Vertical Displacement with Box Height

It was observed that higher maximum surface vertical displacement corresponds with higher box height. This is because the volume of annular space increases as more soil collapse into the annular space. However, culvert height does not have significant impact on surface vertical displacement.

Effect of Box culvert Depth from Surface

Different box depths from surface to the top of the culvert (H_1) were considered to study effect of depth on surface vertical displacement as illustrated in Figure 5-24 and Figure 5-25.

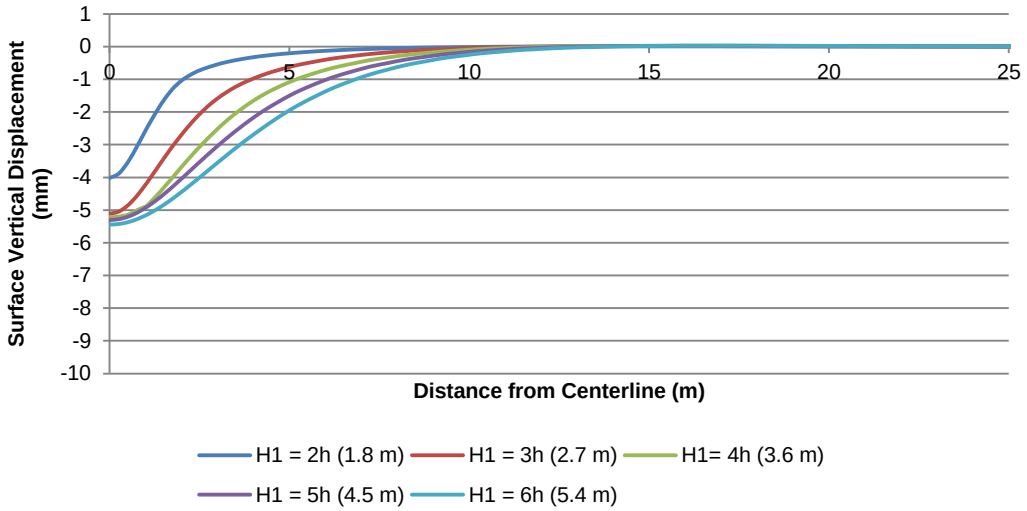

Figure 5-24 Variation of Surface Vertical Displacement with Box Culvert Depth

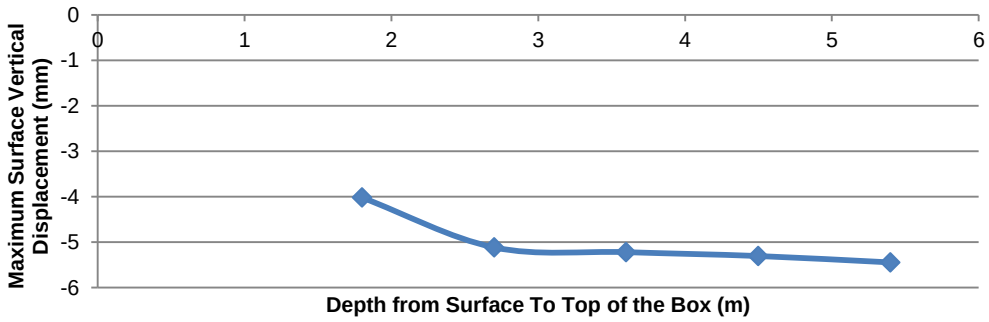

Figure 5-25 Variation of Maximum Surface Vertical Displacement with Depth

Results showed that higher maximum surface vertical displacement corresponds with higher depth. According to Equation 1-1, arching effect decrease with depth increase. This is because the weight of soil prism above the box is increased and, therefore, more displacement is transferred to the surface.

Parameters Participation

The effects of different parameters on maximum surface vertical displacement were studied. However, due to the fact that each factor had a different unit, it was not possible to prioritize parameters effectiveness and rank them based on their participation in determining maximum surface vertical displacement. Regression analysis was conducted in this research to rank parameters. All data were normalized between 0.1 and 0.9 to eliminate the effect of different units (Mamaqani & Najafi, 2014). Equation 5-1 was used for normalization:

$$x_{norm,i} = a + \frac{(x_i - A)(b - a)}{(B - A)} \qquad \text{Equation 5-1}$$

where:

x_i = i^{th} data

a = 0.1 (normalized scale minimum)

b = 0.9 (normalized scale maximum)

A = Data set minimum

B = Data set maximum

According to regression results, coefficients were divided into two categories:

1. Positive coefficients
2. Negative coefficients

Negative coefficients imply that any increase in associated parameters resulted in an increase in maximum surface vertical displacement which is not favorable. On the

contrary, any increase in parameters with positive coefficients resulted in an decrease in the maximum surface vertical displacement which is favorable. Table 5-5 presents regression analysis results.

Table 5-5 Regression Analysis Results (Mamaqani and Najafi, 2014)

Factors	**Coefficients**
Box Width (w)	3.75
Box Height (h)	1.09
Overcut Size (s)	4.45
Depth (H_1)	-7.06
Soil Modulus of Elasticity (E)	-2.56
Soil Friction Angle (ϕ)	0
Soil Dilation Angle (ψ)	0
Soil Unit Weight (γ)	1.54
Soil Cohesion (c)	-10.90

Figure 5-26 illustrates parameters participation percentage in determining maximum surface vertical displacement.

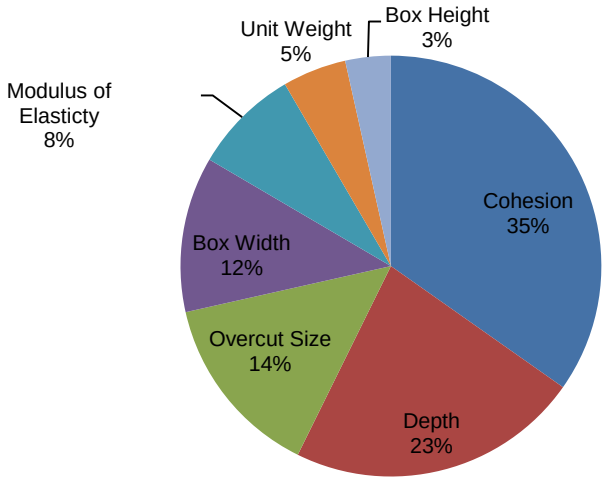

Figure 5-26 Parameters Participation in Determining

Maximum Surface Vertical Displacement (Mamaqani and Najafi, 2014)

It is observed that soil cohesion (c) and soil friction and dilation angles have the highest and lowest effect on determining maximum surface vertical displacement. Both soil friction angle and dilation angle are not presented since their coefficients were negligible.

Finial Artificial Neural Network (ANN) Model

Four combinations of linear and sigmoid transfer functions were considered and model performances were compared as illustrated in Figure 5-27 .

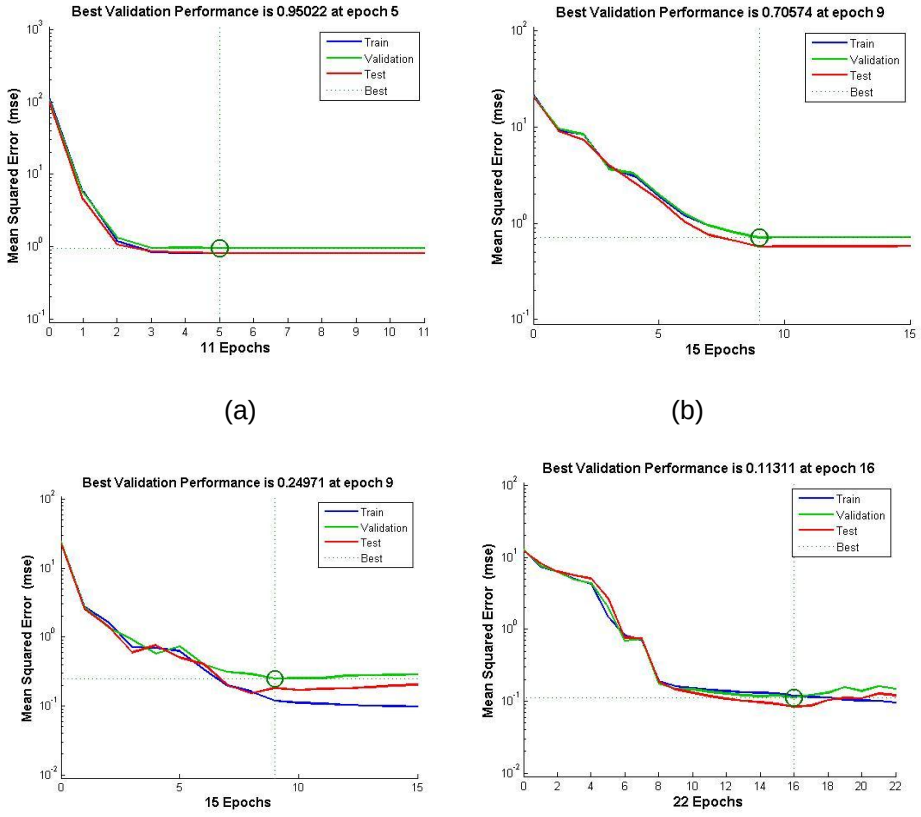

Figure 5-27 Final ANN Model Performance Plot: a) Linear-Linear, b) Linear-Sigmoid c) Sigmoid-Linear, and d) Sigmoid-Sigmoid

It was observed that a model with sigmoid transfer functions in input and output layers had minimum performance which is 0.11.

As discussed in Chapter 2, the next step in model verification is generating and comparing regression plots. Figure 5-28 (a through d) shows the regression plots of considered models.

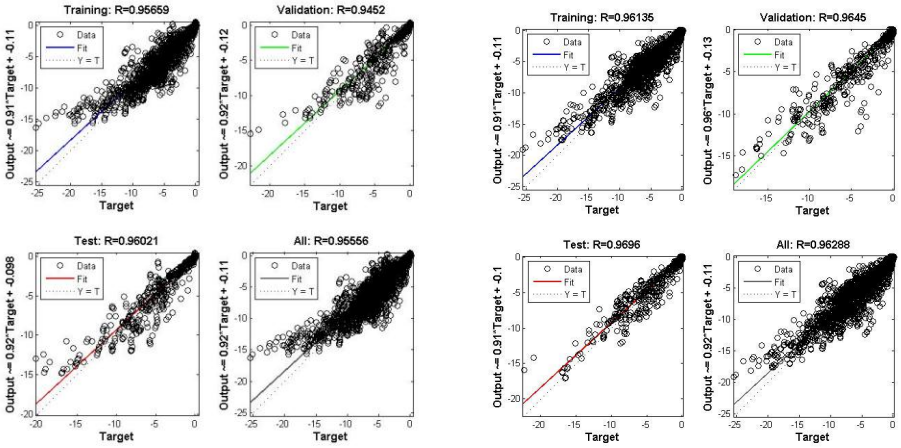

(a) (b)

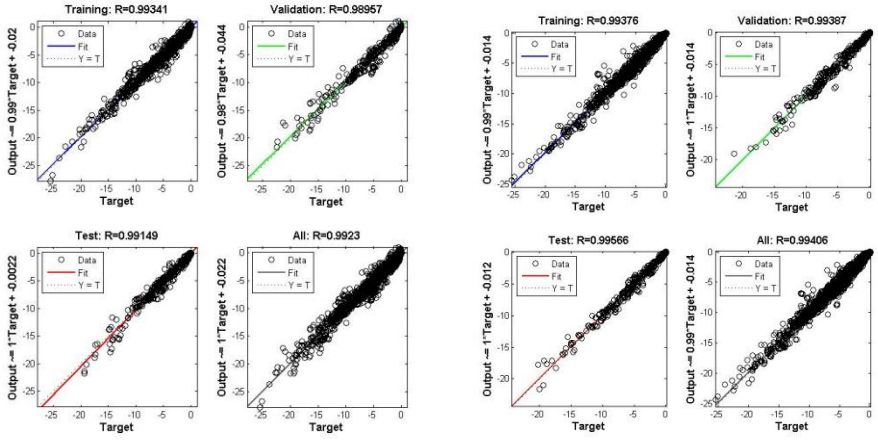

(c) (d)

Figure 5-28 Regression Plots: a) Linear-Linear, b) Linear-Sigmoid

c) Sigmoid-Linear, and d) Sigmoid-Sigmoid

Results showed R value in sigmoid-sigmoid ANN model had the highest value and therefore resulted in more accurate model.

Considering the validation performance and regression results, it was concluded that an ANN model with sigmoid transfer function in both input and output layers leads to more accurate results. Therefore, this model was selected as the final ANN model in this research.

Final ANN Model Validation

New Finite Element Models

Finite element models of new scenarios were generated in PLAXIS and results were recorded. ANN results were also obtained using available inputs for new finite element models, as presented in Table 3-5. Four combinations of Linear and sigmoid transfer functions were used in input and output layer to develop results by ANN model. Figure 5-29 presents maximum surface vertical displacement obtained from PLAXIS and ANN models.

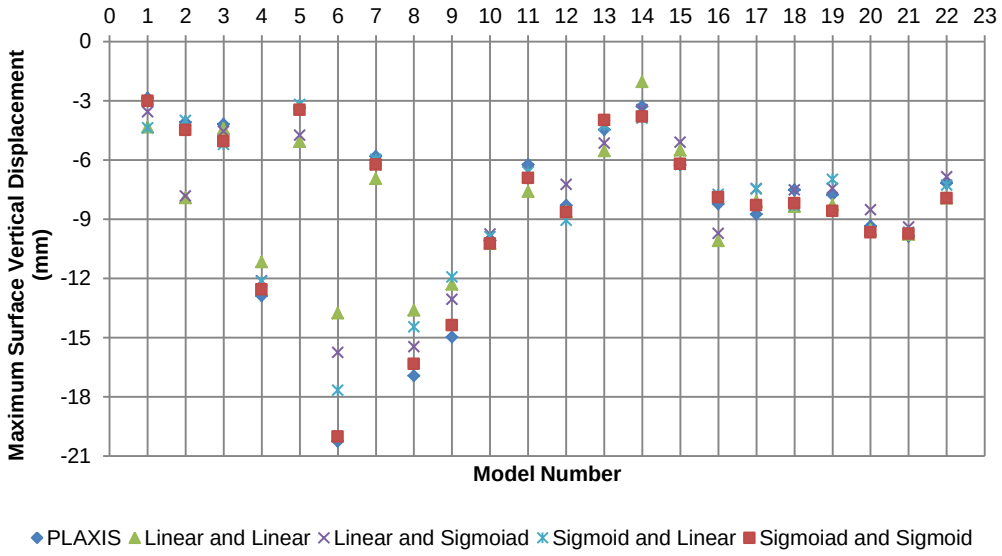

Figure 5-29 Maximum Surface Vertical Displacement Comparisons

To evaluate accuracy of the ANN results with PLAXIS error percentage was introduced and calculated using Equation 4-1.

$$Error\ Percentage\ (\%) = \frac{R_{ANN} - R_{PLAXIS}}{R_{PLAXIS}} \times 100 \qquad \text{Equation 5-2}$$

where:

R_{ANN} = Result obtained by ANN model

R_{PLAXIS} = Result obtained by PLAXIS

A positive error percentage indicates that the ANN result was overestimated compared to PLAXIS results while a negative one indicates underestimation. Figure 5-30 presents error percentages for ANN models. The legend of Figure 5-30 includes standard deviation (Stdv) of each model. Standard deviation shows variation of data from the mean value. A low standard deviation indicates that data are close to the mean while a high standard deviation shows a high variation.

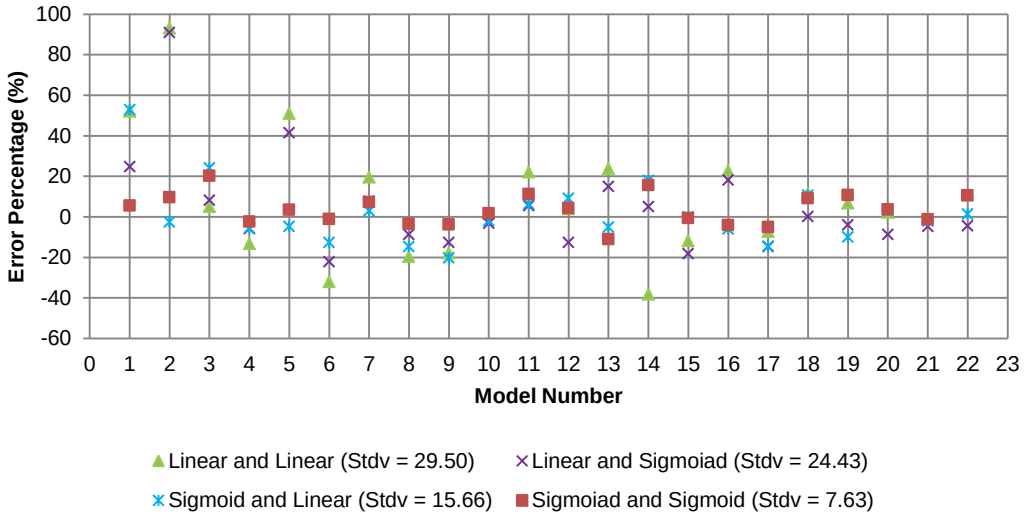

Figure 5-30 Error Percentages for ANN Models

It was observed that ANN model with sigmoid transfer functions in input and output layers had the lowest standard deviation (e.g., 7.63) and calculated the most

accurate results compared with other ANN models. This model is considered as the final ANN model in this research.

As discussed in Chapter 3, Schmidt (1969) and Peck (1969) showed that surface vertical displacement associated with pipe jacking and tunneling can be represented by Gaussian normal distribution as presented in Equation 2-3. Figure 5-31 shows a comparison between surface vertical displacements obtained from PLAXIS and ANN models and the one calculated by empirical method for Scenario #3. Surface vertical displacement comparison for all new finite element models are presented in Appendix G.

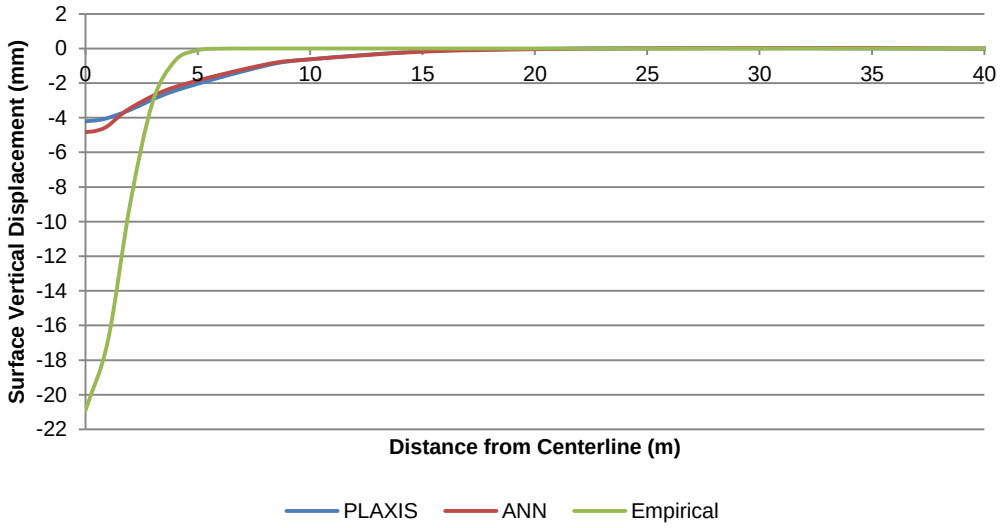

Figure 5-31 Surface Vertical Displacement Obtained by Different Methods in Scenario #3

Results showed that error function originally suggested for pipeline and tunneling projects cannot represent the surface vertical displacement profile in BJ projects. It was observed that installing box culvert underground affects a wider area on surface than installing a pipe culvert. This is because of the rectangular shape of the box culvert which requires wider bore excavation than pipe culvert. Results show that there are good matches between results obtained from ANN model and PLAXIS.

Surface vertical displacements for all 22 new finite element models were obtained from final ANN model and PLACIS. Table 4-8 presents maximum surface vertical displacement calculated by empirical method and results obtained from PLAXIS and ANN models. ANN was able to estimate maximum surface displacement accurately while empirical method overestimated results significantly.

Table 5-6 Maximum Surface Vertical Displacement Obtained from Empirical Method, PLAXIS and ANN Models

Scenario #	S_{max} mm (in.)		
	Empirical	**PLAXIS**	**ANN**
1	-20.3 (-0.80)	-2.9 (-0.11)	-3.0 (-0.12)
2	-32.1 (-1.26)	-4.1 (-0.16)	-4.5 (-0.18)
3	-20.9 (-0.82)	-4.2 (-0.17)	-5.0 (-0.20)
4	-27.2 (-1.07)	-12.9 (-0.51)	-12.6 (-0.50)
5	-42.5 (-1.67)	-3.4 (-0.13)	-3.5 (-0.14)
6	-39.3 (-1.55)	-20.3 (-0.80)	-20.0 (-0.79)
7	-13.8 (-0.54)	-5.8 (-0.23)	-6.2 (-0.24)
8	-41.1 (-1.62)	-16.9 (-0.67)	-16.3 (-0.64)
9	-39.1 (-1.54)	-15.0 (-0.59)	-14.4 (-0.57)
10	-25.5 (-1.00)	-10.1 (-0.40)	-10.2 (-0.40)
11	-15.9 (-0.63)	-6.2 (-0.24)	-6.9 (-0.27)
12	-39.9 (-1.57)	-8.3 (-0.33)	-8.6 (-0.34)
13	-33.4 (-1.31)	-4.5 (-0.18)	-4.0 (-0.16)
14	-17.6 (-0.69)	-3.3 (-0.13)	-3.8 (-0.15)
15	-20.5 (-0.81)	-6.2 (-0.24)	-6.2 (-0.24)
16	-37.0 (-1.46)	-8.2 (-0.32)	-7.9 (-0.31)
17	-21.9 (-0.86)	-8.7 (-0.34)	-8.3 (-0.33)
18	-21.5 (-0.85)	-7.5 (-0.30)	-8.2 (-0.32)
19	-19.1 (-0.75)	-7.8 (-0.31)	-8.6 (-0.34)
20	-32.4 (-1.28)	-9.3 (-0.37)	-9.7 (-0.38)
21	-21.7 (-0.85)	-9.9 (-0.39)	-9.7 (-0.38)
22	-18.7 (-0.74)	-7.2 (-0.28)	-7.9 (-0.31)

An error percentage graph was developed using Equation 5-1. Figure 5-32 illustrates error percentage for both ANN and empirical method with respect to Plaxis results. It is observed that available empirical methods cannot predict maximum surface vertical displacement in BJ projects.

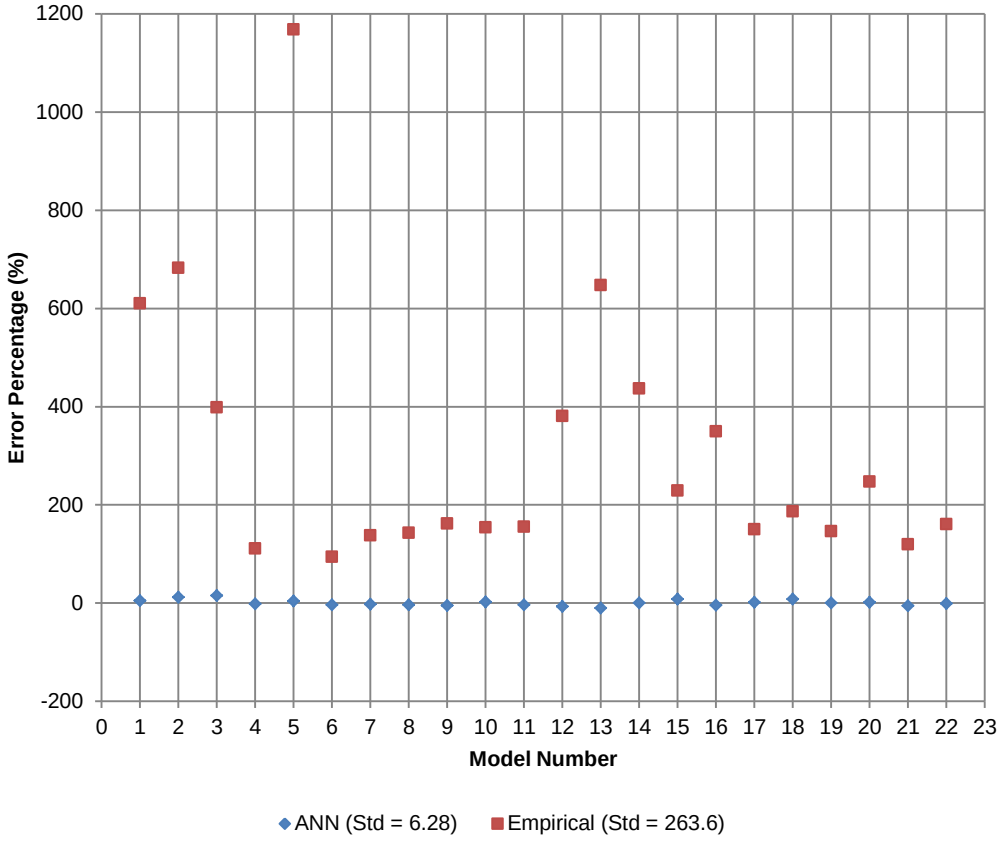

Figure 5-32 Error Percentages for ANN and Empirical Method in New Finite Element Models

Case Studies

Case Study 1: Vernon Project

Due to lack of enough collected surface displacement data from the project and considering a good match between underground displacement results obtained from

PLAXIS modeling and collected data from the project, it was assumed that PLAXIS results for surface displacement was a good representative of the Vernon project for further investigation.

Since the ANN model can only accept one soil layer properties, box culvert surrounding soil layer properties (e.g., layer 3 in Scenario 1 and Layer 2 in Scenario 2), were used as inputs. Figure 5-34 illustrates comparison of results obtained from PLAXIS, ANN and empirical methods for Vernon box jacking project in north side (Scenario #1).

Results showed that the ANN model was able to predict surface vertical displacement accurately compared to PLAXIS results. However, the empirical method overestimated the maximum surface vertical displacement and underestimated settlement trough (channel) width. Errors, observed in Figure 5-34, are due to the fact the only one layer was considered in predicting surface vertical displacement.

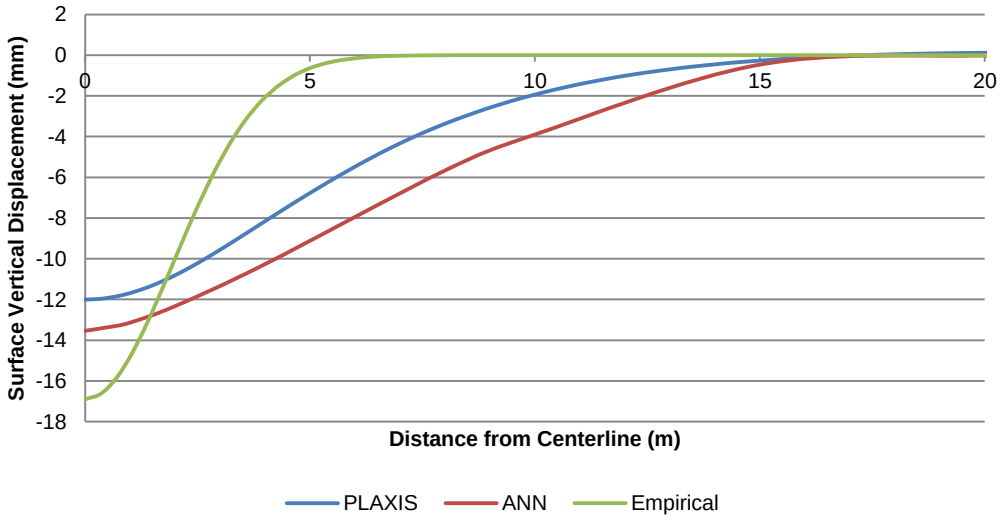

Figure 5-33 Surface Vertical Displacements for Scenario #1

The same procedure was followed to calculate surface vertical displacement in Scenario #2 and #3. Since Scenario #3 contained only one layer, the final ANN model

was able to predict the result more accurately. Figure 5-34 a and b illustrates surface vertical displacement in Scenario #2 and #3.

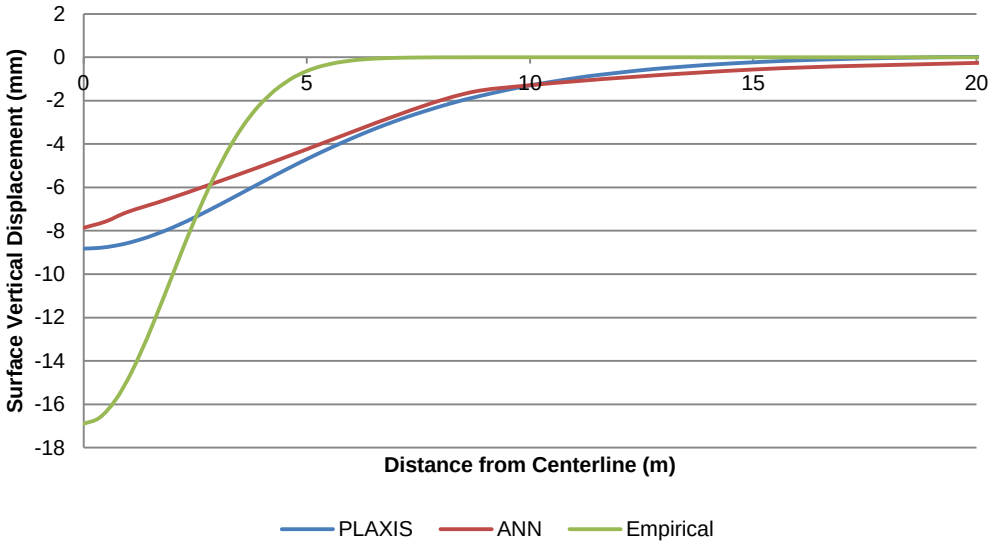

(a)

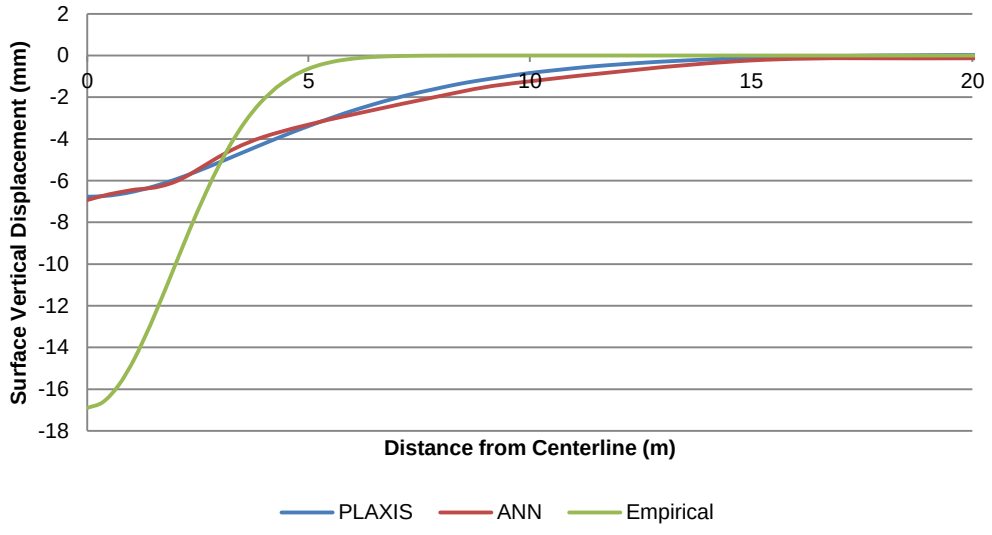

(b)

Figure 5-34 Surface Vertical Displacements: b) Scenario #2, and c) Scenario #3

Case Study 2: Navarro County Project

In this section, results obtained from empirical method, finite element model, and the ANN model are presented and compared with collected data from the project. Collected data from the project were averaged so one surface displacement represent the project.

To calculate surface vertical displacement using the final ANN model, second soil layer properties were considered since the ANN model was able to accept one set of soil properties.

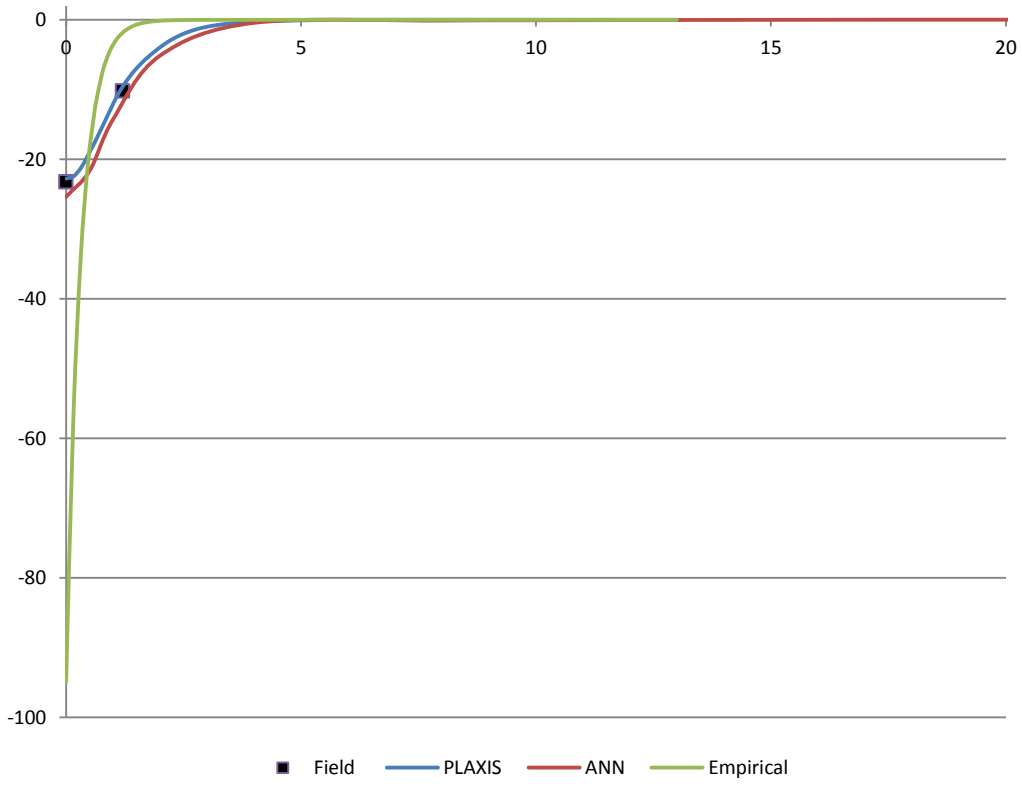

Figure 5-35 Surface Vertical Displacement in Navarro County Project

Contribution

According to regression analysis results presented in this chapter 5, cohesion (c), depth of box culvert from ground surface (H_1) and overcut size (s) had the highest contribution in determining maximum surface vertical displacement. Therefore, these parameters were changed in the initial scenario to develop three 3D prediction graphs using final ANN model results.

Maximum allowable surface settlement for highways and railroads were considered to assess associated risk with the BJ project. Associated risk with box jacking (BJ) was divided into four main categories:

1. Safe (lower than 2.54 mm (0.1 in.)): Safe means that possibility of surface vertical displacement is very low and box jacking project may not damage surface pavement and railroad tracks. Safe BJ project is the most favorable project.
2. Marginal (2.54 to 6.35 mm (0.1 to 0.25 in.)): Marginal means that low displacement is expected on the surface. However, the displacement is within an acceptable range and does not damage the pavement or railroad bed.
3. Critical (6.35 to 12.7 (0.25 to 0.5 in.)): Critical means that caution needs to be taken in the BJ project since significant settlement may occur and damage the pavement or railroad bed.
4. High Risk (higher than 12.7 mm (0.5 in.)): High risk means that there is a high possibility for excessive surface settlement and damage to pavement or railroad bed can be expected.

Figure 5-36 and Figure 5-37 illustrate prediction graphs to determine associated risk with BJ operation when the overcut size (s) are 30 mm (1.18 in.) and 40 mm (1.57 in.) respectively.

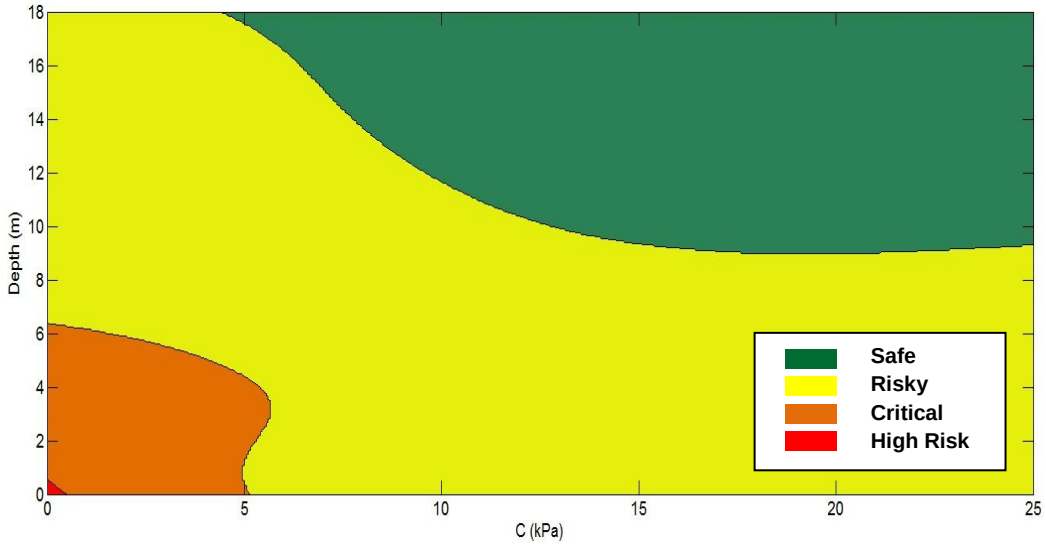

Figure 5-36 Associated Risk for Box Jacking (s = 30 mm or 1.18 in.)

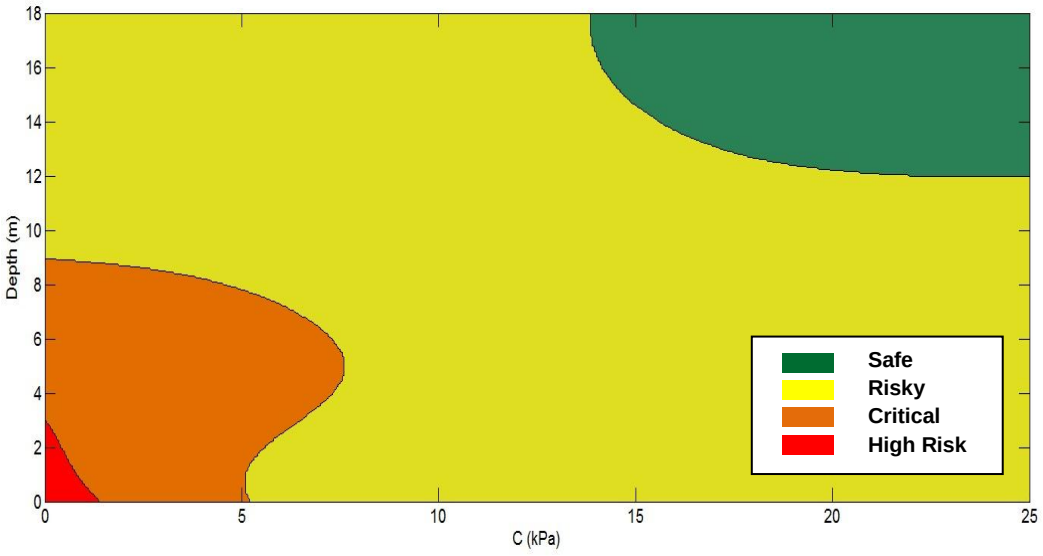

Figure 5-37 Associated Risk for Box Jacking (s = 40 mm or 1.57 in.)

The overcut size (s) was increased to 50 mm (1.98 in.) to develop a prediction graph as illustrated in Figure 5-38.

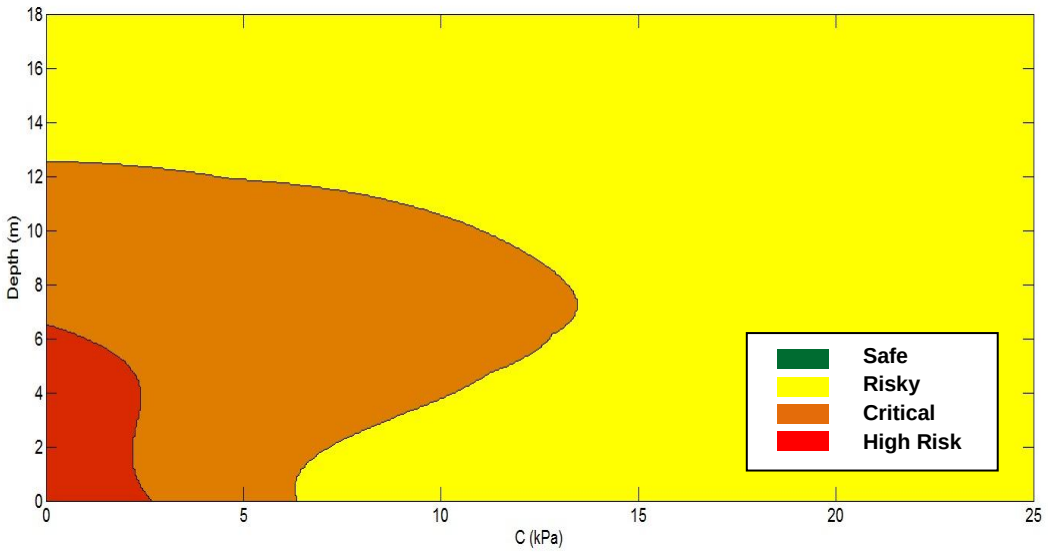

Figure 5-38 Associated Risk for Box Jacking (s = 50 mm or 1.97 in.)

As explained in Chapter 5, the maximum surface vertical displacement is increased when depth and cohesion are decreased. According to Figure 5-36 through Figure 5-38, associated risk with box jacking is decreased as cohesion and depth are increased. Therefore, the high risk area is located near the origin of the graph where depth of the box from surface is shallow and the cohesion of the soil is low. On the other hand, associated risk is the lowest in the opposite corner where both depth and cohesion have the highest amount.

To determine the risk associated in a BJ project, the following steps should be followed:

1. Determine dominant soil cohesion in the project and locate it on the graph
2. Find the depth of the box from ground surface to the top of the box and locate it on the graph

3. Associated risk of the project is determined by intersecting cohesion and depth on the graph.

If it is determined that the project is high risk or critical, the following actions are recommended to reduce the associated risk:

1. Reduce the size of overcut to reduce associated risk
2. Pump bentonite slurry with adequate pressure into the annular space during project execution. High pressure may create heaves on the surface while low pressure may not prevent soil from collapsing into the annular space and settlement.
3. Freeze soil during bore excavation to prevent soil from collapsing during project execution or after project completion.
4. Grout annular space after project completion to stabilize the soil and prevent settlement.
5. Change the depth of the box from the surface by changing the size of the box culvert. For example, the longer side of box can be installed vertically to decrease the depth of the box from ground surface.
6. Reduce the width of the box culvert. Although box width was assumed constant in developing suggested graphs, it was determined that box width has a significant impact on maximum surface vertical displacement and higher width corresponds with higher maximum surface settlement. Therefore, box width can be reduced to lessen the maximum surface vertical displacement.

Continuous surface monitoring is strongly recommended during project execution and after project completion to assure that possible settlement are within acceptable range.

Chapter Summary

This chapter presented sensitivity analysis results and discussed the effects of different factors such as soil unit weight, soil cohesion, and box culvert dimensions on surface vertical displacements. ANN results were compared with results obtained from new finite element models and case studies. The applicability of an empirical method to predict surface vertical displacement in BJ projects was evaluated. At the end, three graphs were suggested to determine associated risk with box jacking using depth of box from surface, cohesion of soil and overcut.

Chapter 6

Conclusions and Recommendations for Future Research

Conclusions

Conclusions of this research can be summarized as below:

1. Results showed that soil cohesion and box depth from surface had the highest impact on surface vertical displacement (settlement) among other parameters such as box dimensions, soil friction angle, soil modulus of elasticity.
2. Soil friction and dilation angles had the lowest impact on surface vertical displacement (settlement).
3. Associated risk with box jacking projects was increased by decrease of soil cohesion and box depth from ground surface.
4. An empirical method, suggested by Milligan and Marshal (1986), was not able to estimate surface displacement associated with box jacking accurately. The method overestimated maximum surface displacement (settlement) and underestimate settlement trough (channel) width.
5. Trained Artificial Neural Network (ANN) was able to estimate surface vertical displacement (settlement) accurately.
6. Arching occurs on top of box culverts and causes less displacement to be transferred to the surface.
7. Vertical stress on top of box culverts was minimum on the box centerline and increased away until it reached its maximum on the edge of box culvert. Then, it decreases away from the edge of box to reach expected value (e.g., γH).

8. None of Terzaghi and Marston's theory was able to estimate vertical stress on top of box culverts. Both theories underestimated vertical stress on top of box culverts.

Recommendations for Future Research

Recommendations for future research can summarized as below:

1. Extend the study to cohesion soils and compare the results with results in this research.
2. Consider the effect of water table fluctuations and its effect on soil properties.
3. Consider traffic load in developing a surface predictive model.
4. Investigate surface vertical displacement associated with box jacking in shallower depths.
5. Consider the effect of bentonite slurry pumping into the annular space on reducing maximum surface vertical displacement.
6. Study arching effect in BJ projects to determine arching zone and vertical stress on top of box culverts.
7. Study possible box settlement during project execution and its effect on surface settlement.
8. Simulate BJ process using 3D models and investigate the effect soil consolidation after completion of the project.

Appendix A

Standard Box Culvert Size

Reinforced Concrete Box Culvert

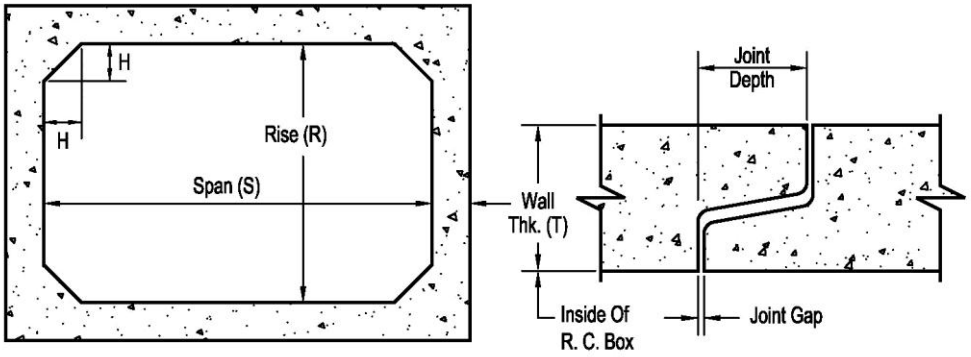

Section thru Box Culvert

Section thru Box Joint

Span (S) → / Rise (R) ↓	Standard Box Culvert Weights (lbs.) per Foot									
	3	4	5	6	7	8	9	10	11	12
2	605	905								
3	705	1025	1425	1885	2410					
4		1155	1575	2060	2600	2800			4880	5700
5			1725	2235	2800	3000	3655	4375		
6				2410	3000	3200	3885	4625	5430	6300
7					3200	3400	4105	4875		
8						3600	4335	5125	5980	6900
9							4555	5375		
10								5625	6530	7500
11									6810	
12										8100
Wall (T)	4	5	6	7	8	8	9	10	11	12
Haunch (H)	7	7,8	7,8	7,8,12	8,12	8,12	12	12	12	12

Notes: Box dimensions may vary depending upon equipment availability.

1. Produced to meet ASTM Specifications.
2. Contact a Concrete Pipe Division representative for details not listed on this sheet.
3. Walls, Slabs and Haunches are designed to meet ASTM / AASHTO standards and project specifications. Rinker 013

Appendix B

PLAXIS Software

PLAXIS is geotechnical finite element software, specially developed for the 2D and 3D analysis of deformation and stability of soil structures, as well as geo-engineering applications such as excavation, foundation, embankments and tunnels. PLAXIS 2D enables users to generate a geometry model and finite element mesh based on a representative vertical cross section of the project by use of a graphical interface. PLAXIS has staged construction feature that enables the user to simulate different construction stages and analysis types. The PLAXIS 2D program can model real situations either by a plane strain or an axisymmetric model. A plane strain model can be used in geometrics with a uniform cross section where strains in z-direction (e.g., perpendicular to the cross section) are assumed to be zero. However, normal stresses in z-direction are considered in the model. An axisymmetric model is used for circular structures where stress and strain are assumed to be identical in any radial direction. Figure B-1 shows examples of plane strain and axisymmetric models.

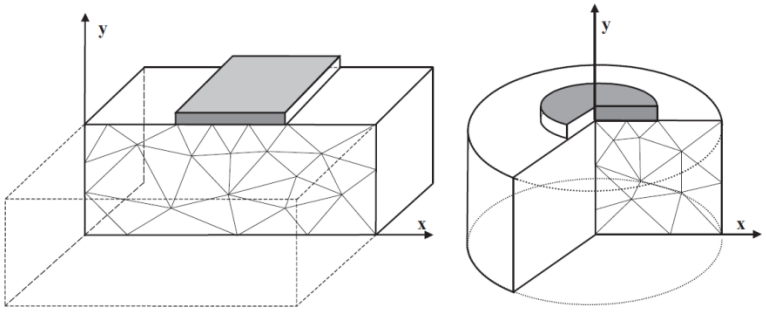

(a) (b)

Figure B-1 Example of PLAXIS Problems: a) Plane Strain,

and b) Axisymmetric (PLAXIS, 2011)

Two types of triangle element, 6-node and 15-node, are available in PLAXIS 2D to model soil layers and structures. 6-node element offers a second order interpolation for displacements and the numerical integration involves three Gauss points (stress points) as presented in Figure B-2.

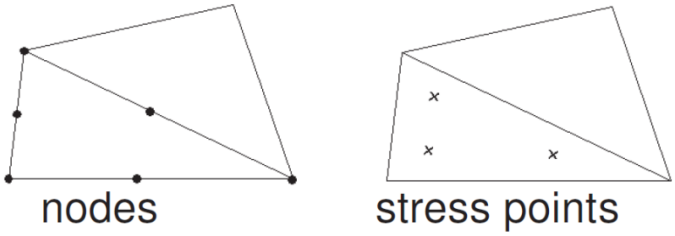

Figure B-2 6-node Triangular Element (PLAXIS, 2011)

A 15-node element, as presented in Figure B-3, provides a fourth order interpolation for displacement and the numerical integration involves twelve Gauss points. The use of a 15-node element leads to more accurate results compared to 6-node element. Moreover, it consumes more memory and results in a slower calculation speed.

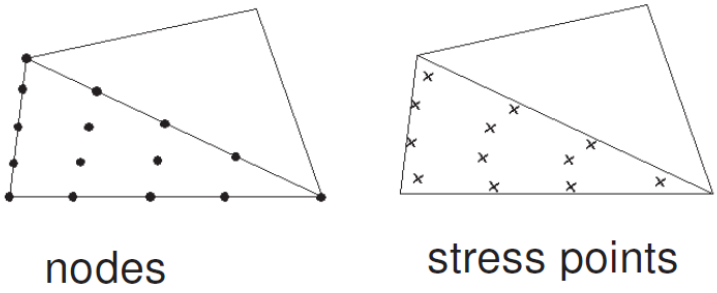

Figure B-3 15-node Element (PLAXIS-2011)

PLAXIS 2D version 2010.01 provides different models to simulate soil behavior. The PLAXIS 2D version 2010.01 has eight built-in material models:

1. Linear elastic model
2. Mohr-Coulomb model (MC)
3. Hardening Soil model (HS)
4. Hardening Soil model with small-strain stiffness (HS small)
5. Soft Soil model (SS)
6. Soft Soil Creep model (SSC)
7. Jointed Rock model (JR)
8. Modified Cam-Clay model (MCC)

Each model can be used to represent a specific type of soil behavior. Linear elastic model uses Hook's law of isotropic linear elasticity to model stiff structures in the soil. MC model is a well-known elastic perfectly-plastic model that estimates a constant average stiffness for the soil layer. HS model is an elastoplastic type of hyperbolic model, formulated in the framework of shear hardening plasticity. HS model involves compression hardening which is suitable to simulate the behavior of sand and gravel as well as softer types of soil such as clays and silts. HS small model is similar to HS model. However, it incorporates strain dependent stiffness moduli that enables the user to simulate different reactions of soils from small strains to large strains. SS model is a Cam-Clay type model that can be used to simulate the behavior of soft soils such as normally consolidated clays and peat. This model assumes that the soil is isotropic, elastoplastic and is not affected by creep. SSC model consists of logarithmic primary and secondary compression and can be used to simulate the time-dependent behavior of soft soils such as normally consolidated clays and peat. JR model is an anisotropic elastic-perfectly plastic model used to simulate the anisotropic behavior of stratified or jointed rock. The model assumes that plastic shearing can occur in a limited number of shearing directions. MCC model assumes a logarithmic relationship between the volumetric strain and the mean effective stress and can be used to simulate the behavior of normally consolidated soft soils (PLAXIS, 2011).

Five types of analysis are available in PLAXIS 2D:

1. Initial stress generation
2. Plastic
3. Plastic drained
4. Consolidation (EPP)
5. Safety
6. Dynamic

The initial stress in the body of the soil is generated by the weight of the material. PLAXIS 2D has two options namely the K_0 procedure and gravity loading to generate initial

stress. The K_0 procedure is suitable for problems with a horizontal surface with all soil layers and phreatic levels parallel to the surface, while gravity loading is applicable for all other cases. K_0 is called a lateral earth pressure coefficient and relates initial horizontal effective stress ($\sigma'_{h,0}$) to the initial vertical effective stress ($\sigma'_{v,0}$). Gravity loading use plastic analysis to generate initial stress based on the volumetric weight of the soil. Plastic calculation uses small deformation theory to carry out an elastic-plastic deformation analysis. Stiffness matrix is calculated based on the original unreformed geometry in the plastic analysis. This type of analysis is widely used to analyze geotechnical projects where time effects can be ignored. Plastic drained analysis is similar to plastic analysis in which undrained behavior is ignored. Consolidation (EPP) analysis is appropriate to analyze the time-dependent development and dissipation of excess pore pressure in saturated clayey soils. PLAXIS provides consolidation analysis to be conducted after an undrained plastic calculation without any additional loading. In safety analysis the failure of the structure is obtained by reducing the strength parameters, tan ϕ and c of the soil. Dynamic analysis is used where stress waves and vibrations need to be considered in soils. Special boundary conditions need to be defined to eliminate the effect of reflection of waves from boundaries (PLAXIS, 2011).

Appendix C

Data Sets

1) 1.8 m x 1.2 m (6 ft x 4 ft)

No.	Gap(cm)	Depth(*D)	SPT	Es(KPa)	ϕ	γ (KN/m3)	c(KPa)
1	5	4	44	29500	37	19.4	7.8
2	3	4	20	17500	34	17.0	10.1
3	4	6	35	25000	36	18.5	16.5
4	5	2	15	15000	33	16.5	4.3
5	5	3	16	15500	33	16.6	6.4
6	3	4	43	29000	37	19.3	22.7
7	5	6	43	29000	37	19.3	6.3
8	4	4	29	22000	35	17.9	15.5
9	4	6	32	23500	35	18.2	11.3
10	4	2	12	13500	32	16.2	14.0
11	5	3	10	12500	32	16.0	13.3
12	3	6	35	25000	36	18.5	8.0
13	4	5	9	12000	32	15.7	7.1
14	5	4	47	31000	38	19.7	10.3
15	4	2	10	12500	32	16.0	17.4
16	5	6	36	25500	36	18.6	19.7
17	5	4	15	15000	33	16.5	0.8
18	4	4	40	27500	37	19.0	20.6
19	3	4	4	9500	30	14.0	23.6
20	5	4	6	10500	31	14.7	11.2
21	3	5	41	28000	37	19.1	2.8
22	3	2	27	21000	35	17.7	3.2
23	3	5	25	20000	34	17.5	18.4
24	5	5	33	24000	35	18.3	18.8
25	4	2	9	12000	32	15.7	19.3
26	3	3	26	20500	34	17.6	10.9
27	4	6	29	22000	35	17.9	12.0
28	3	2	46	30500	37	19.6	10.1
29	5	5	46	30500	37	19.6	20.5
30	3	5	24	19500	34	17.4	16.9
31	5	2	48	31500	38	19.8	2.0
32	3	2	36	25500	36	18.6	22.7
33	3	2	17	16000	33	16.7	2.6
34	4	5	11	13000	32	16.1	2.2
35	4	4	8	11500	31	15.3	4.4

No.	Gap(cm)	Depth(*D)	SPT	Es(KPa)	ϕ	γ (KN/m3)	c(KPa)
36	5	3	5	10000	30	14.3	7.8
37	5	5	44	29500	37	19.4	3.5
38	4	4	41	28000	37	19.1	17.7
39	5	2	9	12000	32	15.7	1.2
40	5	6	32	23500	35	18.2	11.4
41	4	5	42	28500	37	19.2	20.4
42	5	2	24	19500	34	17.4	8.0
43	5	6	30	22500	35	18.0	22.0
44	3	6	48	31500	38	19.8	0.8
45	4	3	20	17500	34	17.0	13.1
46	5	3	36	25500	36	18.6	11.2
47	3	3	49	32000	38	19.9	5.1
48	3	6	34	24500	36	18.4	0.5
49	4	3	22	18500	34	17.2	3.8
50	3	2	28	21500	35	17.8	22.5

2) 1.8 m x 1.8 m (6 ft x 6 ft)

No.	Gap(cm)	Depth(*D)	SPT	Es(KPa)	ϕ	γ (KN/m3)	c(KPa)
1	5	6	17	16000	33	16.7	3.2
2	4	3	5	10000	30	14.3	2.4
3	5	3	39	27000	36	18.9	7.5
4	5	3	18	16500	33	16.8	12.3
5	5	5	31	23000	35	18.1	21.7
6	4	2	17	16000	33	16.7	7.9
7	4	4	35	25000	36	18.5	14.0
8	5	5	18	16500	33	16.8	2.8
9	5	2	36	25500	36	18.6	22.0
10	3	4	33	24000	35	18.3	21.9
11	3	4	39	27000	36	18.9	17.6
12	5	3	29	22000	35	17.9	13.5
13	4	2	26	20500	34	17.6	9.3
14	4	4	40	27500	37	19.0	3.6
15	3	2	40	27500	37	19.0	0.5
16	4	4	45	30000	37	19.5	2.7
17	4	4	41	28000	37	19.1	13.3
18	3	3	36	25500	36	18.6	9.9
19	3	4	10	12500	32	16.0	10.5

No.	Gap(cm)	Depth(*D)	SPT	Es(KPa)	ϕ	γ (KN/m3)	c(KPa)
20	4	2	34	24500	36	18.4	20.9
21	5	3	49	32000	38	19.9	11.2
22	4	5	29	22000	35	17.9	15.3
23	4	4	19	17000	33	16.9	8.8
24	3	4	30	22500	35	18.0	3.7
25	4	3	20	17500	34	17.0	0.1
26	4	4	42	28500	37	19.2	13.2
27	5	6	44	29500	37	19.4	3.7
28	5	4	15	15000	33	16.5	0.5
29	4	5	10	12500	32	16.0	2.6
30	4	6	33	24000	35	18.3	1.8
31	5	2	43	29000	37	19.3	20.1
32	5	2	20	17500	34	17.0	4.4
33	3	2	15	15000	33	16.5	23.4
34	5	4	47	31000	38	19.7	5.1
35	5	3	43	29000	37	19.3	21.2
36	3	5	8	11500	31	15.3	7.7
37	3	5	31	23000	35	18.1	5.1
38	3	6	19	17000	33	16.9	23.6
39	4	2	28	21500	35	17.8	8.4
40	3	2	41	28000	37	19.1	15.0
41	3	3	6	10500	31	14.7	9.4
42	4	4	8	11500	31	15.3	18.9
43	5	4	16	15500	33	16.6	20.8
44	3	3	15	15000	33	16.5	13.8
45	3	3	9	12000	32	15.7	6.7
46	4	5	25	20000	34	17.5	20.7
47	4	3	30	22500	35	18.0	1.8
48	3	6	34	24500	36	18.4	7.8
49	4	3	36	25500	36	18.6	11.7
50	5	5	16	15500	33	16.6	7.2

3) 2.4 m x 1.2 m (8 ft x 4 ft)

No.	Gap(cm)	Depth(*D)	SPT	Es(KPa)	ϕ	γ (KN/m3)	c(KPa)
1	4	3	41	28000	37	19.1	1.2
2	3	5	33	24000	35	18.3	20.3
3	4	2	31	23000	35	18.1	10.0

No.	Gap(cm)	Depth(*D)	SPT	Es(KPa)	ϕ	γ (KN/m3)	c(KPa)
4	4	2	40	27500	37	19.0	2.9
5	5	4	43	29000	37	19.3	7.3
6	5	6	44	29500	37	19.4	10.2
7	4	4	7	11000	31	15.0	12.4
8	4	6	32	23500	35	18.2	9.1
9	5	3	17	16000	33	16.7	7.3
10	3	2	4	9500	30	14.0	13.6
11	3	2	18	16500	33	16.8	8.1
12	3	4	31	23000	35	18.1	7.1
13	4	3	26	20500	34	17.6	12.8
14	5	3	15	15000	33	16.5	3.5
15	5	6	22	18500	34	17.2	1.0
16	3	6	46	30500	37	19.6	12.9
17	4	2	14	14500	33	16.4	1.0
18	5	5	47	31000	38	19.7	12.9
19	5	4	43	29000	37	19.3	16.1
20	4	2	23	19000	34	17.3	20.2
21	4	3	25	20000	34	17.5	22.8
22	5	5	32	23500	35	18.2	15.0
23	4	4	12	13500	32	16.2	0.7
24	5	4	31	23000	35	18.1	11.8
25	5	2	48	31500	38	19.8	11.9
26	3	3	34	24500	36	18.4	3.6
27	4	4	48	31500	38	19.8	9.3
28	5	2	40	27500	37	19.0	4.4
29	4	5	15	15000	33	16.5	2.7
30	3	5	26	20500	34	17.6	9.9
31	4	2	49	32000	38	19.9	8.7
32	4	5	9	12000	32	15.7	10.8
33	4	3	18	16500	33	16.8	4.5
34	5	6	28	21500	35	17.8	18.1
35	3	4	6	10500	31	14.7	9.8
36	3	5	11	13000	32	16.1	6.1
37	5	2	16	15500	33	16.6	13.7
38	4	6	6	10500	31	14.7	16.3
39	5	3	41	28000	37	19.1	18.5
40	4	2	32	23500	35	18.2	3.0

No.	Gap(cm)	Depth(*D)	SPT	Es(KPa)	ϕ	γ (KN/m3)	c(KPa)
41	3	3	7	11000	31	15.0	17.9
42	3	2	10	12500	32	16.0	19.8
43	3	6	8	11500	31	15.3	0.3
44	3	2	10	12500	32	16.0	1.2
45	3	2	22	18500	34	17.2	15.8
46	5	2	7	11000	31	15.0	4.6
47	5	2	17	16000	33	16.7	19.9
48	3	4	32	23500	35	18.2	11.7
49	3	6	8	11500	31	15.3	13.2
50	4	6	35	25000	36	18.5	16.1

4) 2.4 m x 2.4 m (8 ft x 8 ft)

No.	Gap(cm)	Depth(*D)	SPT	Es(KPa)	ϕ	γ (KN/m3)	c(KPa)
1	4	5	44	29500	37	19.4	18.3
2	5	6	18	16500	33	16.8	8.7
3	3	5	21	18000	34	17.1	18.3
4	4	4	47	31000	38	19.7	12.4
5	3	5	33	24000	35	18.3	7.5
6	5	6	34	24500	36	18.4	19.2
7	3	4	9	12000	32	15.7	4.6
8	5	3	31	23000	35	18.1	3.4
9	4	4	30	22500	35	18.0	21.6
10	5	2	5	10000	30	14.3	1.8
11	5	4	25	20000	34	17.5	17.2
12	4	6	41	28000	37	19.1	1.4
13	5	5	47	31000	38	19.7	16.9
14	3	5	48	31500	38	19.8	9.3
15	4	3	15	15000	33	16.5	7.5
16	4	2	5	10000	30	14.3	8.4
17	5	6	30	22500	35	18.0	8.0
18	4	4	41	28000	37	19.1	6.6
19	4	6	5	10000	30	14.3	18.7
20	3	2	38	26500	36	18.8	13.9
21	3	6	33	24000	35	18.3	21.1
22	3	6	7	11000	31	15.0	10.0
23	3	3	24	19500	34	17.4	0.7
24	3	4	11	13000	32	16.1	5.8

No.	Gap(cm)	Depth(*D)	SPT	Es(KPa)	ϕ	γ (KN/m3)	c(KPa)
25	3	5	49	32000	38	19.9	7.8
26	5	5	16	15500	33	16.6	23.8
27	4	2	49	32000	38	19.9	6.2
28	5	3	48	31500	38	19.8	21.7
29	5	2	22	18500	34	17.2	23.8
30	3	2	13	14000	32	16.3	1.5
31	4	2	38	26500	36	18.8	11.6
32	4	5	44	29500	37	19.4	15.2
33	3	6	25	20000	34	17.5	13.4
34	3	3	39	27000	36	18.9	21.4
35	5	5	18	16500	33	16.8	1.2
36	4	5	27	21000	35	17.7	22.7
37	5	4	9	12000	32	15.7	17.6
38	4	4	42	28500	37	19.2	4.8
39	3	4	40	27500	37	19.0	13.8
40	4	3	22	18500	34	17.2	3.7
41	4	6	26	20500	34	17.6	2.9
42	4	5	30	22500	35	18.0	23.8
43	5	4	10	12500	32	16.0	20.6
44	5	5	17	16000	33	16.7	22.1
45	5	2	41	28000	37	19.1	9.9
46	5	6	24	19500	34	17.4	6.2
47	5	5	34	24500	36	18.4	22.2
48	3	6	7	11000	31	15.0	11.8
49	5	3	8	11500	31	15.3	14.0
50	5	4	26	20500	34	17.6	3.5

5) 3 m x 1.5 m (10 ft x 5 ft)

No.	Gap(cm)	Depth(*D)	SPT	Es(KPa)	ϕ	γ (KN/m3)	c(KPa)
1	3	2	41	28000	37	19.1	13.9
2	5	4	29	22000	35	17.9	1.2
3	4	4	38	26500	36	18.8	14.3
4	4	5	27	21000	35	17.7	0.0
5	5	6	14	14500	33	16.4	19.1
6	3	2	21	18000	34	17.1	1.6
7	4	2	12	13500	32	16.2	18.5
8	5	2	32	23500	35	18.2	4.5

No.	Gap(cm)	Depth(*D)	SPT	Es(KPa)	ϕ	γ (KN/m3)	c(KPa)
9	5	5	36	25500	36	18.6	18.1
10	5	3	14	14500	33	16.4	6.5
11	5	5	46	30500	37	19.6	5.0
12	5	5	12	13500	32	16.2	7.9
13	5	2	12	13500	32	16.2	7.9
14	3	3	4	9500	30	14.0	10.4
15	3	6	32	23500	35	18.2	16.5
16	4	5	41	28000	37	19.1	3.5
17	5	5	32	23500	35	18.2	5.2
18	4	6	11	13000	32	16.1	20.9
19	3	5	4	9500	30	14.0	10.1
20	4	2	5	10000	30	14.3	6.5
21	3	6	31	23000	35	18.1	20.6
22	3	5	43	29000	37	19.3	23.1
23	5	4	23	19000	34	17.3	19.5
24	4	3	46	30500	37	19.6	21.9
25	5	3	31	23000	35	18.1	17.4
26	4	4	27	21000	35	17.7	17.7
27	4	6	32	23500	35	18.2	23.0
28	5	3	23	19000	34	17.3	19.9
29	5	2	5	10000	30	14.3	21.6
30	5	2	8	11500	31	15.3	15.8
31	3	2	9	12000	32	15.7	8.0
32	4	6	22	18500	34	17.2	0.6
33	4	5	8	11500	31	15.3	14.1
34	3	3	38	26500	36	18.8	20.1
35	5	5	23	19000	34	17.3	0.6
36	4	3	14	14500	33	16.4	10.4
37	4	2	49	32000	38	19.9	22.3
38	5	6	25	20000	34	17.5	0.2
39	3	5	4	9500	30	14.0	0.3
40	3	2	41	28000	37	19.1	11.9
41	4	3	17	16000	33	16.7	14.4
42	5	2	8	11500	31	15.3	6.6
43	4	2	21	18000	34	17.1	17.1
44	5	6	38	26500	36	18.8	10.7
45	4	2	34	24500	36	18.4	23.2

No.	Gap(cm)	Depth(*D)	SPT	Es(KPa)	ϕ	γ (KN/m3)	c(KPa)
46	3	3	23	19000	34	17.3	5.2
47	3	5	25	20000	34	17.5	1.4
48	5	2	43	29000	37	19.3	1.2
49	3	4	41	28000	37	19.1	9.9
50	4	5	12	13500	32	16.2	13.6

6) 3 m x 3 m (10 ft x 10 ft)

No.	Gap(cm)	Depth(*D)	SPT	Es(KPa)	ϕ	γ (KN/m3)	c(KPa)
1	4	4	36	25500	36	18.6	20.1
2	3	3	43	29000	37	19.3	22.1
3	5	5	23	19000	34	17.3	9.5
4	5	3	22	18500	34	17.2	12.8
5	4	5	25	20000	34	17.5	12.8
6	3	4	27	21000	35	17.7	16.0
7	4	4	34	24500	36	18.4	23.0
8	5	4	23	19000	34	17.3	1.8
9	4	6	19	17000	33	16.9	1.3
10	3	2	28	21500	35	17.8	21.2
11	5	6	17	16000	33	16.7	8.2
12	3	2	11	13000	32	16.1	4.6
13	4	6	6	10500	31	14.7	14.5
14	4	2	23	19000	34	17.3	23.3
15	4	5	48	31500	38	19.8	15.1
16	5	5	35	25000	36	18.5	7.9
17	3	4	32	23500	35	18.2	1.7
18	5	6	41	28000	37	19.1	0.8
19	3	5	35	25000	36	18.5	3.3
20	5	6	37	26000	36	18.7	20.2
21	3	6	41	28000	37	19.1	16.0
22	4	5	39	27000	36	18.9	6.1
23	5	5	10	12500	32	16.0	5.8
24	5	5	47	31000	38	19.7	13.6
25	3	4	33	24000	35	18.3	3.9
26	5	5	40	27500	37	19.0	15.7
27	3	2	19	17000	33	16.9	3.2
28	5	3	10	12500	32	16.0	22.5
29	5	2	10	12500	32	16.0	10.2

No.	Gap(cm)	Depth(*D)	SPT	Es(KPa)	ϕ	γ (KN/m3)	c(KPa)
30	5	4	29	22000	35	17.9	8.4
31	4	6	13	14000	32	16.3	15.0
32	5	4	25	20000	34	17.5	7.4
33	3	6	19	17000	33	16.9	3.6
34	5	2	33	24000	35	18.3	17.1
35	4	3	36	25500	36	18.6	6.7
36	4	4	12	13500	32	16.2	21.1
37	4	3	20	17500	34	17.0	21.3
38	3	5	49	32000	38	19.9	9.5
39	5	6	46	30500	37	19.6	10.6
40	4	5	44	29500	37	19.4	7.4
41	3	5	49	32000	38	19.9	23.7
42	3	6	42	28500	37	19.2	18.9
43	3	6	28	21500	35	17.8	21.2
44	4	6	14	14500	33	16.4	20.5
45	4	4	26	20500	34	17.6	19.5
46	4	2	28	21500	35	17.8	1.7
47	3	5	37	26000	36	18.7	8.2
48	5	4	19	17000	33	16.9	19.8
49	4	2	46	30500	37	19.6	15.8
50	5	2	24	19500	34	17.4	18.6

Appendix D

MATLAB Neural Network Code

```
Inputs = x
targets = t

% Create a Feed Forward Network
hiddenLayerSize = 10;
net = feedforwardnet(hiddenLayerSize);
net.numLayers = 2
%Transfer Functions
net.layers{1}.transferFcn='tansig'
net.layers{2}.transferFcn='tansig'

% Choose Input and Output Pre/Post-Processing Functions
net.inputs{1}.processFcns = {'removeconstantrows','mapminmax'};
net.outputs{2}.processFcns = {'removeconstantrows','mapminmax'};


% Setup Division of Data for Training, Validation, Testing
% For a list of all data division functions type: help nndivide
net.divideFcn = 'dividerand';  % Divide data randomly
net.divideMode = 'sample';  % Divide up every sample
net.divideParam.trainRatio = 70/100;
net.divideParam.valRatio = 15/100;
net.divideParam.testRatio = 15/100;

net.trainFcn = 'trainlm';  % Levenberg-Marquardt

% Choose a Performance Function
net.performFcn = 'mse';  % Mean squared error

% Choose Plot Functions
net.plotFcns = {'plotperform','plottrainstate','ploterrhist', ...
  'plotregression', 'plotfit'};
% Training Parameters
net.trainParam.epochs = 1000
net.trainParam.goal = 0
net.trainParam.max_fail = 6
net.trainParam.min_grad = 1e-7
net.trainParam.mu = 0.001
net.trainParam.mu_dec = 0.1
net.trainParam.mu_inc = 10
net.trainParam.mu_max = 1e10
net.trainParam.show = 25
net.trainParam.showCommandLine = 0
net.trainParam.showWindow = 1

% Train the Network
[net,tr] = train(net,inputs,targets);

% Test the Network
outputs = net(inputs);
errors = gsubtract(targets,outputs);
performance = perform(net,targets,outputs)
```

```
% Recalculate Training, Validation and Test Performance
trainTargets = targets .* tr.trainMask{1};
valTargets = targets  .* tr.valMask{1};
testTargets = targets  .* tr.testMask{1};
trainPerformance = perform(net,trainTargets,outputs)
valPerformance = perform(net,valTargets,outputs)
testPerformance = perform(net,testTargets,outputs)

% View the Network
view(net)
predict = sim(net,sample)

%Plots
figure, plotperform(tr)
figure, plottrainstate(tr)
figure, plotfit(net,inputs,targets)
figure, plotregression(targets,outputs)
figure, ploterrhist(errors)
```

Appendix E

GEOKON Pressure Transducer

VW Piezometers & Pressure Transducers

Applications
For the measurement of...

- Ground water elevations
- Pore water pressures
- Pump tests
- Uplift pressures in dam foundations
- Hydraulic pressures in tanks and pipelines
- Wick drain efficiency
- Water pressures behind tunnel linings

• Model 4500C, 4500S, 4500H, 4500DP and 4500HD Vibrating Wire Piezometers (front to back)

Operating Principle

The transducer uses a pressure sensitive diaphragm with a vibrating wire element attached to it. The diaphragm is welded to a capsule which is evacuated and hermetically sealed. Fluid pressures acting upon the outer face of the diaphragm cause deflections of the diaphragm and changes in tension and frequency of the vibrating wire. The changing frequency is sensed and transmitted to the readout device by an electrical coil acting through the walls of the capsule.

Piezometers incorporate a porous filter stone ahead of the diaphragm, which allows the fluid to pass through but prevents soil particles from impinging directly on the diaphragm.

Advantages and Limitations

The 4500 Series Vibrating Wire Piezometers and Pressure Transducers have outstanding long-term stability and reliability, and low thermal zero shift. Cable lengths of several kilometers are no problem and the frequency output signal is not affected by changing cable resistances (caused by splicing, changes of length, terminal contact resistances, etc.), nor by penetration of moisture into the electronic circuitry.

A thermistor located in the housing permits the measurement of temperatures at the piezometer location.

All-stainless steel or titanium construction and evacuation of the capsule guarantees a high level of corrosion resistance. Integral gas discharge tubes inside the main housing protect against lightning damage.

Standard porous filters are made from sintered 316 stainless steel. High air-entry ceramic filters are available for use in applications requiring that air be prevented from passing through the filter.

Vented versions of all models are available to provide automatic compensation for barometric pressure fluctuations. Negative pressures up to 1 Bar can be measured.

Vibrating wire pressure transducers are not suitable for the measurement of rapidly changing pressures: for these purposes Model 3400 transducers should be used.

Model 4500S/SV/SH/AL/ALV Standard Piezometers

• Model 4500S (front) and Model 4500AL (rear) Standard Piezometers.

The Model 4500S/SV Standard Piezometer is designed to measure fluid pressures such as ground water elevations and pore pressures when buried directly in embankments, fills, etc. It is also suitable for installation inside boreholes, observation wells and standard (>19 mm diameter) piezometer riser pipe.

The Model 4500SH is designed with a heavy duty housing for pressures that exceed 3 MPa.

The Model 4500AL is designed for low-pressure ranges. The vented version (Model 4500ALV) provides automatic compensation for barometric pressure changes. Thermistors are included to measure temperatures.

Model 4500DP Drive Point Piezometers

• Model 4500DP Drive Point Piezometers.

The Model 4500DP Drive Point Piezometer has the transducer located inside a housing with an EW drill rod thread and removable pointed nose cone. When threaded onto the end of EW drill rods, the unit can be pushed directly into soft ground with the signal cable located inside the drill rod. This model is ideally suited for use in soft clays and landfills. The piezometer may be recovered at the end of the job.

Models are also available that are similar in construction to the 4500DP but which use standard metric threads allowing for installation using cone penetrometer and other drill rods with adapters.

Model 4500B/BV/C Small Diameter Piezometers

• Model 4500C (front) and Model 4500B (rear) Small Diameter Piezometers.

These piezometers are designed to enable the automation of small diameter piezometer standpipes. The 4500B/BV fits inside 19 mm pipe and the 4500C inside 12 mm pipe.

Model 4500HD Heavy Duty Piezometer

• Model 4500HD Heavy Duty Piezometer.

The Model 4500HD Heavy Duty Piezometer is designed for direct burial in fills and dam embankments. The 4500HD is used in conjunction with heavily armored cable to withstand earth movements during construction. Recommended for use in earth dams.

Model 4500H/HH Pressure Transducers

• *Model 4500H Pressure Transducer.*

The Model 4500H and 4500HH Pressure Transducers are supplied with a ¼-18 NPT pipe thread fitting to permit the transducer to be coupled directly into hydraulic or pneumatic pressure lines. Other pipe thread sizes are also available.

Model 4500HT High Temperature Piezometer

• *Model 4500HT High Temperature Piezometer.*

The Model 4500HT High Temperature Piezometer is designed for applications for temperatures up to 230°C. These sensors are supplied with either mineral insulated cables or Teflon cables inside stainless steel tubing. *For further details, please see the Model 4500HT data sheet.*

Model 4500Ti Titanium Piezometer

• *Model 4500Ti Titanium Piezometer.*

The Model 4500Ti is designed specifically for use in highly corrosive environments such as landfills and leach fields. Also used in critical areas where long term survivability is essential, for example, as in nuclear waste repositories and aggressive mine tailings. All exterior surfaces are made from titanium.

Model 4580 Pressure Transducer

• *Model 4580 Pressure Transducer.*

The Model 4580 Pressure Transducers are designed for very low fluid pressure measurements, such as groundwater elevations in wells, water levels in streams, weirs, flumes, etc. Changes in water levels of as little as 0.2 mm can be measured. Non vented types can be used as a barometer to measure atmospheric pressure changes.

Model 4500AR Autoresonant Piezometer

• *Model 4500AR "Autoresonant" Piezometer.*

The Model 4500AR "Autoresonant" Piezometer is designed for use with existing data acquisition systems incapable of reading standard (pluck and read) vibrating wire sensors. It can also be used where low frequency (< 20 Hz) dynamic measurements are required.

The Model 4500AR is powered using a 6-24 VDC supply, which yields a 5 V square wave output at the sensor frequency. This high-output offers excellent noise immunity and enhanced signal transmission over long (300 m+) cables. The Model 4500AR is available in standard pressure ranges, with corresponding resolution, linearity and accuracy.

Appendix F

Horizontal Inclinometer

Horizontal Digitilt Inclinometer Probe

Applications

Horizontal inclinometers are used to obtain profiles of settlement or heave. Typical applications include monitoring settlement and heave under storage tanks, embankments, dams, and landfills.

Operation

The horizontal system consists of inclinometer casing, a horizontal probe, control cable, pull cable, and a readout unit.

Casing is installed in a horizontal trench or borehole with one set of grooves aligned to vertical. If the far end of the casing is not accessible, a dead-end pulley and cable-return pipe are installed with the casing.

The probe, control cable, pull-cable, and readout are used to survey the casing. The initial survey establishes the profile of the casing. Subsequent surveys reveal changes in the profile if ground movement occurs.

The Digitilt probe employs a force-balanced servo-accelerometer to measure tilt in the plane of the probe wheels. During a survey, tilt measurements are obtained at half-meter or 2-foot intervals as the probe is drawn from one end of the casing to the other.

The probe is then reversed end-for-end and drawn through the casing a second time. Tilt measurements from the reversed probe are used to eliminate any error due to sensor bias and to generate checksums for validating the survey.

Settlement and heave are calculated as L(sine q1 - sine q0), where L is the measurement interval, q1 is the current tilt, and q0 is the initial tilt.

Settlement profiles are generated by summing displacements and plotting them.

Advantages

Differential Settlement: Horizontal inclinometers provide full profiles of differential settlement.

Simple Operation: Horizontal inclinometer surveys are simple and relatively quick. Unlike other profilers, there are no reservoirs or pressure sources to adjust and maintain.

Proven Reliability: The Digitilt inclinometer probe has earned a world-wide reputation for high precision and durability.

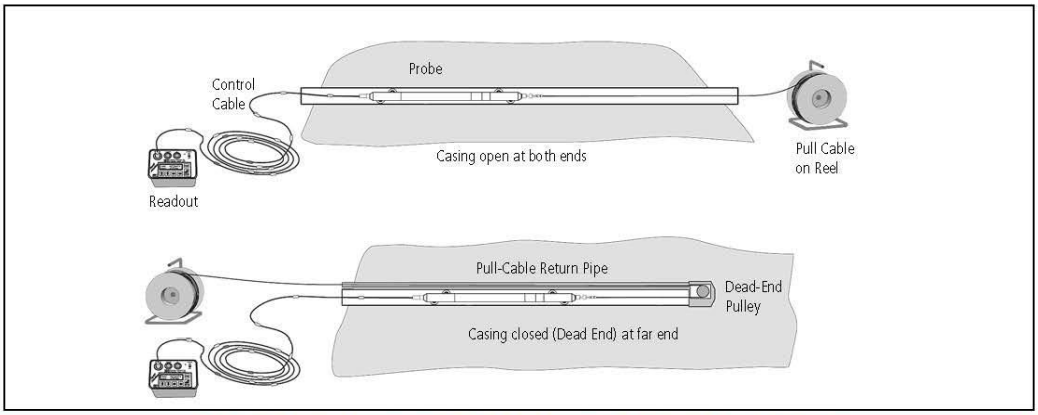

HORIZONTAL DIGITILT PROBE

Horizontal Probe, Metric-Units . . .50303510
Horizontal Probe, English-Units . .50303500

Digitilt inclinometer probe includes a carrying case, accessories and an instruction manual. Control cable and readout are not included.

	Metric	English
Sensor Type	Analog force-balanced servo-accelerometers x 2	
Wheel Base	500 mm	24 inch
Cal Range*	±30°	±30°
Sys Resolution*	0.01 mm	0.0006"
Sys Accuracy*	±6 mm / 25m	±0.3"/ 100'
Precision	±0.01% FS	
Temp	-20 to +50 °C	-4 to +122 °F
Size	38x650 mm	1.5 x 39"
Weight	4.6 kg	10.6 lb
Material	Stainless Ste	
Casing Req	70 or 85mm	

Calibrated Range: Metric and English unit probes are calibrated to ±30° and have an over-range to ±53° and ±42° respectively.

System Resolution: The resolution derived from a two-pass survey converted to mm and inches per standard interval.

System Accuracy: Specifications were derived empirically from the analysis of a large number of surveys and include errors introduced by casing, probe, cable, readout, and operator. Casing was installed within 3 degrees of vertical. Operators followed recommended survey practices. After correcting for systematic errors, the best accuracy obtainable is ±1.4 mm per 50 readings with metric systems and ±0.05 inch per 50 readings with English systems.

CONTROL CABLE

50m Control Cable, Complete. . . .50601050
100m Control Cable, Complete. . .50601100

150 ft Control Cable, Complete . .50601003
300 ft Control Cable, Complete . .50601004

Depth Marks: Metric cable has 0.5m depth marks English cable has 2 foot marks. Marks are molded onto the cable jacket and cannot slip.

Construction: Cable is supplied with no splices or surface defects. Kevlar core provides tensile strength. Dacron torsion braid counters twist and provides dimensional stability. Polyurethane jacket resists chemicals and abrasions and stays flexible in cold temperatures.

Custom Length Cables: Lengths up to 300m (1000 ft) are available on special order. Extension cables are also available.

DIGITILT DATAMATE READOUT

Digitilt DataMate II 50310900

Readout includes hand switch, battery charger with international plugs, and USB cable for PC.

Compatibility: Digitilt probes, both vertical and horizontal, Digitilt tiltmeters, and spiral sensors.

Survey Types: 2-pass surveys for inclinometer probes; 4-pass surveys for spiral sensors.

Minimum Reading Interval: 0.5 m for metric systems and 12 inches for English systems.

Display: Two line backlit LCD shows readings in traditional sine units: 25000 sine (angle) for metric systems and 20000 sine (angle) for English.

Memory Capacity: 160 installations and 32000 A & B axis readings.

Battery: 6 volt, 6 Ah, lead-acid gell cell powers readout and probe up to 16 hours per charge.

Temp Rating: -20 to 50°C (-4 to 122°F).

Case: Aluminum case is splash proof. Connectors are waterproof when capped or in use.

Size & Weight: 127 x 178 x 178 mm at 3 kg. (5 x 7 x 7" at 6.5 lb).

DIGIPR02 SOFTWARE

DigiPro2 Software . . . . . Download
DigiPro2 License Key 50310101

DigiPro2 software is an essential component of the classic system. It has two modes, basic and advanced.

DigiPro2 Basic is free to use and provides all the functions necessary to retrieve surveys from the DataMate and make simple plots.

DigiPro2 Advanced provides correction routines, reports, and many other features that enabled by purchase of a license key. Features are described in a separate datasheet and on the website.

PULL CABLE

Pull Cable 50402310
Extra Carabiner 02750012
Extra Saddle Clamp. 02700067

Pull cable is 1/8" stranded stainless steel cable and is used to draw probe to far end of casing. Order one pull cable for each casing installation. If using a dead-end pulley, length of pull cable should be at least twice the length of the casing.

A carabiner and saddle clamp are included with the probe. These are installed on the pull cable and left in the casing with the pull cable. Additional carabiners, saddle clamps, (and pull cable) should be ordered if there is more than one casing installation to be monitored.

DEAD-END PULLEY

Dead-End Pulley 50302951
Cable-Return Pipe. 50711104
Coupling for Pipe 50711604

Dead-end pulley is required when far end of casing is not accessible. Rated for casing up to 60 m (200') long.

Cable-return pipe is used with dead-end pulley. 1/2" schedule 40 PVC pipe is supplied in 10" (3.05 m) lengths.

Couplings are used to join lengths of pipe. PVC cement is required for assembly.

SLIP-RING REEL

200 m (650') capacity 50503100
300 m (1150') capacity 50503300

Slip-ring cable reel allows the readout to remain connected while the reel is operated. Includes jumper cable to connect reel to readout.

STORAGE REEL

70 m (230') capacity 50502050
100 m (360') capacity 50502110

Sturdy storage reels have large diameter hub keeps cable neat when not in use. 30, 50, and 100 m reels are heavy-duty plastic. 200 m reel is steel.

www.slopeindicator.com
solutions@slope.com
DGSI East 2175 West Park Court, Stone Mountain, GA USA 30087 Tel: +1-770-465-7557
DGSI West 12123 Harbour Reach Drive, Mukilteo, WA, USA 98275 Tel: +1-425-493-6200

Appendix G

Horizontal Inclinometer

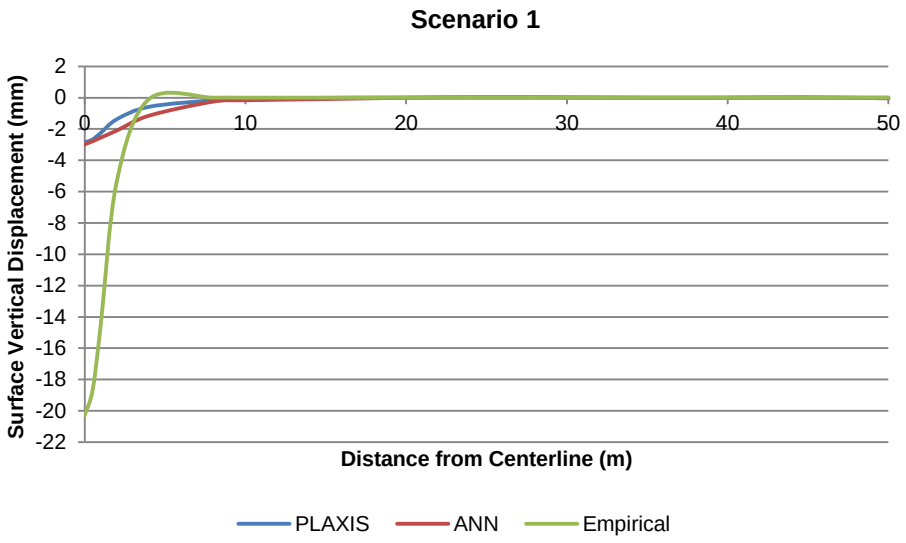
Scenario 1
Surface Vertical Displacement (mm)
2
0
-2
-4
-6
-8
-10
-12
-14
-16
-18
-20
-22
0
10
20
30
40
50
Distance from Centerline (m)
PLAXIS
ANN
Empirical

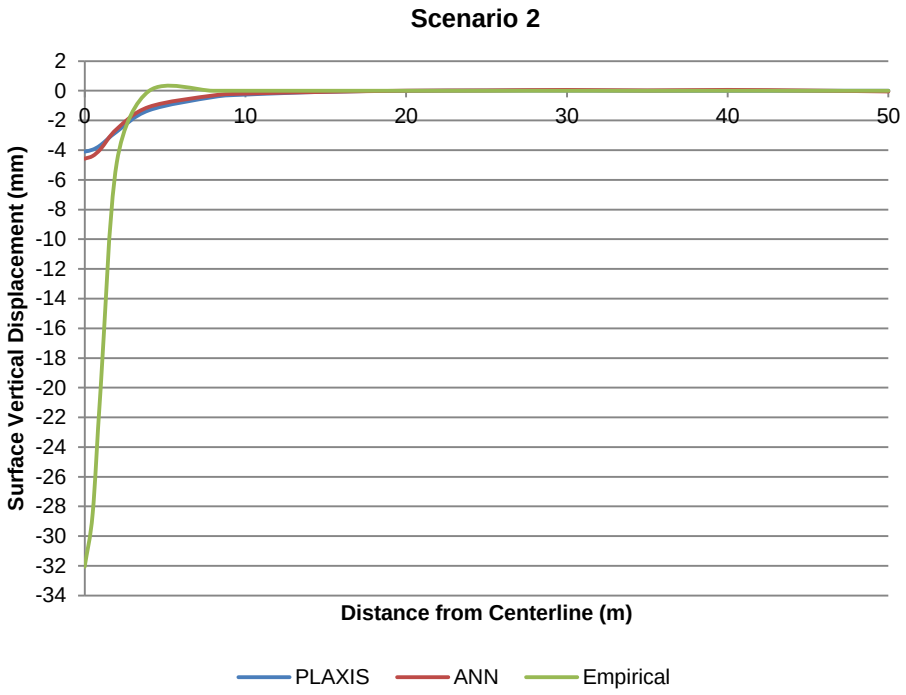
Scenario 2
Surface Vertical Displacement (mm)
2
0
-2
-4
-6
-8
-10
-12
-14
-16
-18
-20
-22
-24
-26
-28
-30
-32
-34
0
10
20
30
40
50
Distance from Centerline (m)
PLAXIS
ANN
Empirical

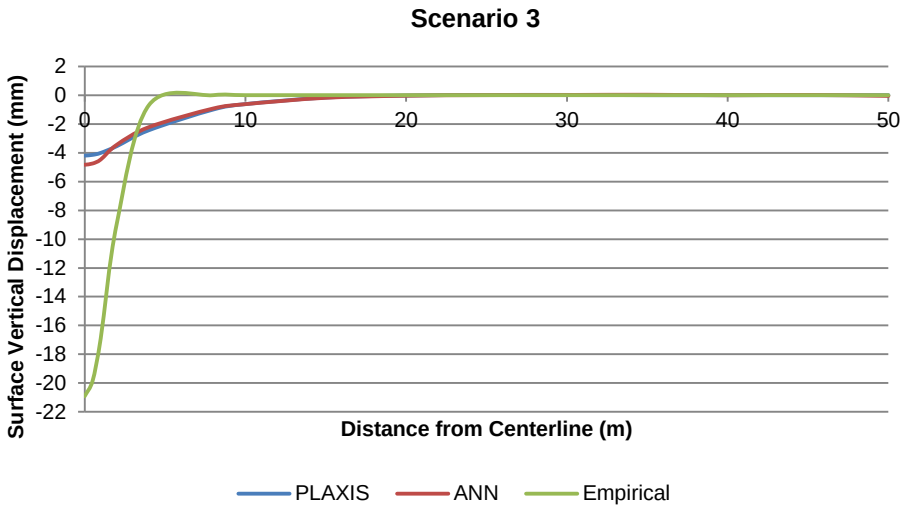
Scenario 3
Surface Vertical Displacement (mm)
2
0
-2
-4
-6
-8
-10
-12
-14
-16
-18
-20
-22
0
10
20
30
40
50
Distance from Centerline (m)
PLAXIS
ANN
Empirical

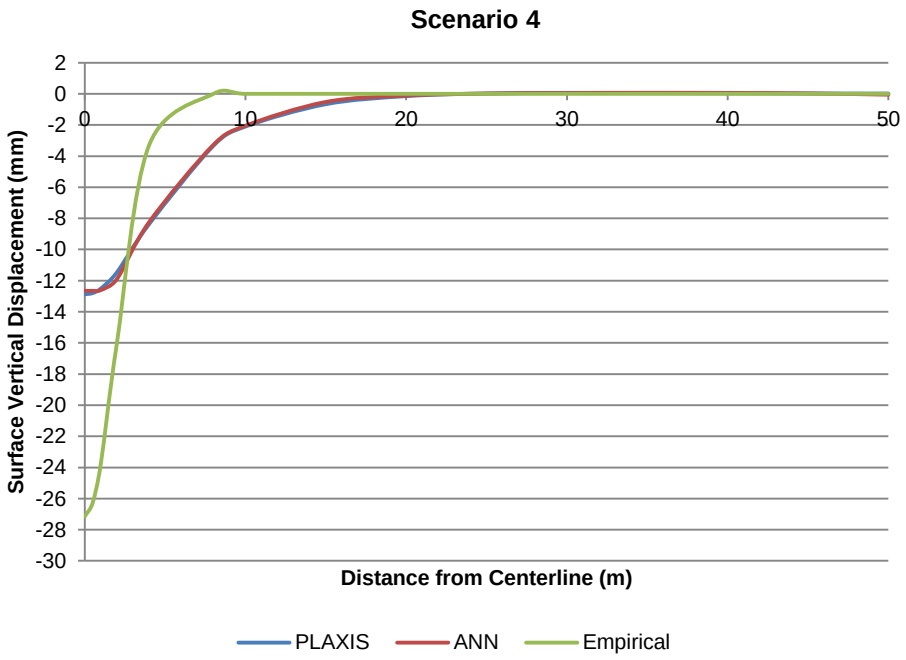
Scenario 4
Surface Vertical Displacement (mm)
2
0
-2
-4
-6
-8
-10
-12
-14
-16
-18
-20
-22
-24
-26
-28
-30
0
10
20
30
40
50
Distance from Centerline (m)
PLAXIS
ANN
Empirical

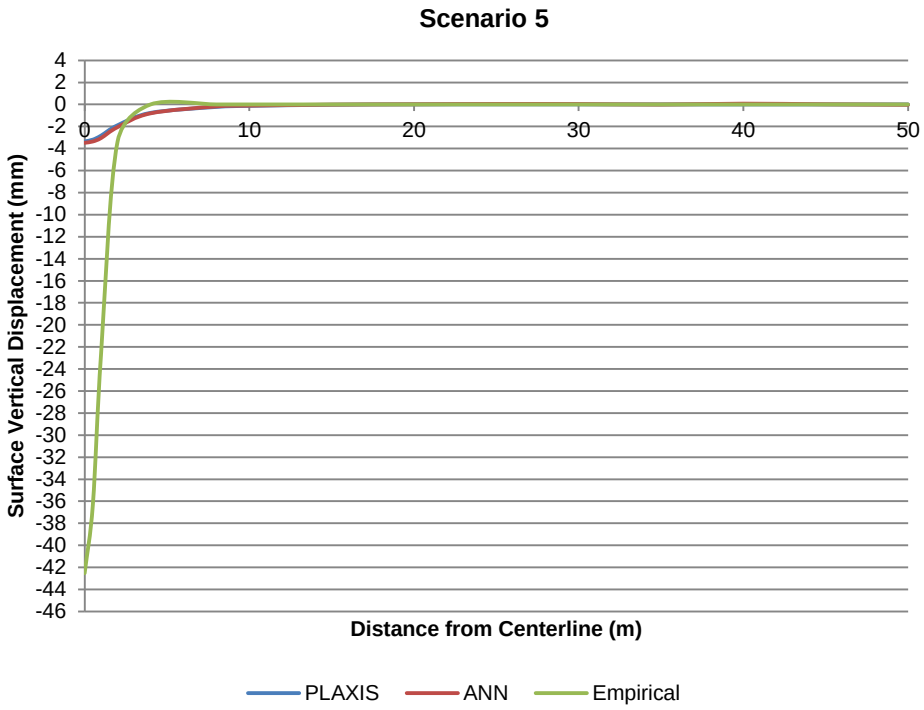
Scenario 5
Surface Vertical Displacement (mm)
4
2
0
-2
-4
-6
-8
-10
-12
-14
-16
-18
-20
-22
-24
-26
-28
-30
-32
-34
-36
-38
-40
-42
-44
-46
0
10
20
30
40
50
Distance from Centerline (m)
PLAXIS
ANN
Empirical

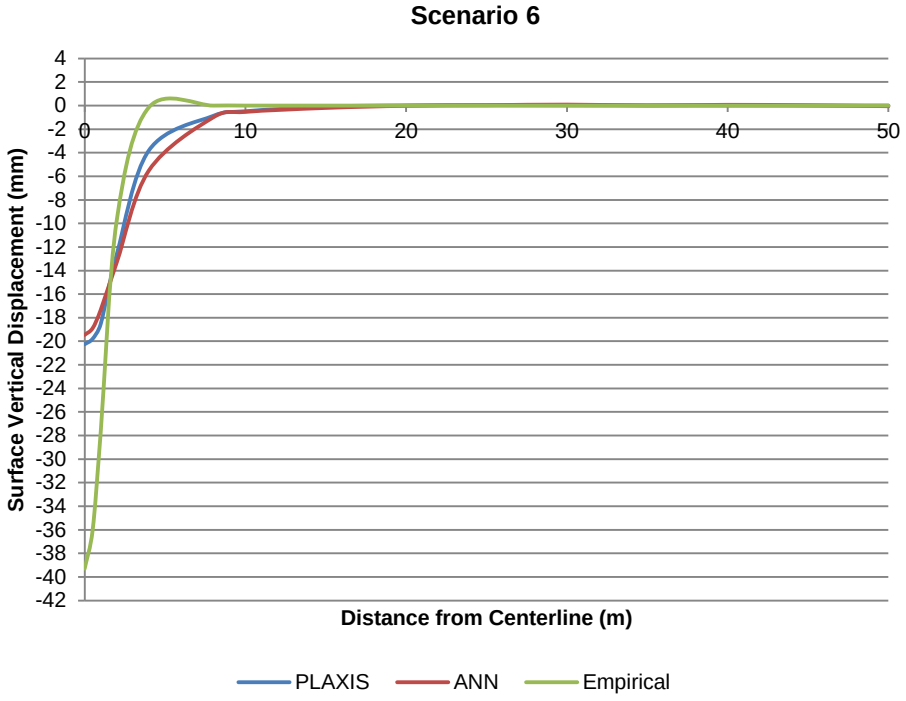
Scenario 6
Surface Vertical Displacement (mm)
4
2
0
-2
-4
-6
-8
-10
-12
-14
-16
-18
-20
-22
-24
-26
-28
-30
-32
-34
-36
-38
-40
-42
0
10
20
30
40
50
Distance from Centerline (m)
PLAXIS
ANN
Empirical

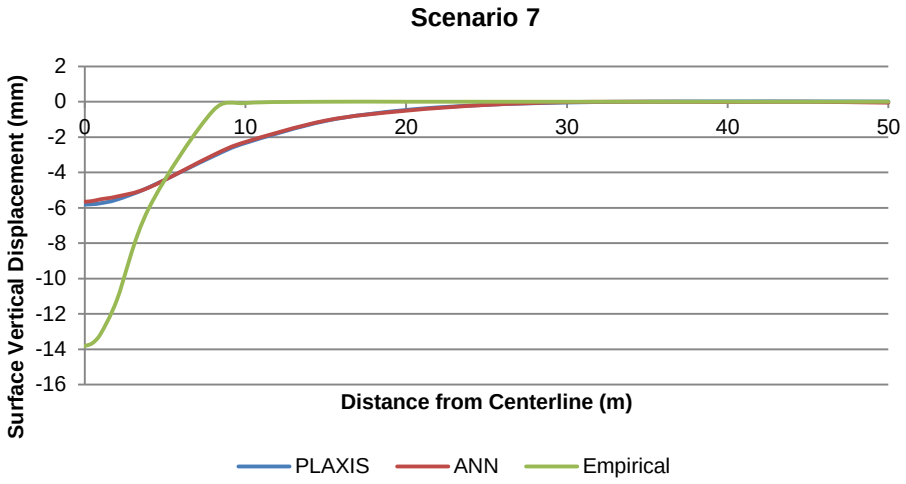
Scenario 7
Surface Vertical Displacement (mm)
2
0
-2
-4
-6
-8
-10
-12
-14
-16
0
10
20
30
40
50
Distance from Centerline (m)
PLAXIS
ANN
Empirical

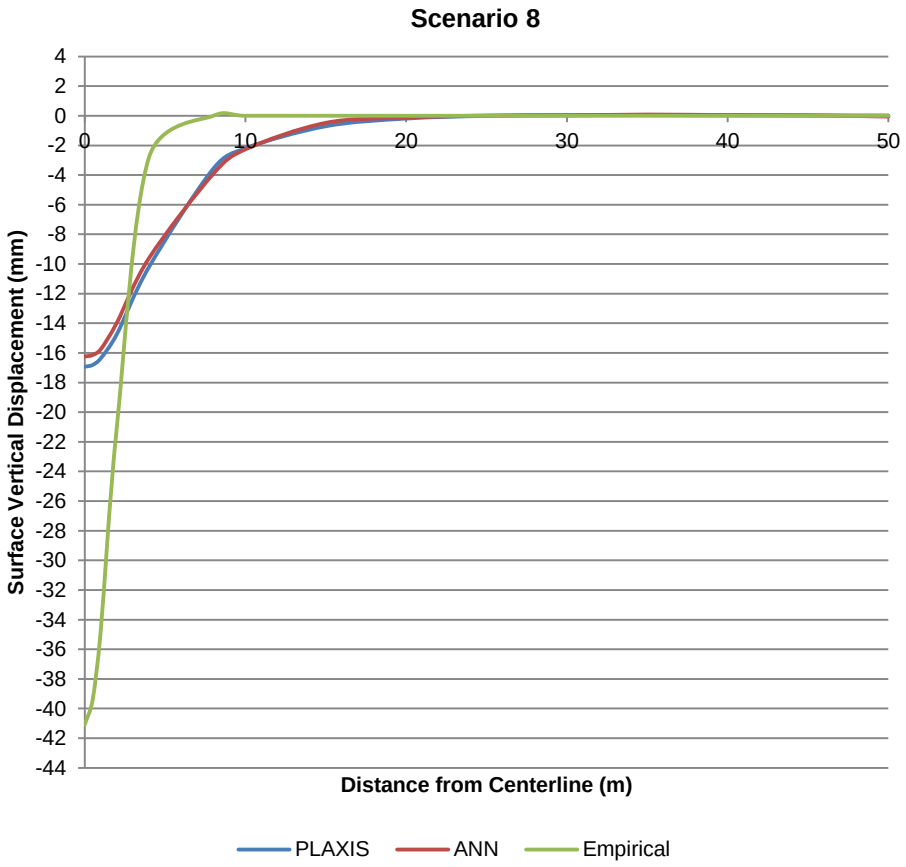
Scenario 8
Surface Vertical Displacement (mm)
4
2
0
-2
-4
-6
-8
-10
-12
-14
-16
-18
-20
-22
-24
-26
-28
-30
-32
-34
-36
-38
-40
-42
-44
0
10
20
30
40
50
Distance from Centerline (m)
PLAXIS
ANN
Empirical

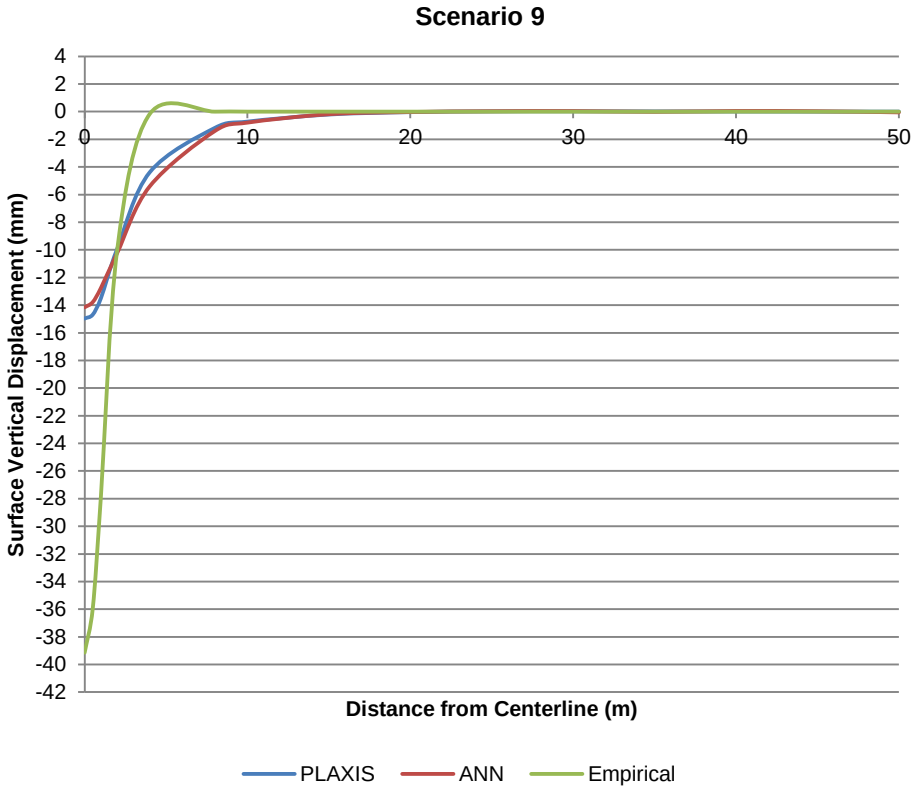
Scenario 9
Surface Vertical Displacement (mm)
Distance from Centerline (m)
PLAXIS
ANN
Empirical

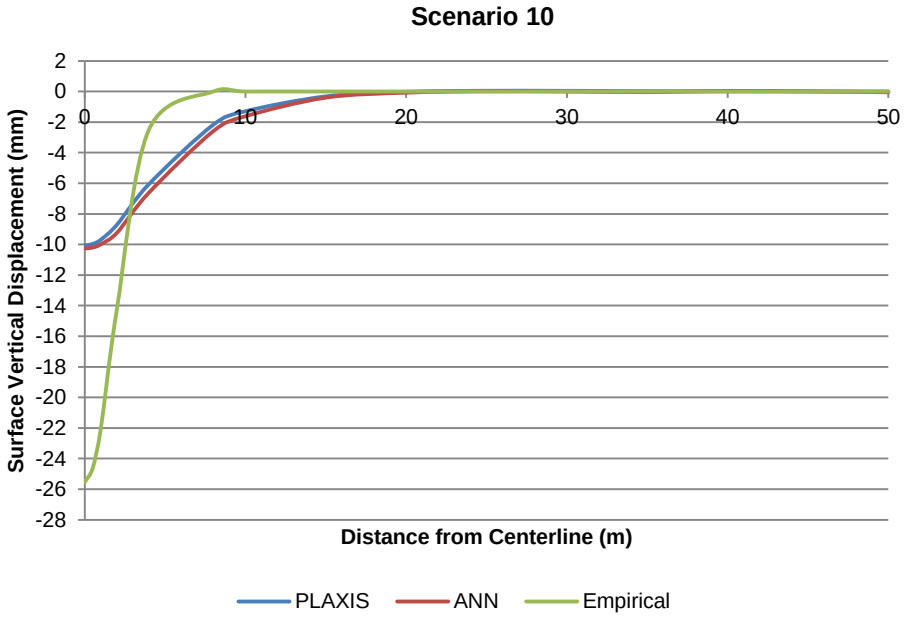
Scenario 10
Surface Vertical Displacement (mm)
Distance from Centerline (m)
PLAXIS
ANN
Empirical

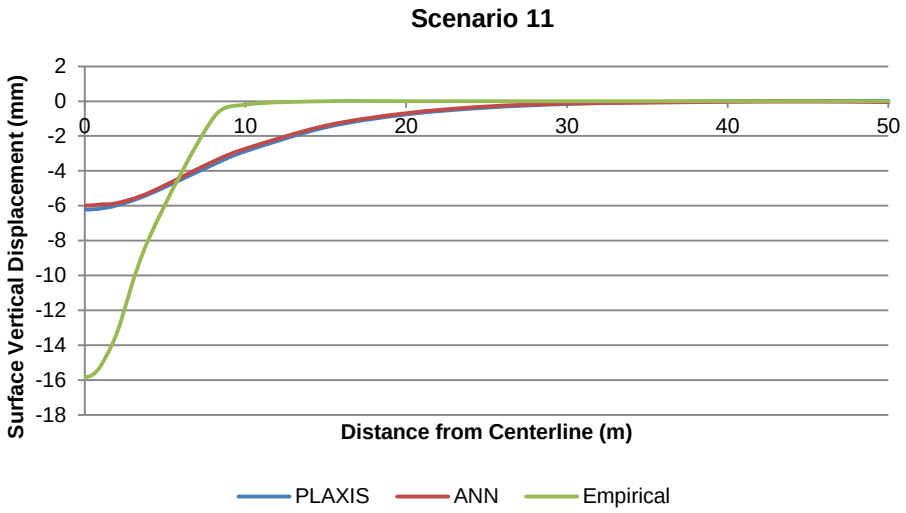
Scenario 11
Surface Vertical Displacement (mm)
2
0
-2
-4
-6
-8
-10
-12
-14
-16
-18
0
10
20
30
40
50
Distance from Centerline (m)
PLAXIS
ANN
Empirical

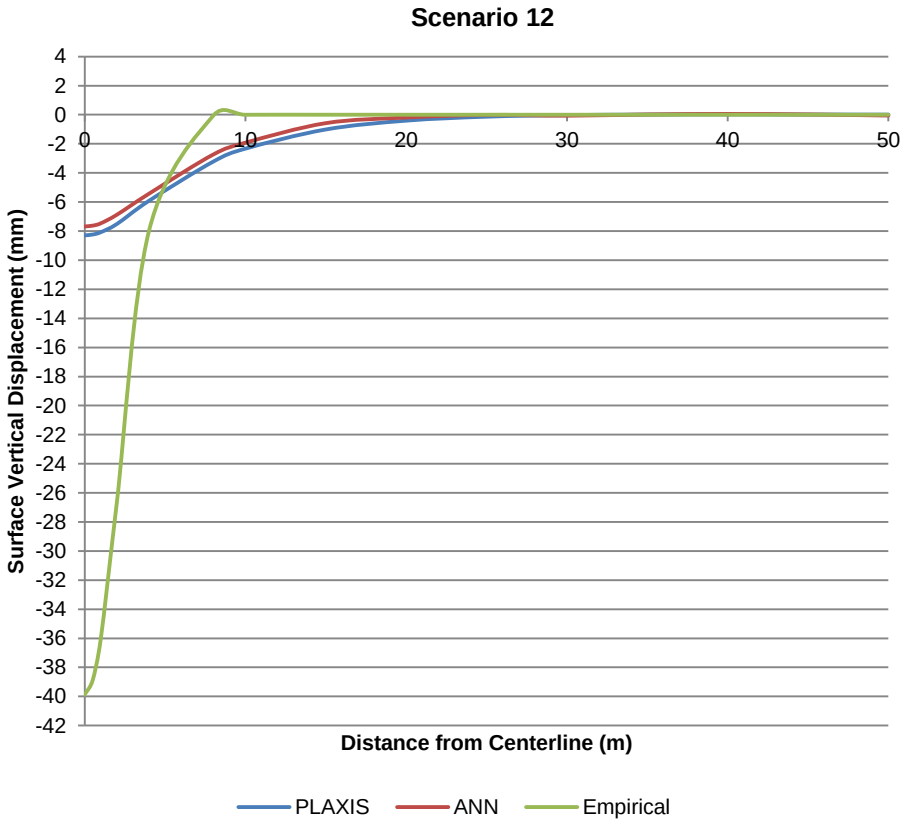
Scenario 12
Surface Vertical Displacement (mm)
4
2
0
-2
-4
-6
-8
-10
-12
-14
-16
-18
-20
-22
-24
-26
-28
-30
-32
-34
-36
-38
-40
-42
0
10
20
30
40
50
Distance from Centerline (m)
PLAXIS
ANN
Empirical

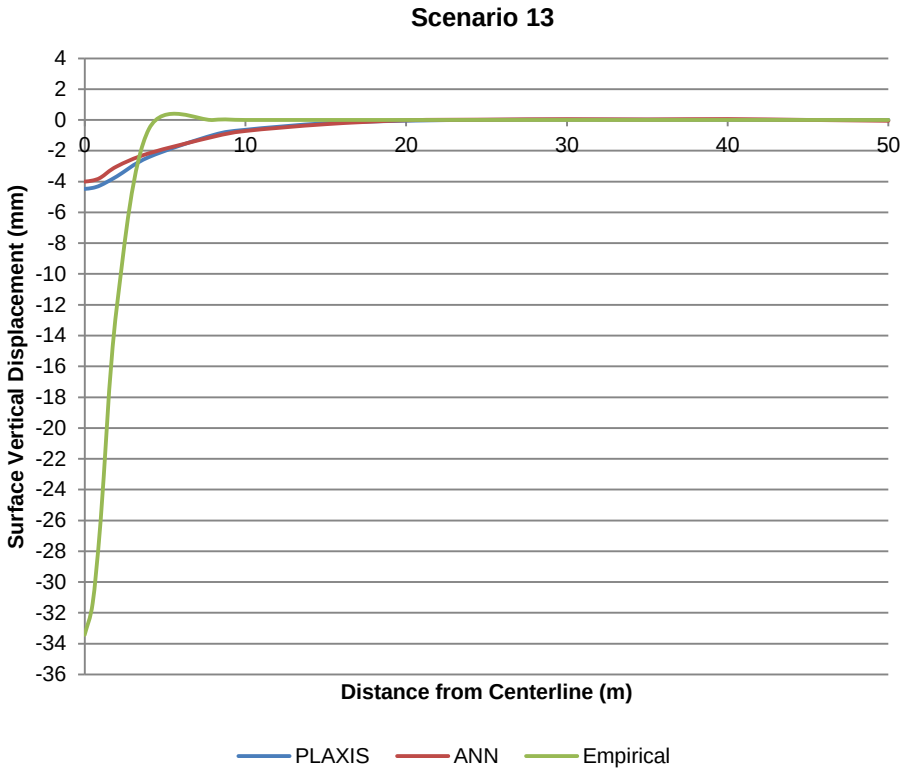
Scenario 13
Surface Vertical Displacement (mm)
4
2
0
-2
-4
-6
-8
-10
-12
-14
-16
-18
-20
-22
-24
-26
-28
-30
-32
-34
-36
0
10
20
30
40
50
Distance from Centerline (m)
PLAXIS
ANN
Empirical

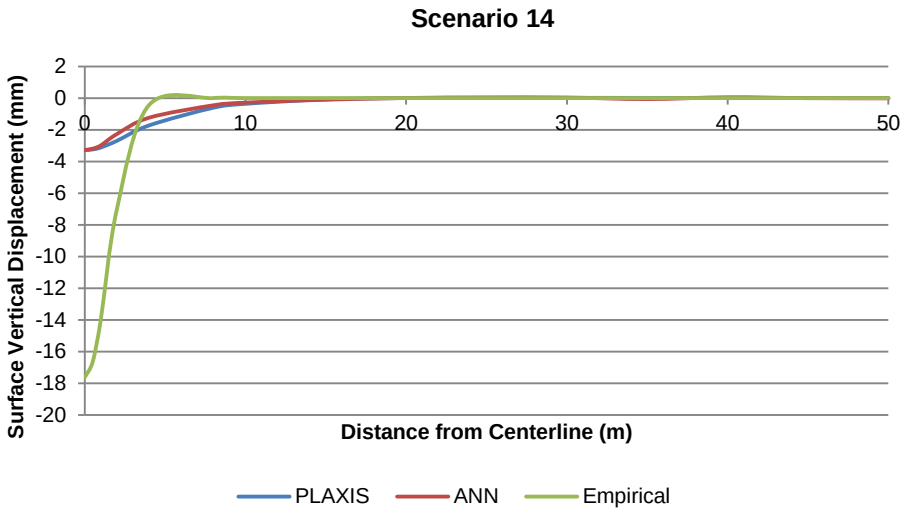
Scenario 14
Surface Vertical Displacement (mm)
2
0
-2
-4
-6
-8
-10
-12
-14
-16
-18
-20
0
10
20
30
40
50
Distance from Centerline (m)
PLAXIS
ANN
Empirical

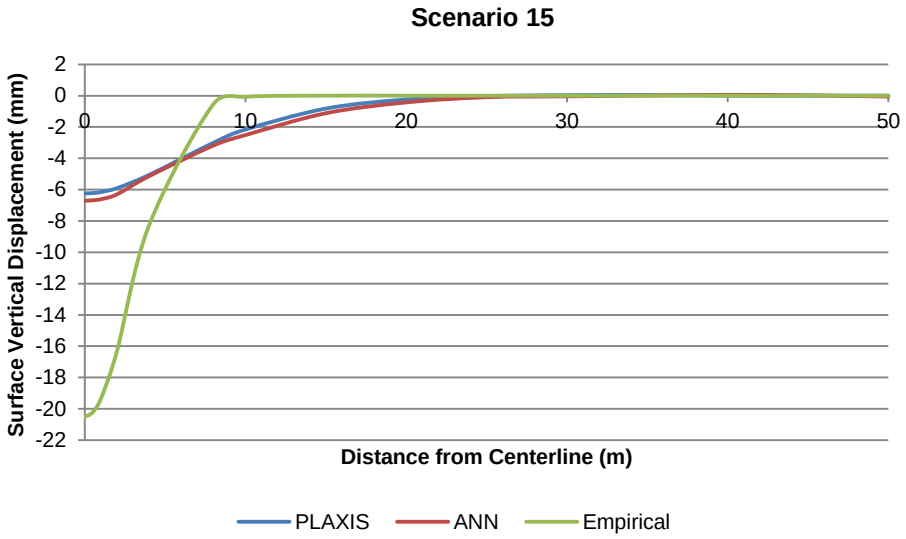
Scenario 15
Surface Vertical Displacement (mm)
2
0
-2
-4
-6
-8
-10
-12
-14
-16
-18
-20
-22
0
10
20
30
40
50
Distance from Centerline (m)
PLAXIS
ANN
Empirical

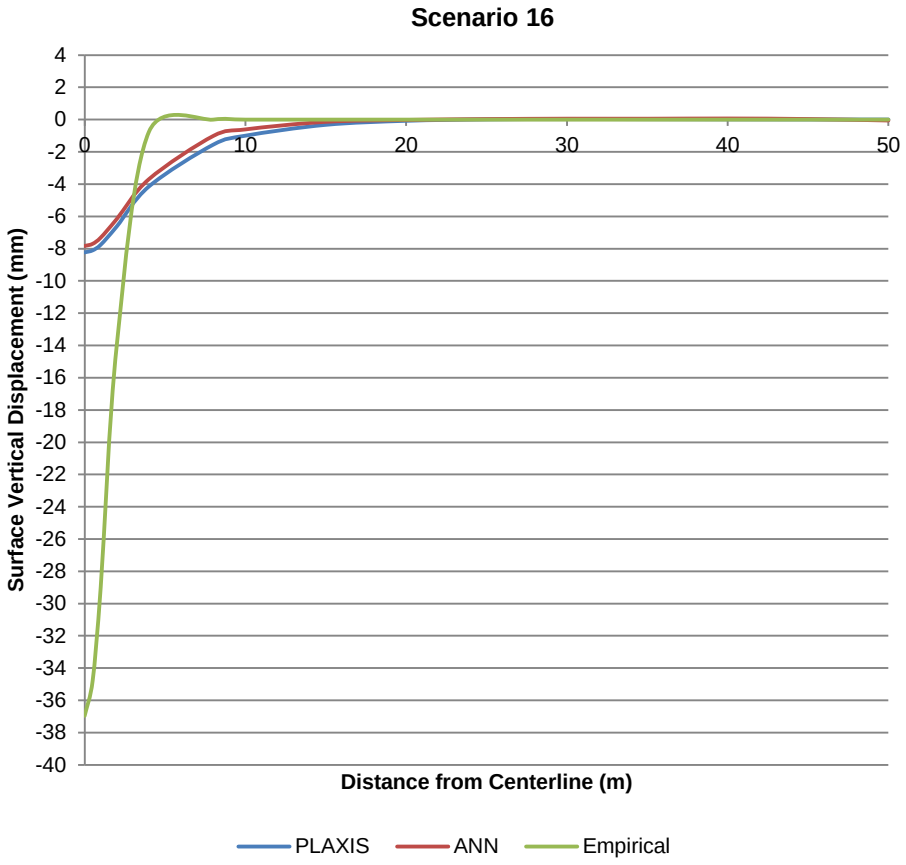
Scenario 16
Surface Vertical Displacement (mm)
4
2
0
-2
-4
-6
-8
-10
-12
-14
-16
-18
-20
-22
-24
-26
-28
-30
-32
-34
-36
-38
-40
0
10
20
30
40
50
Distance from Centerline (m)
PLAXIS
ANN
Empirical

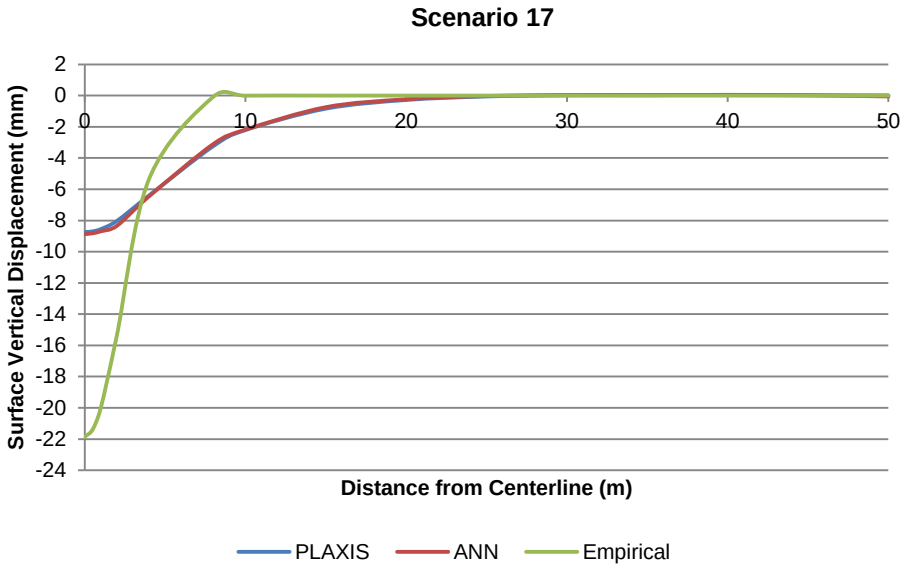
Scenario 17
Surface Vertical Displacement (mm)
2
0
-2
-4
-6
-8
-10
-12
-14
-16
-18
-20
-22
-24
0
10
20
30
40
50
Distance from Centerline (m)
PLAXIS
ANN
Empirical

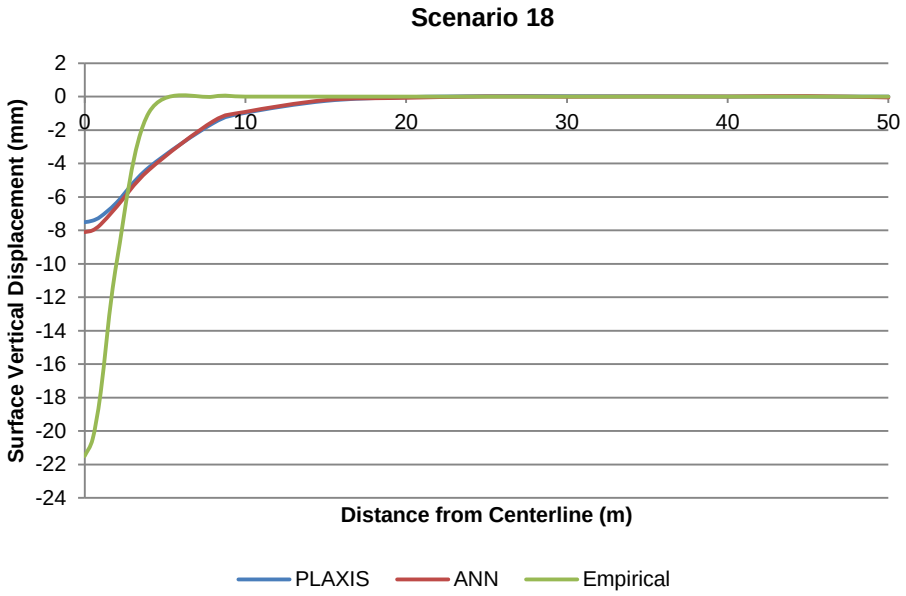
Scenario 18
Surface Vertical Displacement (mm)
2
0
-2
-4
-6
-8
-10
-12
-14
-16
-18
-20
-22
-24
0
10
20
30
40
50
Distance from Centerline (m)
PLAXIS
ANN
Empirical

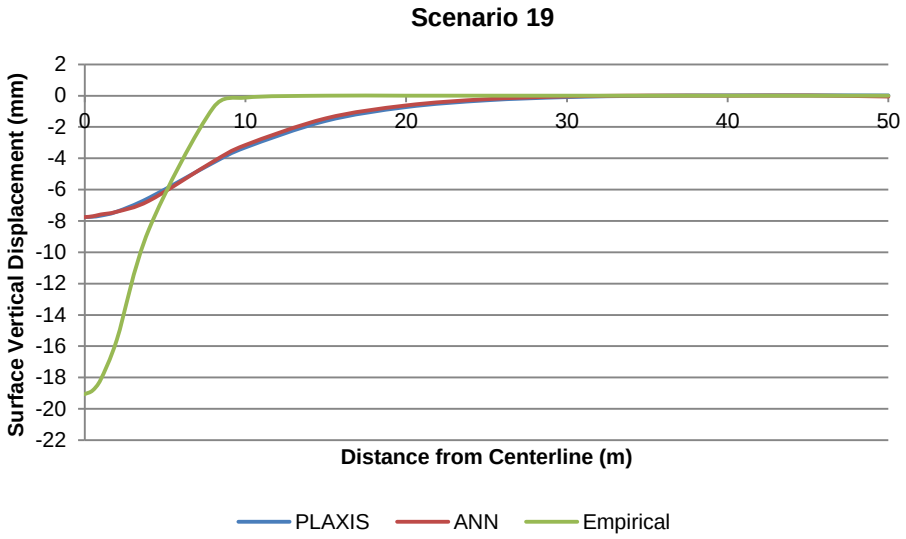
Scenario 19
Surface Vertical Displacement (mm)
2
0
-2
-4
-6
-8
-10
-12
-14
-16
-18
-20
-22
0
10
20
30
40
50
Distance from Centerline (m)
PLAXIS
ANN
Empirical

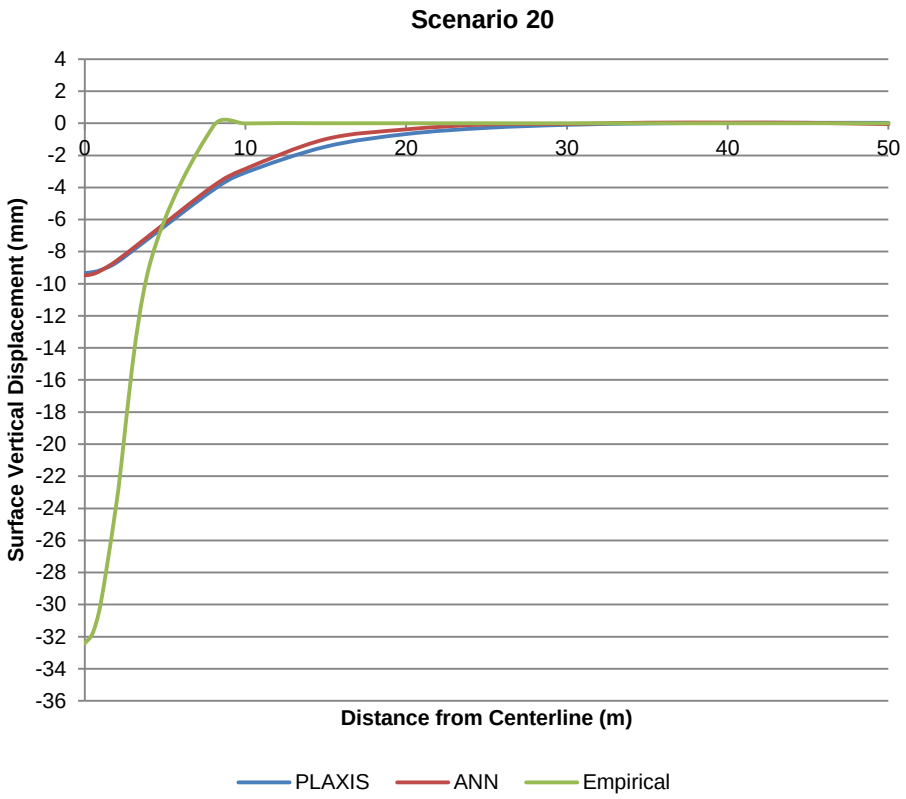
Scenario 20
Surface Vertical Displacement (mm)
4
2
0
-2
-4
-6
-8
-10
-12
-14
-16
-18
-20
-22
-24
-26
-28
-30
-32
-34
-36
0
10
20
30
40
50
Distance from Centerline (m)
PLAXIS
ANN
Empirical

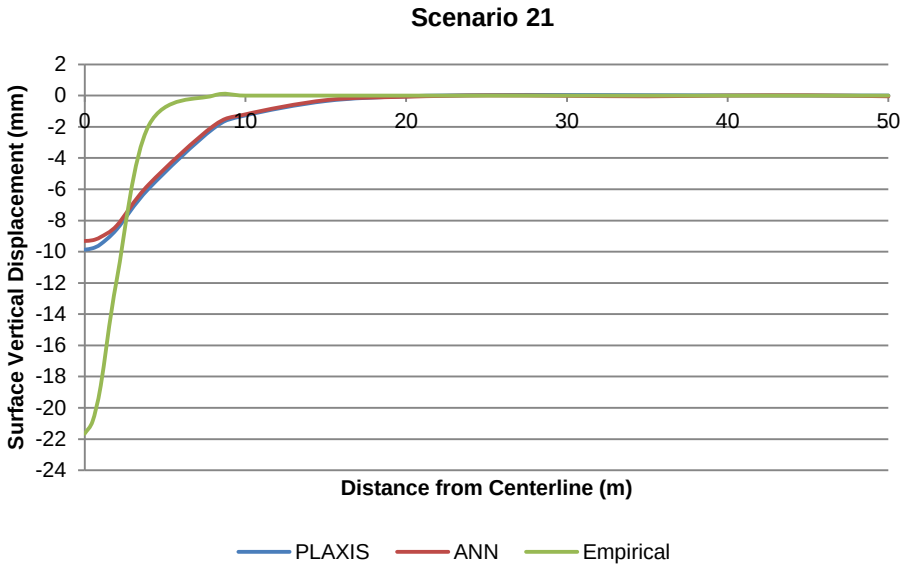
Scenario 21
Surface Vertical Displacement (mm)
2
0
-2
-4
-6
-8
-10
-12
-14
-16
-18
-20
-22
-24
0
10
20
30
40
50
Distance from Centerline (m)
PLAXIS
ANN
Empirical

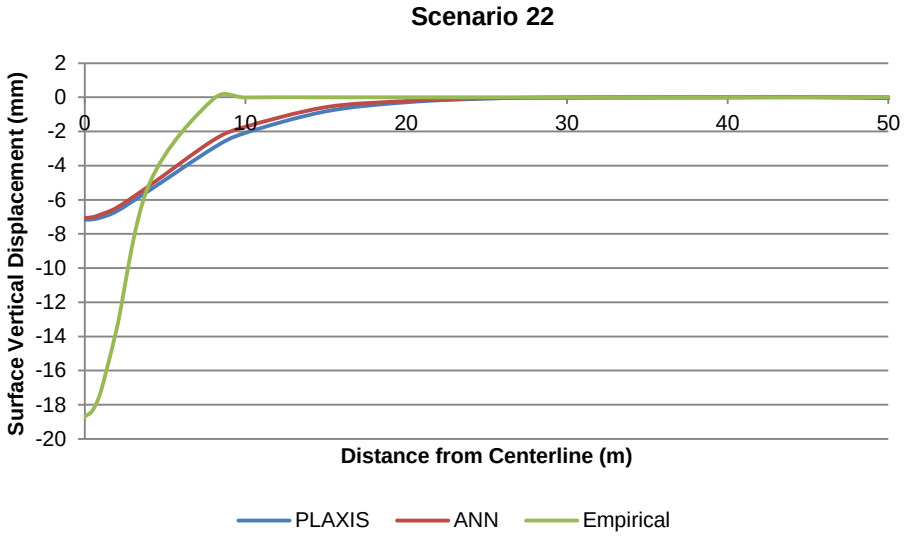
Scenario 22
Surface Vertical Displacement (mm)
2
0
-2
-4
-6
-8
-10
-12
-14
-16
-18
-20
0
10
20
30
40
50
Distance from Centerline (m)
PLAXIS
ANN
Empirical

List of Abbreviations

Abbreviation	Description
ANN:	Artificial Neural Network
BJ:	Box Jacking
FEM:	Finite Element Modeling
HAB:	Horizontal Auger Boring
HDD:	Horizontal Directional Drilling
HI:	Horizontal Inclinometer
MT:	Microtunneling
PJ:	Pipe Jacking
SPT:	Standard Penetration Test
TCM:	Trenchless Construction Method
TRM:	Trenchless Renewal Method
TT:	Trenchless Technology
TxDOT:	Texas Department of Transportation
USCS:	Unified Soil Classification System
UT:	Utility Tunneling

References

Association of Pipelines. Retrieved 02 10, 2014, from AOPL: http://www.aopl.org/

Bennett, D. (1998). *Jacking Force and Ground Deformations Associated with Microtunneling.* Urbana, IL.: Ph.D. Dissertation, The University of Illinois.

Bolton, M. D. (1986). The Strength and Dilatancy of Sands. *Geotechnique 36*, 65-78.

Budhu, M. (2011). *Soil Mechanics and Foundations.* Hoboken, NJ: John Wiley & Sons, Inc.

Cording, E., & Hansmire, W. (1975). Displacements around Soft Ground Tunnels. Buenos Aires, Argentina: 5th Pan American Congress on Soil Mechanics and Foundation Engineering.

Desai, Y. M., Eldho, T. I., & Shah, A. H. (2011). *Finite Element Method with Application in Engineering.* New Delhi: Dorling Kindersley (India) Pvt. Ltd.

DGSI. (2013, August). *Slope Indicator*. Retrieved February 2014, from http://www.slopeindicator.com/pdf/digitilt-horizontal-inclinometer-probe-datasheet.pdf

Duan, Z. . (2001). *Ground Movement Associated with Microtunneling.* Luisiana: Luisiana Tech University.

Evans, C. (1983). *An Examination of Arching in Granular Soils.* Massachusetts: Massachusetts Institute of Technology (MIT).

GEOKON. (2014). Retrieved May 21, 2014, from Pressure Transducer: http://www.geokon.com/

Hossaini, S. M., Shaban, M., & Talebnejad, A. (2012). Relationship Between Twin Tunnels Distance and Surface Subsidance in Soft Ground of Tabriz Metro-IRAN. *Coal Operators' Conference*.

Humes. (2013). *Box Culverts.* Australia: Humes.

Hung, J., Monsees, J., Munfah, N., & Wisniewski, J. (2009). *Technical Manual for Design and Construction of Road Tunnels - Civil Element.* New York, NY: Parsons Brinckerhoff, Inc.

Iseley, T., & Gokhale, S. (1997). *Trenchless Installation of conduits Beneath Roadways.* Washington D.C.: National Academy Press.

Lawrence, J. (1994). *Introduction to Neural Network.* Nevada: California Sceintific Software.

Lee, C.-J., Chiang, K.-H., & Kuo, C.-M. (2004). Ground Movement and Tunnel Stability When Tunneling in Sandy Ground. *chinese Institute of Engineers*, 1021-1032.

Lenz R.W. (2011).”Pavement Design Guide.” Texas Department of Transportation (TxDOT).

Liu, W.-T., & Lu, X.-Y. (2012). 3D Numirical Analysis of Soil Structure Interaction Behaviors of Pipe Jacking Construction. *Applied Mechanics and Materials*, 534-538.

Mair, R., Taylor, R., & Bracegirdle, A. (1993). Subsurface Settlement Profiles Above Tunnels in Clays. *Geotechnique*, 315-320.

Mamaqani, B., & Najafi, M. (2014). Settlement Analysis of Box Jacking Projects. *ASCE Pipeline .* Portland, OR: American Society of American Society (ASCE).

Martos, F. (1958). Concerning and Approximate Equation of the Subsidence Trough and its Time Factors. *International Strata Control Congress*, 191-205.

Nair, R., & Taylor, R. (1993). Subsurface Settlement Profiles Above Tunnels in Clay. *Geotechnique 43(2)*, 315-320.

Najafi, M. (2013). *Trenchless Technology; Planning, Equipment, and Methods.* New York: McGraw-Hill Companies.

Najafi, M. (2010). *Trenchless TechnologyPiping: Installation and Inspection.* New York: McGraw-Hill Companies.
Najafi, M., & Gokhale, S. (2004). *Trenchless Technology; Pipeline and Utility Design, Construction, and Renewal.* New York: McGill-Hill.
O'Reilly, M. (1991). Ground Movements Associated with Pipe Installation and Tunneling. *10th European Conference on Soil Mechanics and Foundation Engineer*, 907-910.
O'Reilly, Myles, P., & B.M., N. (1982). Settlements Above Tunnels in the United Kingdom -Their Magnitude and Prediction. *Proceeding of Tunneling '82*.
O'Reilly, Nichael, P., & C.D.F., R. (1990). Ground Movements Associated with Pipejacking and Trenchling. *No-Dig 90*.
OSHA. (2002). *29 CFR 1926 SOHA Construction Industry Regulations.* Davenport, Iowa.
Peck, R. (1969). Deep Excavations and Tunneling in Soft Ground. State of the Art Report. (pp. 225-290). Mecico City: 7th International Conference on Soil Mechanics and Foundation Engineering.
Piehl, R. (2005). *Summary of Trenchless Technology for Use With USDA Forest Service Culverts.* Washington D.C.: The U.S. Department of Agriculture (USDA).
Plaxis. (2011). *Plaxis Tutorial.* Plaxis.
Potts, D. (1976). *Behaviour of Lined and Unlined Tunnels in Sand.* Cambridge: University of Cambridge.
Rogers, C., & O'Reily, M. (1991). Ground Movements Associated with Pipejacking and Trenching. *Proceedings of the International Conference on Soil Mechanics and Foundation Engineering* (pp. 907-910). Florence, Italy: Publ by A.A. Balkema, Rotterdam, Netherlands.
Sagaseta. (1987). Analysis of Underained Soil Deformation Due to Ground Loss. *Geotechnique 37*, 301-320.
Schmidt, B. (1969). Settlements and Ground Movements Associated with Tunneling in Soil. Urbana, IL: PhD Dissertation, University of Illinois.
Shou, K. J., & Chang, F. W. (2006). Analysis of Pipe-Soil Interaction for a Miniature Pipejacking. *Journal of Mechanics*, 213-220.
Stein, D. (2005). *Trenchless Technology for Installation of Cables and Pipelines.* Bochum: Stein & Partnet GmbH.
Tavakoli, H. (2012). “Productivity Analysis of Box Jacking.” M.S. Thesis, The University of Texas at Arlington, Arlington, TX.
Taylor, S., & Winsor, D. (1998). Developments in Tunnel Jacking. *Jacked Tunnel Design and Construction*.
Terzaghi, K. (1943). *Theorotical Soil Mechanics.* New York: John Wiley and Sons.
Terzaghi, K., Peck, R. B., & Mesri, G. (1996). *Soil Mechanics in Engineering Practice.* New York: John Wiley & Sons, Inc.
Tien, H.-J. (1990). *A Literature Study of the Arching Effect.* Cambrdige, MA: MAssachusetts Institute of Technology (MIT).
U.S. Army Corps of Engineers. (2003). *Guidelines and Standards for Implementation of* Electronic *Document Management Systems*. Retrieved February 23, 2014, from http://www.archives.gov/records-mgmt/toolkit/pdf/ID114.pdf
Wallin, M., Wallin, K., & Bennett, D. (2008). Analysis and Mitigation of Settlement Risks in New Trenchless Installations. *No-Dig Conference and Exhibition*.
Wu, B., & Lee, C. (2003). Ground Movements and Collapse Mechanism Induced by Tunneling in Clayey Soil. *International Journal of Physical Modelling of Geotechnics*, 15-29.

Biographical Information

Babak H. Mamaqani was born February 14, 1984, in Tehran, IRAN. He received his bachelor degree in Civil Engineering from Tabriz Azad University, Tabriz, IRAN in 2007. Then, he continued his education in civil engineering and received his master's degree in Structural/Earthquake Engineering from the International Institute of Earthquake Engineering and Seismology (IIEES), Tehran, IRAN in 2010. Meanwhile, he worked as a Project Engineer and Design Engineer for a construction company, Rezvan Makan Co, and participated in different types of civil engineering projects within construction, structural, pipeline industries. With great motivation and enthusiasm for developing higher-level skills and knowledge in the area of construction and pipeline engineering, he decided to pursue his Ph.D. in civil engineering. He was accepted into the graduate program of the University of Texas at Arlington in 2010 and worked with Dr. Mohammad Najafi who served as his advisor. As a graduate student, he worked on several research projects which provided instruction and explored innovative research in ways to handle high-density polyethylene (HDPE) and large-diameter pipeline repair and maintenance. Most importantly, he was able to work with the Texas Department of Transportation (TxDOT) through a collaborative program with UTA where he was able to investigate the different applications and methods of trenchless technology like horizontal directional drilling (HDD) and Pipe/Box Jacking. This study led to the writing of this dissertation and inspired a lasting interest in trenchless technology.